

# The Physics of Space Weather: What We Know Now and What Are the Current and Future Challenges?

Bruce T. Tsurutani<sup>1</sup>, Gurbax S. Lakhina<sup>2</sup>, Rajkumar Hajra<sup>3</sup>

<sup>1</sup>Pasadena, Calif, USA

<sup>2</sup>Indian Institute for Geomagnetism, Navi Mumbai, India

<sup>3</sup>National Atmospheric Research Laboratory, Gadanki, India

## ABSTRACT

Major geomagnetic storms are caused by unusually intense solar wind southward magnetic fields that impinge upon the Earth's magnetosphere (Dungey, 1961). How can we predict the occurrence of future interplanetary events? Do we currently know enough of the underlying physics and do we have sufficient observations of solar wind phenomena that will impinge upon the Earth's magnetosphere? We view this as the most important challenge in Space Weather. We discuss the case for magnetic clouds (MCs), interplanetary sheaths upstream of interplanetary coronal mass ejections (ICMEs), corotating interaction regions (CIRs) and solar wind high-speed streams (HSSs). The sheath- and CIR-related magnetic storms will be difficult to predict and will require better knowledge of the slow solar wind and modeling to solve. For interplanetary space weather, there are challenges for understanding the fluences and spectra of solar energetic particles (SEPs). This will require better knowledge of interplanetary shock properties as they propagate and evolve going from the Sun to 1 AU (and beyond), the upstream slow solar wind and energetic "seed" particles. Dayside aurora, triggering of nightside substorms, and formation of new radiation belts can all be caused by shock and interplanetary ram pressure impingements onto the Earth's magnetosphere. The acceleration and loss of relativistic magnetospheric "killer" electrons and prompt penetrating electric fields in terms of causing positive and negative ionospheric storms are reasonably well understood, but refinements are still needed. The forecasting of extreme events (extreme shocks, extreme solar energetic particle events, and extreme geomagnetic storms ("Carrington" events or greater)) are also

31 discussed. Energetic particle precipitation [into the atmosphere](#) and ozone destruction is  
32 briefly discussed. For many of the studies, the Parker Solar Probe, Solar Orbiter,  
33 Magnetospheric Multiscale Mission (MMS), Arase, and SWARM data will be useful.

34

## 35 **1. INTRODUCTION**

### 36 **1.1. Some Comments on the History of [the Physics of Space Weather](#)**

37

38 Space Weather is a new term for a topic [that actually began over a century and a half ago](#). It is just  
39 [that with the space age beginning in 1957 \(with the launch of Sputnik\) and soon thereafter, many](#)  
40 [scientifically instrumented satellites led to an explosion of knowledge of the physics of Space](#)  
41 [Weather. However it is useful to review some of the early scientific studies that occurred prior to](#)  
42 [1957](#). Prior to the space age (where we have satellites orbiting the Earth, probing interplanetary  
43 space and viewing the Sun in UV, EUV and X-ray wavelengths), it was clearly realized that solar  
44 phenomena caused geomagnetic activity at the Earth. For example, Carrington (1859) noted that  
45 there was a magnetic storm that followed ~17 h 40 min after the well-documented optical solar  
46 flare which he reported. This storm (Chapman and Bartels, 1940) was only more recently studied  
47 in detail by Tsurutani et al. (2003) and Lakhina et al. (2012), but the hints of a causal relationship  
48 was there in 1859. [After Carrington \(1959\) published his seminal paper](#), Hale (1931), Newton  
49 (1943) and others showed that magnetic storms were delayed by several days from intense solar  
50 flares. These types of magnetic storms are now known to be caused by [either their associated](#)  
51 [interplanetary coronal mass ejections \(ICMEs\) or their upstream sheaths](#). Details will be discussed  
52 later in this review.

53

54 Maunder (1904) showed that geomagnetic activity often had a ~27 day recurrence. [This periodicity](#)  
55 [was associated with some mysteriously unseen \(by visible light\) feature on the Sun](#). Chree (1905,  
56 1913) showed that these data were statistically significant, thus inventing the Chree “superposed  
57 epoch analysis”, a [scientific data analysis](#) technique which is [still](#) used today. The mysteriously  
58 unseen solar features responsible for the geomagnetic activity were called “M-regions” by Bartels  
59 (1934) where the “M” stood for “magnetically active”. It is now known that M-regions are coronal  
60 holes (Krieger et al., 1973), solar regions from which [solar wind high-speed streams \(HSSs\)](#)  
61 emanate, causing geomagnetic activity at the Earth (Sheeley et al., 1976, 1977; Tsurutani et al.

62 1995). The current status of geomagnetic activity associated with HSSs and the future work  
63 needed to better understand and to predict the various facets of Space Weather events will be  
64 discussed later.

65  
66 With the advent of rockets and satellites, the near-Earth interplanetary medium has been probed  
67 by magnetic field, plasma, and energetic particle detectors. The Sun has been viewed in many  
68 different wavelengths. The Earth's auroral regions have recently been viewed by UV imagers  
69 giving a global view of auroras including the dayside. The ionosphere has been probed by global  
70 positioning system (GPS) dual frequency radio signals, allowing a global map of the ionospheric  
71 total electron content (TEC) in relatively high spatial and temporal resolution. The purpose of this  
72 review article will be to give a reasonably thorough review of some of the major Space Weather  
73 effects in the magnetosphere, ionosphere and atmosphere and in interplanetary space, in order to  
74 explain what the solar and interplanetary causes are or are expected to be. The most useful part of  
75 this review will be to focus on what future advances in Space Weather might be in the next 10 to  
76 25 years. In particular we will mention what outstanding problems the Parker Solar Probe, Solar  
77 Orbiter, MMS, Arase, ICON, GOLD, and SWARM data might be useful in solving.

78  
79 Our discussion will first start with phenomena that occur most frequently during solar maxima  
80 (flares, CMEs and ICME-induced magnetic storms). We will explain to the reader what is meant  
81 by an ICME and why we distinguish this from a CME. Next, phenomena associated with the  
82 declining phase of the solar cycle will be addressed. These include corotating interaction regions  
83 (CIRs) and HSSs, which cause high-intensity long-duration continuous AE activity (HILDCAA)  
84 events, and the acceleration and loss of magnetospheric relativistic electrons. We will then return  
85 to the topic of interplanetary shocks and their acceleration of energetic particles in interplanetary  
86 space and also their creating new radiation belts inside the magnetosphere. Interplanetary shock  
87 impingement onto the magnetosphere create dayside auroras and also trigger nightside substorms.  
88 Prompt penetration electric fields during magnetic storm main phases will be discussed in terms  
89 of the consequences of positive and negative ionospheric storms, depending on the local time of  
90 the observation and the phase of the magnetic storm. Two relatively new topics, that of  
91 supersubstorms (SSSs) and the possibility of precipitating magnetospheric relativistic electrons

92 affecting atmospheric weather will be discussed. A glossary will be provided to give definition of  
93 the terms used in this review article.

94  
95 There have been some recent books/articles that touch on the many topics of the physics of Space  
96 Weather, however not in the same way that we will attempt to do here. We recommend the  
97 interested reader: “*From the Sun: Auroras, Magnetic Storms, Solar Flares, Cosmic Rays*” by Suess  
98 and Tsurutani (1989), “*Magnetic Storms*” by Tsurutani, Kamide, Gonzalez, Arballo (1997a),  
99 “*Storm-Substorm Relationship*” by Sharma, Kamide, Lakhina (2004), “*Recurrent Magnetic*  
100 *Storms: Corotating Solar Wind Streams*” by Tsurutani, McPherron, Gonzalez, Lu, Sobral,  
101 Gopalswamy (2006a), “*The Sun and Space Weather*” by Hanslmeier (2007), “*Physics of Space*  
102 *Storms: From the Solar Surface to the Earth*” by Koskinen (2011), and “*Extreme Events in*  
103 *Geospace: Origins, Predictability and Consequences*” by Buzulukova (2018). Because Space  
104 Weather is an enormous field/topic, not all facets of it have ever been covered in one book. The  
105 present authors are active researchers in the field and will attempt to introduce new viewpoints and  
106 topics not covered in the above works.

## 107 108 **1.2. Organization of Paper**

109  
110 The concept of magnetic reconnection is introduced first for the non-space plasma reader.  
111 **Magnetic reconnection** is the physical process responsible for transferring solar wind energy into  
112 the magnetosphere during magnetic storms. We have organized the rest of the paper by discussing  
113 **Space Weather** phenomena by solar cycle intervals. However it should be mentioned that this is  
114 not totally successful since some phenomena span all parts of the solar cycle.

115  
116 Solar maximum phenomena such as **CMEs**, **ICMEs**, fast shocks, sheaths, and the forecasting of  
117 geomagnetic storms associated with the above are covered in **Subsections 2.1 to 2.4**. The **Space**  
118 **Weather** phenomena associated with the declining phase of the solar cycle are discussed in **Section**  
119 **3.0**. Topics such as CIRs, CIR storms, **HSSs**, embedded Alfvén wave trains **within HSSs**,  
120 **HILDCAA** events, relativistic magnetospheric electron acceleration and loss, and electron  
121 precipitation and ozone depletion are discussed in **Subsections 3.1 to 3.6**. Although interplanetary  
122 shocks are primarily features associated with fast ICMEs and thus **primarily** a solar maximum

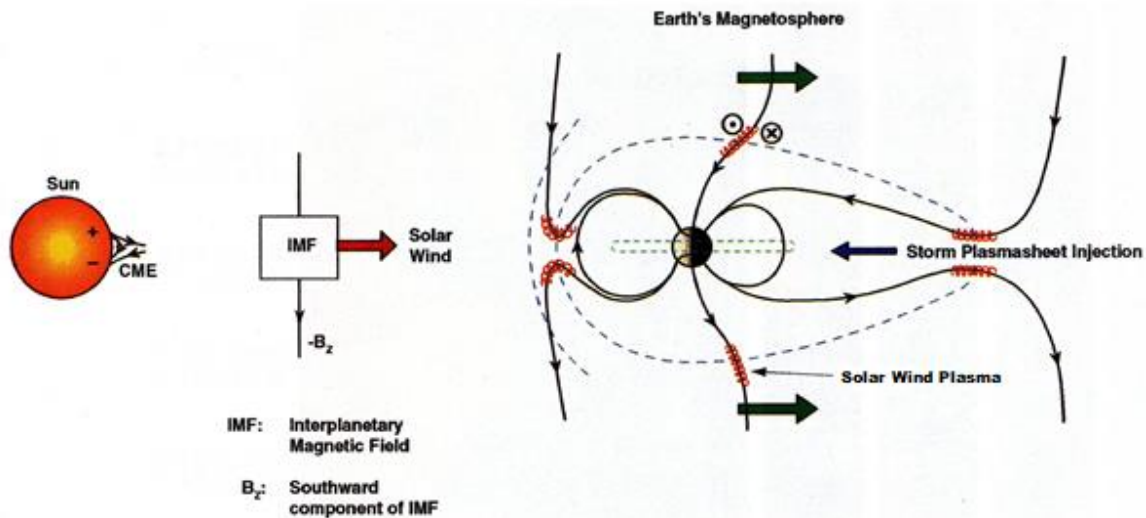
123 phenomenon, shocks can also bound CIRs (~20% of the time) at 1 AU during the solar cycle  
124 declining phase as well. Shocks and the high density plasmas that they create can input ram energy  
125 into the magnetosphere. Topics such as solar cosmic ray particle acceleration, dayside auroras,  
126 triggering of nightside substorms and the creation of new magnetospheric radiation belts are  
127 covered in Subsections 4.1 to 4.4. Solar flares and ionospheric TEC increases is another Space  
128 Weather effect causing direct solar-ionospheric coupling not involving interplanetary space nor  
129 the magnetosphere. This is briefly discussed in Section 5.0. Prompt penetration electric fields  
130 (PPEFs) and ionospheric TEC increases (and decreases) occurs during magnetic storms. Although  
131 the biggest effects are observed during ICME magnetic storms (solar maximum), effects have been  
132 noted in CIR magnetic storms as well. This is discussed in Section 6.0. The “Carrington” magnetic  
133 storm is the most intense magnetic storm in recorded history. The aurora associated with the storm  
134 reached 23° from the geomagnetic equator (Kimball, 1960), the lowest in recorded history. Since  
135 this event has been used as an example for extreme Space Weather and events of this type are a  
136 problem for the U.S. Homeland Security, we felt that there should be a separate section on this  
137 topic, Section 7.0. We also discuss the possibility of events even larger than the Carrington storm  
138 occurring. In Section 8.0 auroral SSSs are discussed. Why is this topic covered in this paper? It  
139 is possible that SSSs which occur within superstorms are the actual causes for the extreme  
140 ionospheric currents, geomagnetically induced currents (GICs), that are responsible for potential  
141 power grid failures and not the geomagnetic storms themselves. Section 9.0 gives our  
142 summary/conclusions for the physics and the possibility of forecasting Space Weather events.  
143 Section 10.0 is a glossary of Space Weather terms used by researchers in the field. Most of the  
144 definitions were carefully constructed in a previous book (Suess and Tsurutani, 1998). These  
145 should be useful for an ionospheric person looking up solar terms, etc. It could be particularly  
146 useful for the non-space plasma readership as well.

147

## 148 **2. RESULTS: Solar Maximum**

### 149 **2.1. Southward Interplanetary Magnetic Fields, Magnetic Reconnection and Magnetic** 150 **Storms**

151



152  
 153 Figure 1. Magnetic reconnection powering geomagnetic storms and substorms. Adapted from  
 154 Dungey (1961).

155  
 156 Figure 1 shows the Dungey (1961) scenario of magnetic reconnection. A one-to-one relationship  
 157 between southward **interplanetary** magnetic fields (**IMFs**) and magnetic storms has been shown by  
 158 Echer et al. (2008a) for 90 **intense** ( $Dst < -100$  nT) magnetic storms that occurred during **solar**  
 159 **cycle 23**. If the **IMF** is directed southward, it will interconnect with the Earth's magnetopause  
 160 northward magnetic fields (the Earth's north magnetic pole is located in the southern hemisphere  
 161 near the south rotational pole). The solar wind drags the interconnected magnetic fields and plasma  
 162 downstream (in the antisunward direction). The open magnetic fields then reconnect in the tail.  
 163 Reconnection leads to strong convection of the plasmasheet into the nightside magnetosphere.

164  
 165 What is known by theory and verified by observations is that the stronger the southward  
 166 component of the **IMF and the stronger the solar wind velocity convecting the magnetic field**, the  
 167 stronger the solar wind-magnetospheric system is driven (e.g., Gonzalez et al., 1994). Intense IMF  
 168  $B_{south}$  in MCs (and sheaths) drive intense magnetic reconnection at the dayside magnetopause  
 169 and intense reconnection on the nightside. Strong nightside magnetic reconnection leads to strong  
 170 inward convection of the plasmasheet. The stronger the magnetotail reconnection, the stronger the  
 171 inward convection. Via conservation of the first two adiabatic invariants (Alfvén, 1950), the  
 172 greater the convection, the greater the energization of the radiation belt particles.

173

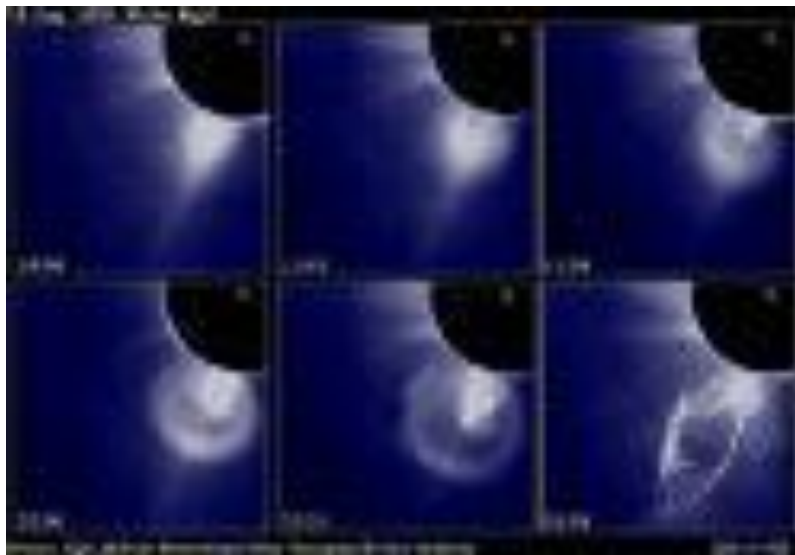
174 As the midnight sector plasmashet is convected inward to lower L, the initially ~100 eV to 1 keV  
175 plasmashet electrons and protons are adiabatically compressed (kinetically energized) so that the  
176 perpendicular (to the ambient magnetic field) energy becomes greater than the parallel energy.  
177 This leads to plasma instabilities, wave growth and wave-particle interactions (Kennel and  
178 Petschek, 1966). The resultant effect is the “diffuse aurora” caused by the precipitation of the ~10  
179 to 100 keV electrons and protons into the upper atmosphere/lower ionosphere. At the same time  
180 double layers are formed just above the ionosphere, giving rise to ~1 to 10 keV “monoenergetic”  
181 electron acceleration and precipitation in the formation of “discrete auroras” (Carlson et al., 1998).

182  
183 *If the IMF southward component is particularly intense, this can lead to a magnetic storm with Dst*  
184 *< -100 nT. The Dst decrease is caused by strong convection of the plasmashet into the inner part*  
185 *of the magnetosphere and the formation of an intensified ring current. This ring current produces*  
186 *a diamagnetic field which causes the reduced field strength at surface of the Earth. This is the*  
187 *magnetic storm main phase.*

188  
189 After the southward field decreases or changes orientation to northward fields, the magnetic storm  
190 recovers. The recovery is associated with a multitude of physical processes associated with the  
191 loss of the energetic ring current particles: charge exchange, Coulomb collisions, wave-particle  
192 interactions and convection out the dayside magnetopause (West et al., 1972; Kozyra et al. 1997,  
193 2006a; Jordanova et al., 1998; Daglis et al. 1999). A typical time for storm recovery is ~10 to 24  
194 h (Burton et al., 1975; Hamilton et al., 1988; Ebihara and Ejiri, 1998; O’Brien and McPherron,  
195 2000; Dasso et al., 2002; Kozyra et al., 2002; Wang et al., 2003; Weygand and McPherron, 2006;  
196 Monreal MacMahon and Llop, 2008).

197  
198 **2.2. Coronal Mass Ejections (CMEs), Interplanetary Coronal Mass Ejections (ICMEs) and**  
199 **Magnetic Storms**

200



201  
 202 Figure 2. A sequence of images showing the emergence of parts of a CME coming from the Sun.  
 203 The time sequence starts at the upper left and ends at the lower right. Taken from Illing and  
 204 Hundhausen (1986).

205  
 206 What are the solar and interplanetary sources of intense IMFs that lead to magnetic reconnection  
 207 at Earth and intense magnetic storms? What we know from space age observations is that these  
 208 magnetic fields come from parts of a CME, a giant blob of plasma and magnetic fields which are  
 209 released from the Sun associated with solar flares and disappearing filaments (Tang et al., 1989).  
 210 Figure 2 shows the emergence of a CME from behind a solar occulting disc. The time sequence  
 211 starts at the upper left, goes to the right and then to the bottom left, and ends at the bottom right.  
 212 The three parts of a CME are best noted in the image on the bottom left. There is a bright outer  
 213 loop most distant from the Sun, followed by a “dark region”, and then closest to the Sun is the  
 214 solar filament.

### 215 216 **2.3. Forecasting Magnetic Storms and Extreme Storms Associated with ICMEs**

217  
 218 We will precede ourselves and state here that for the limited number of cases studied to date, the  
 219 most geoeffective part of the CME is the “dark region”. Interplanetary scientists (Burlaga et al.,  
 220 1981; Choe et al., 1982; Tsurutani and Gonzalez, 1994) have identified this as the low plasma beta  
 221 region called a magnetic cloud (MC), first identified by Burlaga et al.(1981) and Klein and Burlaga  
 222 (1982) in interplanetary space by magnetic field and plasma measurements. When there are



223 southward component magnetic fields within the MC (thought to typically be a giant fluxrope), a  
224 magnetic storm results (Gonzalez and Tsurutani, 1987; Gonzalez et al. 1994; Tsurutani et al.,  
225 1997b; Zhang et al., 2007; Echer et al. 2008a).

226  
227 It should be noted that fast CMEs and intense MC fields are relatively rare. The SOHO LASCO  
228 instrument has observed > 10,000 CMEs but only ~5% have speeds faster than ~700 km/s. Only  
229 very few have speeds > 2,000 km/s and these are coming from coronal regions associated with  
230 Active Regions (ARs) (personal communications with referee, 2019).

231  
232 Interplanetary and magnetospheric scientists have developed the term ICME or interplanetary  
233 CME because it is not currently known (for individual events) how the CME evolves as it  
234 propagates from the Sun to the Earth and beyond. Leamon et al. (2004) in comparing interplanetary  
235 MCs to associated solar active regions found that there was little or no relationship, compelling  
236 the authors to conclude that “MCs are formed during magnetic reconnection and are not simple  
237 eruptions of preexisting coronal structures”. Yurchyshyn et al. (2007) in a similar study found that  
238 “for the majority of interplanetary MCs, the fluxrope axis orientation changed less than 45° going  
239 from the Sun to 1 AU”. Palmerio et al. (2018) found “for the majority of cases, the flux rope tilt  
240 angles rotated several tens of degrees (between the Sun and the Earth) while 35% changed by more  
241 than 90°”. 3D MHD simulations have shown that CMEs can be severely distorted as they interact  
242 with different types of interplanetary structures as they propagate through interplanetary space  
243 (Odstrcil and Pizzo, 1999a,b). The latter authors have shown that the CME distortion is  
244 substantially different when it interacts with the streamer belt (heliospheric plasma sheet/HPS)  
245 than with an HSS. The distortion of the CME can make the ICME unrecognizable at a distance  
246 further away from the Sun.

247  
248 More detailed topics not covered in Palmerio et al. (2018) or in Odstrcil and Pizzo (1999a,b) are  
249 the topics of the fate of the principal features of CMEs as discussed by Illing and Hundhausen  
250 (1986). For example, the bright outer loops are seldomly identified at 1 AU (one rare case was  
251 identified by Tsurutani et al., 1998) and the filaments are typically not found within the ICME at  
252 1 AU. The first filament detection at 1 AU was not reported until 1998 (Burlaga et al., 1998). For  
253 more recent observations of filaments at 1 AU, we direct the reader to Lepri and Zurbuchen (2010).

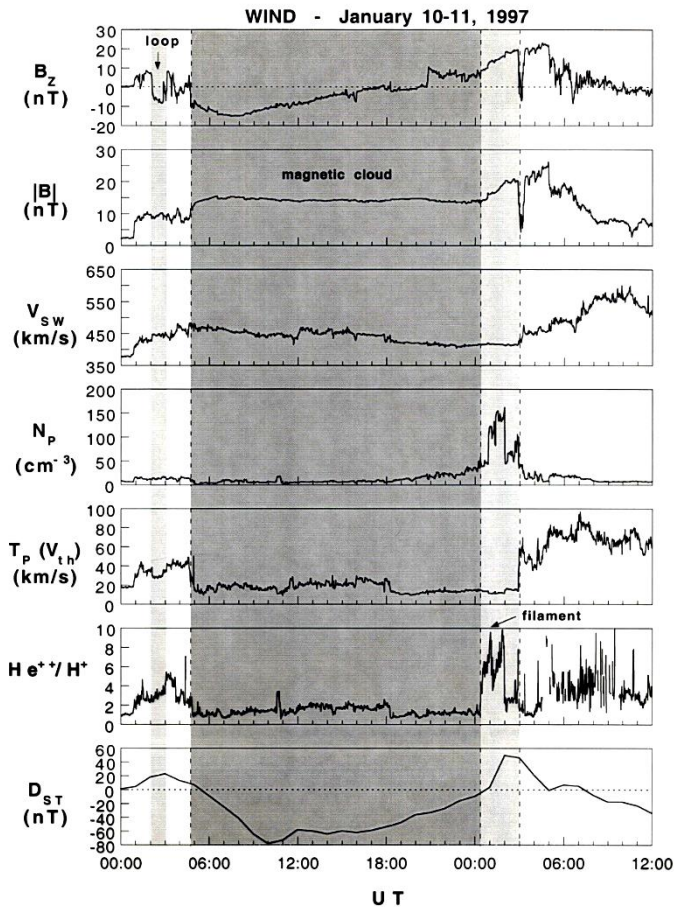
254 Where have the bright outer loops and filaments gone to? Have they simply detached only to  
255 impinge onto the magnetosphere at a later time, or do they go back into the Sun? [Or is it possible](#)  
256 [that many CMEs do not have filaments at their bases?](#) [Remote imaging observations from](#)  
257 [STEREO should be able to answer these questions. New in situ results from](#) Parker Solar Probe,  
258 Solar Orbiter and ACE plus ground-based solar observations could perhaps [help address the](#)  
259 [plasma physics of why typical ICMEs do not have attached filaments.](#)

260

261 It should be remarked that the high density solar filaments could be extremely geoeffective if they  
262 collided with the Earth's magnetosphere (this is covered later in Section 3.2.5). Is it possible for  
263 the MC to rotate so that initially southward magnetic fields become northward components? Can  
264 the MC fields be compressed or expanded by interplanetary interactions? Can magnetic  
265 reconnection be taking place within the ICME between the solar corona and 1 AU as suggested by  
266 Manchester et al. (2006) and Kozyra et al., (2013)? If so, how often does this occur and can it be  
267 predicted? [Modeling and examining the Parker Solar Probe and Solar Orbiter data \(for studies on](#)  
268 [the same ICME\) could help us understand whether the MCs evolve as they propagate through](#)  
269 [interplanetary space.](#)

270

271 Of course the most important goal for [Space Weather](#) is predicting the southward magnetic fields  
272 within the ICME. This extremely difficult task is the holy grail of [Space Weather](#). It is more  
273 important than predicting the time of the release of a CME, its speed and its direction.



274

275

276 Figure 3. An ICME detected at 1 AU just upstream of the Earth.

277

278 Figure 3 shows a rare case of an ICME at 1 AU where all three parts of a CME are detected. The  
 279 MC is indicated by the shaded region in the figure. The outer loop was identified by Tsurutani et  
 280 al. (1998) and the filament by Burlaga et al. (1998).

281

282 From top to bottom are the IMF  $B_z$  component (in geocentric solar magnetospheric/GSM  
 283 coordinates), the field magnitude, the solar wind velocity, density, temperature and the  $\text{He}^{++}/\text{H}^+$   
 284 ratio. The bottom panel gives the ground based Dst index whose amplitude is used as an indicator  
 285 of the occurrence of a magnetic storm. Dst becomes negative when the Earth's magnetosphere is  
 286 filled with storm-time energetic  $\sim 10\text{-}300$  keV electrons and ions (Williams et al., 1990). Dessler  
 287 and Parker (1959) and Sckopke (1966) have shown that the amount of magnetic decrease is linearly  
 288 related to the total kinetic energy of the enhanced radiation belt particles. This is because the

289 energetic particles which comprise the storm-time ring current, through gradient drift of the  
290 charged particles, form a diamagnetic current which decreases the Earth's magnetic field inside  
291 the current. We refer the reader to Sugiura (1964) and Davis and Sugiura (1966) for [further](#)  
292 discussions of the Dst index. The Dst index is a one hr index. More recently a 1 min SYM-H index  
293 (Iyemori, 1990; Wanliss and Showalter, 2006) has been developed. This is more useful for high  
294 time resolution studies. Both indices are produced by the Kyoto Data Center.

295  
296 In this example (top panel of Figure 3) the MC fields start with a strong southward ( $B_z < 0$  nT)  
297 component and then later turns northward. In the bottom panel, the magnetic storm Dst index  
298 becomes negative with very little delay from the southward magnetic fields. The energy transfer  
299 mechanism is magnetic reconnection, as discussed [earlier](#) in Section 2.1. The high density filament  
300 (fourth panel from the top) is present after the MC passage. Values as high as  $\sim 160 \text{ cm}^{-3}$  have been  
301 detected. These values are extreme values ([the](#) nominal solar wind density [is](#)  $\sim 3$  to  $5 \text{ cm}^{-3}$ :  
302 Tsurutani et al., 2018a). The high densities impinging on the magnetosphere in this case caused  
303 [compression of the magnetosphere and](#) the Dst index to reach  $\sim +55$  nT.

304  
305 The stronger the southward component of the MC fields, the more intense the magnetic storm at  
306 the Earth. In extreme cases storms with intensities of  $\text{Dst} < -250$  nT can occur (Tsurutani et al.  
307 1992a; Echer et al. 2008b). An empirical relationship between the speed of the MC at 1 AU and  
308 its magnetic intensity has been shown by Gonzalez et al. (1998). A hypothetical explanation is the  
309 “melon seed model”: squeezing a melon seed will cause it to squirt out, squeezing it harder will  
310 make it come out fast. A larger magnetic field will require greater pressure to release it. However  
311 a [substantial](#) MHD or plasma kinetic model is [needed](#) to explain [the physics of](#) this empirical  
312 relationship [in more detail](#).

313  
314 Because extremely strong MC magnetic fields are needed to produce extreme magnetic storms  
315 like the “Carrington” event (Tsurutani et al., 2003; Lakhina and Tsurutani, 2017), one should focus  
316 on extremely fast events for forecasting purposes. The geoeffective interplanetary dawn-to-dusk  
317 electric field is  $V_{\text{sw}} \times B_{\text{south}}$ . Because Gonzalez et al (1998) have shown that  $|B|$  is empirically  
318 proportional to  $V_{\text{sw}}$ , the dawn-to-dusk interplanetary electric field has a  $V_{\text{sw}}^2$  dependence. The  
319 Carrington ICME took  $\sim 17$  hr 40 min to go from the Sun to Earth (Carrington, 1859), causing the

320 largest magnetic storm in history. The minimum Dst has been estimated to be -1760 nT. However  
321 the August 1972 event was even faster, taking only ~14 h 40 min to go from the Sun to Earth  
322 (Vaisberg and Zastenker 1976; Zastenker et al. 1978). Although the 1972 MC was indeed extreme  
323 in speed and magnetic field intensity, the direction of the magnetic field was northward and thus  
324 there was geomagnetic quiet following the MC impingement onto the magnetosphere (Tsurutani  
325 et al. 1992b). So again, predicting the ICME magnetic field direction is paramount in importance  
326 for Space Weather applications.

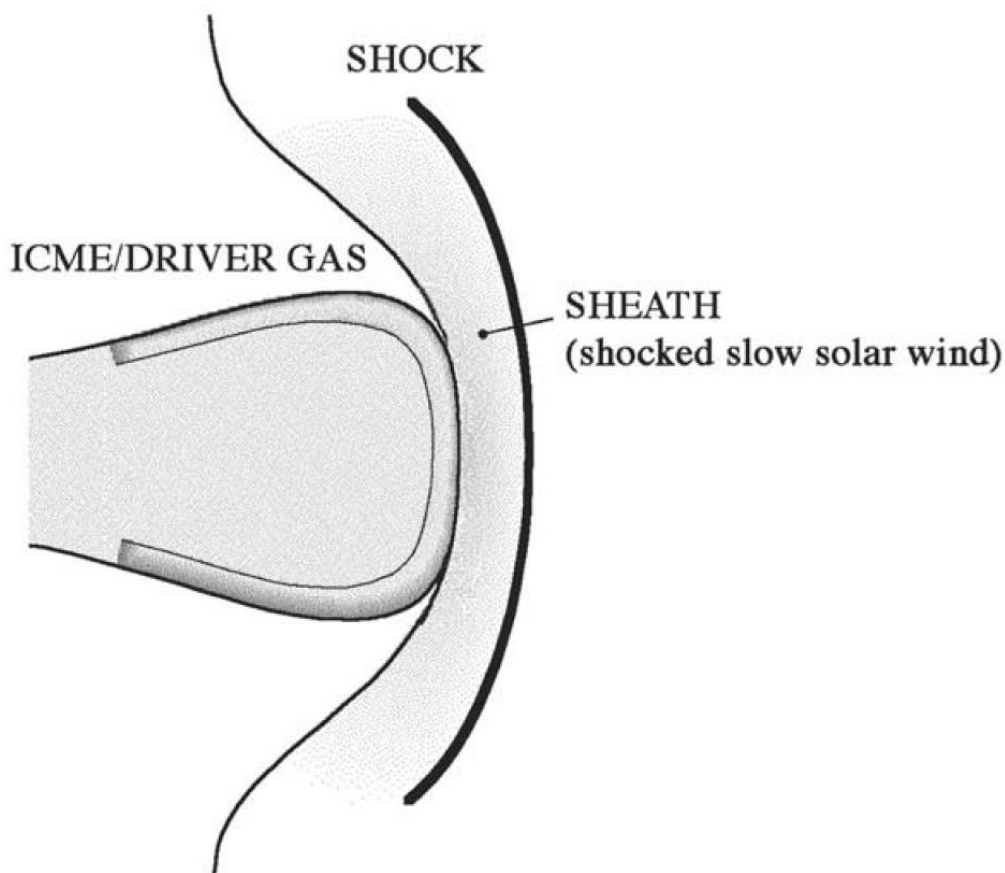
327

328 Modeling ICME propagation in interplanetary space during disturbed AR periods has met only  
329 limited success (Echer et al., 2009; Mostl et al., 2015; Hajra et al., 2019). Sometimes it is difficult  
330 to even identify to which flare or disappearing filament a detected ICME is related (see Tang et  
331 al., 1989; Hajra et al., 2019). Hajra et al. (2019) have noted a halo CME event that did not reach  
332 the Earth. The propagation times from the Sun to 1 AU has often been in error by days (Zhao and  
333 Dryer, 2014). The additional information provided by the Parker Solar Probe and Solar Orbiter  
334 and examination of present ICME propagation codes could help improve the ability to make more  
335 accurate forecasts.

336

#### 337 **2.4. Fast Shocks, Sheaths and Magnetic Storms**

338



339  
 340 Figure 4. A schematic of an interplanetary sheath antisunward of an ICME. In this diagram the  
 341 Sun is on the left (not shown).

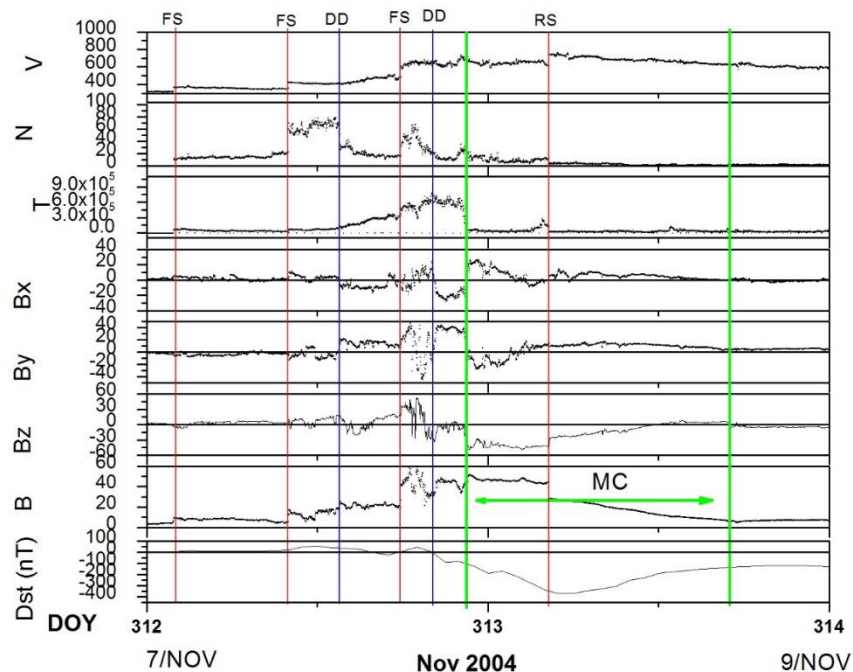
342  
 343 Figure 4 shows a schematic of a shock and sheath upstream of an ICME. “Fast” CMEs/ICMEs can  
 344 create upstream fast forward shocks (Tsurutani et al., 1988). By “fast” it is meant that the  
 345 CME/ICME is moving at a speed higher than the upstream magnetosonic (fast wave mode) speed  
 346 relative to the upstream plasma and by “forward” we mean that the shock is propagating in the  
 347 same direction as the “driver gas” or the CME/ICME, antisunward. When a shock is formed, it  
 348 compresses the upstream plasma and magnetic fields. In this terminology, the upstream direction  
 349 is the direction in which the shock is propagating (antisunward in this case) and the downstream  
 350 direction is towards the Sun (see Kennel et al., 1985 and Tsurutani et al., 2011 for details on  
 351 shocks). The compressed plasma and magnetic fields downstream of the shock is the “sheath”.  
 352 The shock and sheath are not part of the CME/ICME. The origin of this plasma and magnetic  
 353 fields is the slow solar wind altered by shock compression. This is important to [understand](#) if one

354 wishes to predict magnetic storms caused by interplanetary sheath southward magnetic fields. It  
 355 should be noted that “slow” ICMEs have been detected at 1 AU (Tsurutani et al., 1994a). These  
 356 phenomena do not have upstream shocks and sheaths, as expected. However the southward MC  
 357 magnetic fields still cause magnetic storms.

358

359 Kennel et al. (1985) used MHD simulations to show that the plasma densities and magnetic field  
 360 magnitudes downstream of shocks are roughly related to the shock magnetosonic Mach numbers.  
 361 This [theoretical](#) relationship holds up to a Mach number of  $\sim 4$ . For higher Mach numbers MHD  
 362 predicts that the compression will remain at a factor of  $\sim 4$ . Since interplanetary shocks detected  
 363 at 1 AU typically have Mach numbers only of 1 to 3 (Tsurutani and Lin, 1985; Echer et al., 2011;  
 364 Meng et al. 2019a), 1 to 3 are the typical shock magnetic field and density compression [ratios](#)  
 365 detected at 1 AU. One question for future studies is “does the MHD relationships of magnetic  
 366 field magnitude and density jumps hold for extreme shocks?” If not, there will be important  
 367 consequences for extreme [Space Weather](#).

368



369

370 Figure 5. An example of three fast forward shocks pumping up the interplanetary magnetic field  
 371 intensity. Taken from Tsurutani et al. (2008a).

372  
373 Figure 5 shows a complex interplanetary event that was selected by the CAWSES II team to study  
374 in detail. The full information on this event from the Sun to the atmosphere can be found in the  
375 special issue: Large Geomagnetic Storms of Solar Cycle 23  
376 ([https://agupubs.onlinelibrary.wiley.com/doi/toc/10.1002/\(ISSN\)1944-8007.CYCLE231](https://agupubs.onlinelibrary.wiley.com/doi/toc/10.1002/(ISSN)1944-8007.CYCLE231)). What  
377 is important is that this event was associated with a solar active region (AR) and the results are  
378 quite important in terms not only for interplanetary disturbance phenomena but also for  
379 geomagnetic activity at the Earth.

380  
381 From top to bottom in Figure 5 are the solar wind speed, density, and temperature, the IMF B<sub>x</sub>,  
382 B<sub>y</sub> and B<sub>z</sub> components and the magnetic field magnitude in solar magnetospheric (GSM)  
383 coordinates. In this coordinate system,  $\mathbf{x}$  points in the direction of the Sun,  $\mathbf{y}$  is  $(\boldsymbol{\Omega} \times \mathbf{x})/|\boldsymbol{\Omega} \times \mathbf{x}|$   
384 where  $\boldsymbol{\Omega}$  is the Earth's south magnetic pole and  $\mathbf{z}$  completes the right hand system. The magnetic  
385 storm Dst index is given at the bottom. Fast forward shocks are denoted by the three vertical red  
386 lines on 7 November 2004. There are sudden increases in the velocity, density, temperature and  
387 magnetic field magnitude at all three events. The Rankine-Hugoniot relationships have been  
388 applied to the plasma and magnetic field data and the analysis did determine that they are indeed  
389 fast shocks.

390  
391 The point of showing this interplanetary event is to indicate that each shock pumps up the  
392 interplanetary sheath magnetic field by factors of ~2 to 3. The initial magnetic field magnitude  
393 started with a value of ~4 nT and at the peak value after the three shocks, it reached a value of ~60  
394 nT. This final value was higher than the MC magnetic field, which was ~45 nT. Details  
395 concerning the shocks and compressions can be found in the original paper for readers who are  
396 interested. What is important here is how intense interplanetary magnetic fields are created. They  
397 can come from the MCs themselves or the sheaths, as shown here. However, in this case the  
398 southward magnetic fields that caused the magnetic storm came from the MC and not the sheath.

399  
400 In the above example it is believed that three fast forward shocks were associated with three ICMEs  
401 released from the AR. The longitudinal extent of shocks are, however, wider than the MCs, so



402 only one MC was detected in the event. A similar situation was found for the August 1972 event  
403 discussed earlier.

404  
405 It should be noted that a fast reverse wave (here by “reverse” we mean that the wave is propagating  
406 in the solar direction) was detected during the Figure 5 event. It is identified as the red vertical line  
407 on 8 November. In detailed examination of the Rankine-Hugoniot conservation equations, this  
408 wave was found to propagate at a speed below the upstream magnetosonic speed and thus was a  
409 magnetosonic wave and not a shock. This reverse wave caused a decrease in the MC magnetic  
410 field (and the southward component) and thus the start of the recovery phase of the magnetic storm.  
411 The reader should note that fast reverse waves and shocks are also important for geomagnetic  
412 activity. A detailed discussion of shock and discontinuity effects on geomagnetic activity can be  
413 found in Tsurutani et al. (2011).

414

#### 415 **2.4.1. Forecasting ICME sheath magnetic storms**

416

417 Determination of the IMF Bz component in the sheaths will be a difficult task. To do this, more  
418 effort [in understanding](#) the slow solar wind plasma, magnetic fields [and their variations](#) will be  
419 required. To date, there has been little effort expended in this area. This is, however easy for us to  
420 hope for, but in practice is far more difficult to do. Use of data from Solar Probe, Solar Orbiter and  
421 a 1 AU spacecraft such as ACE [could](#) help in these analyses.

422

423 This problem has recently been emphasized by results from Meng et al. (2019a). Meng et al. have  
424 shown that superstorms ( $Dst < -250$  nT) that occurred during the space age (1957 to present) are  
425 mostly driven by sheath fields or a combination of sheath plus a following magnetic cloud (MC).

426

427 Substorms are generated by lower intensity southward magnetic fields with the process of  
428 magnetic reconnection being the same as above. However substorm plasmashet injections only  
429 go in to  $L \sim 4$ , the outer part of the magnetosphere (Soraas et al., 2004). The auroras associated  
430 with substorms appear in the “auroral zone”,  $60^\circ$  to  $70^\circ$  magnetic latitude (MLAT). Magnetic  
431 storms associated with much larger IMF B<sub>south</sub> are detected at subauroral zone latitudes.

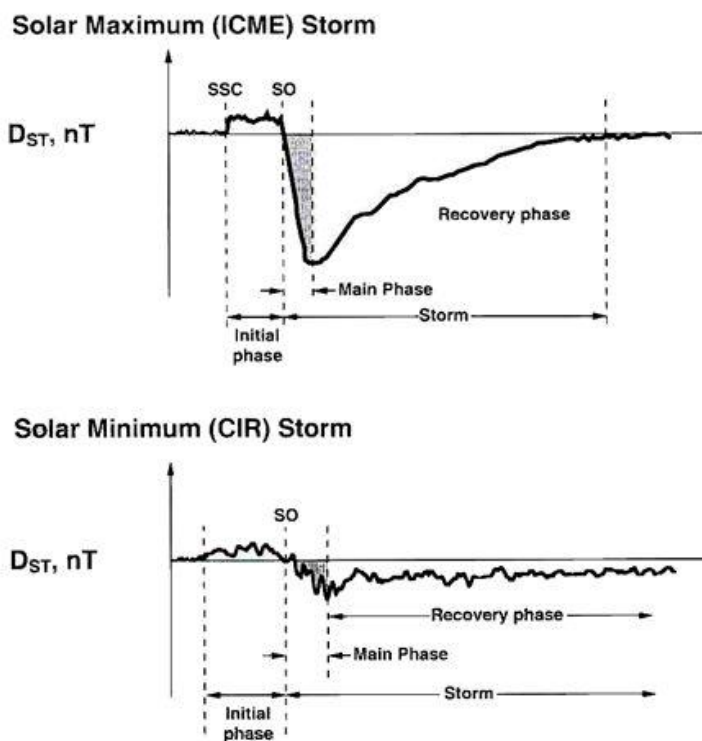
432

433

### 3.0. RESULTS: Declining Phase of the Solar Cycle

434

#### 3.1. Corotating Interaction Region (CIR) Magnetic Storms



435

436 Figure 6. The magnetic Dst profiles of a CIR magnetic storm (bottom) and an ICME magnetic  
 437 storm (top). Taken from Tsurutani (2000).

438

439 During the declining phase of the solar cycle a different type of solar and interplanetary activity  
 440 dominates the [physical](#) cause of magnetic storms, that of Corotating Interaction Regions (CIRs).  
 441 [HSSs emanating from coronal holes \(CHs\) interact with the slow solar wind and form CIRs at their](#)  
 442 [interaction interfaces](#). The magnetic storms caused by CIRs are quite different from storms caused  
 443 by ICMEs and/or their sheaths. Figure 6 shows the difference in profiles of two different types of  
 444 magnetic storms. The profile of a CIR magnetic storm is shown on the bottom and that of a shock  
 445 sheath ahead of an ICME MC magnetic storm on top.

446

447 The ICME MC magnetic storm Dst profile, discussed briefly earlier (see Figure 3), is reasonably  
 448 easy to identify (top panel). There is a sudden, ~tens of second duration positive increase in Dst  
 449 which is caused by the sudden increase in solar wind ram pressure [due to](#) the passage of the sheath

450 high density jump downstream of the shock. This compresses the magnetosphere, creating the  
451 sudden impulse (SI<sup>+</sup>: see Joselyn and Tsurutani, 1990) detected everywhere on the ground (Araki  
452 et al., 2009). Later, in either the sheath or the MC there may be a southward IMF which causes  
453 the magnetic storm. If there is a southward component in the MC, it is usually smoothly varying  
454 in intensity and direction. This leads to a smooth monochromatic storm main phase as seen in the  
455 Dst index (and illustrated in [Figures 3 and 6](#)). The loss of the ring current particles is [the cause of](#)  
456 [the](#) storm recovery phase. The details of storm recovery phase durations and causative mechanisms  
457 will be an interesting topic for magnetospheric scientists to study in the near future. The Arase  
458 mission data will be quite useful for these studies.

459  
460 The bottom panel of Figure 6 shows the typical profile of a CIR magnetic storm. It is quite different  
461 from a [sheath-MC](#) magnetic storm profile. There is no SI<sup>+</sup> associated with the beginning of the  
462 geomagnetic disturbance. This is because CIRs detected at 1 AU typically are not led by fast  
463 forward shocks (Smith and Wolf, 1976; Tsurutani et al. 1995). The positive increase in Dst is  
464 associated with the impact of a high density region near the heliospheric current sheet (HCS)  
465 (Smith et al., 1978; Tsurutani et al. 2006b) called the heliospheric plasmashet ([HPS](#); Winterhalter  
466 et al., 1994) and/or associated with the compressed plasma at the leading edge of the CIR. These  
467 are slow solar wind plasma densities. The most distinguishing feature of the CIR storm main phase  
468 is the lack of smoothness, in sharp contrast to the MC magnetic storm. This irregular Dst storm  
469 main phase is caused by large Bz fluctuations within the CIR.

470  
471 CIR magnetic fields have magnitudes of ~20 to 30 nT and typically do not reach the much higher  
472 intensities that MC fields [typically](#) do. For this reason and also because of the [IMF](#) Bz fluctuations,  
473 CIR magnetic storms [usually](#) have intensities  $Dst \geq -100$  nT ([small or no](#) magnetic storms).  
474 Extreme magnetic storms with  $Dst < -250$  nT caused by CIRs are rare, if they occur at all (none  
475 [were](#) found in the Meng et al. 2019a study). However it is clear that compound events involving  
476 both CIRs, [sheaths ahead of ICMEs](#) and ICMEs could certainly cause extreme magnetic storm  
477 events.

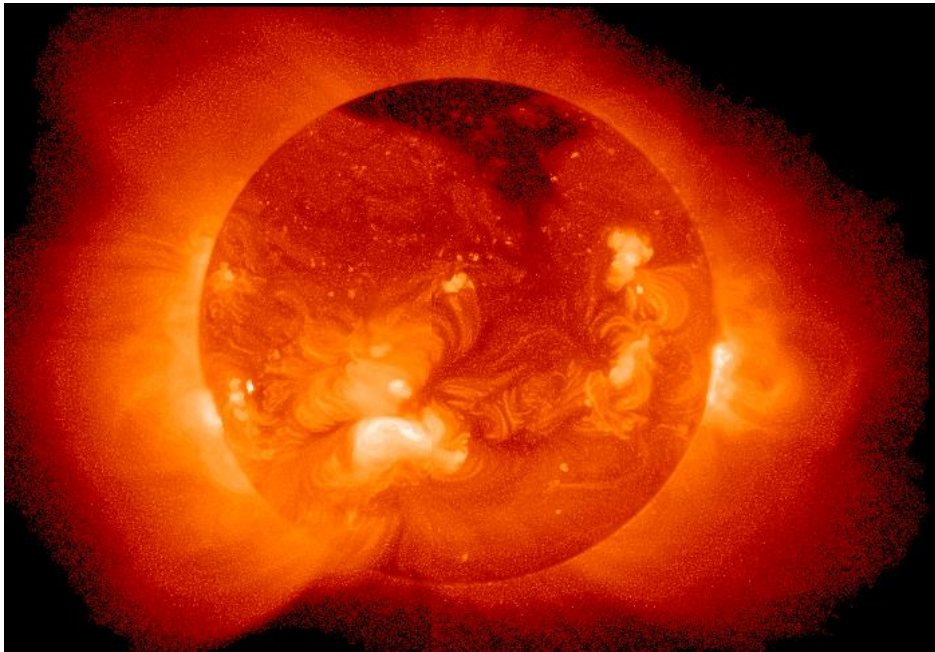
478  
479 CIR related magnetic storms occur most frequently during the declining phase of the solar cycle  
480 and ICME magnetic storms typically occur near the maximum phase of the solar cycle. However,

481 it should be noted that both CIR storms and sheath and/or ICME MC magnetic storms can occur  
482 during any phase of the solar cycle. We have simply ordered things by solar cycle so that it will  
483 be easier to give the reader the general picture of Space Weather.

484

### 485 3.2 Coronal Holes, High Speed Solar Wind Streams and Geomagnetic Activity

#### 486 3.2.1. Coronal holes and high speed solar wind streams



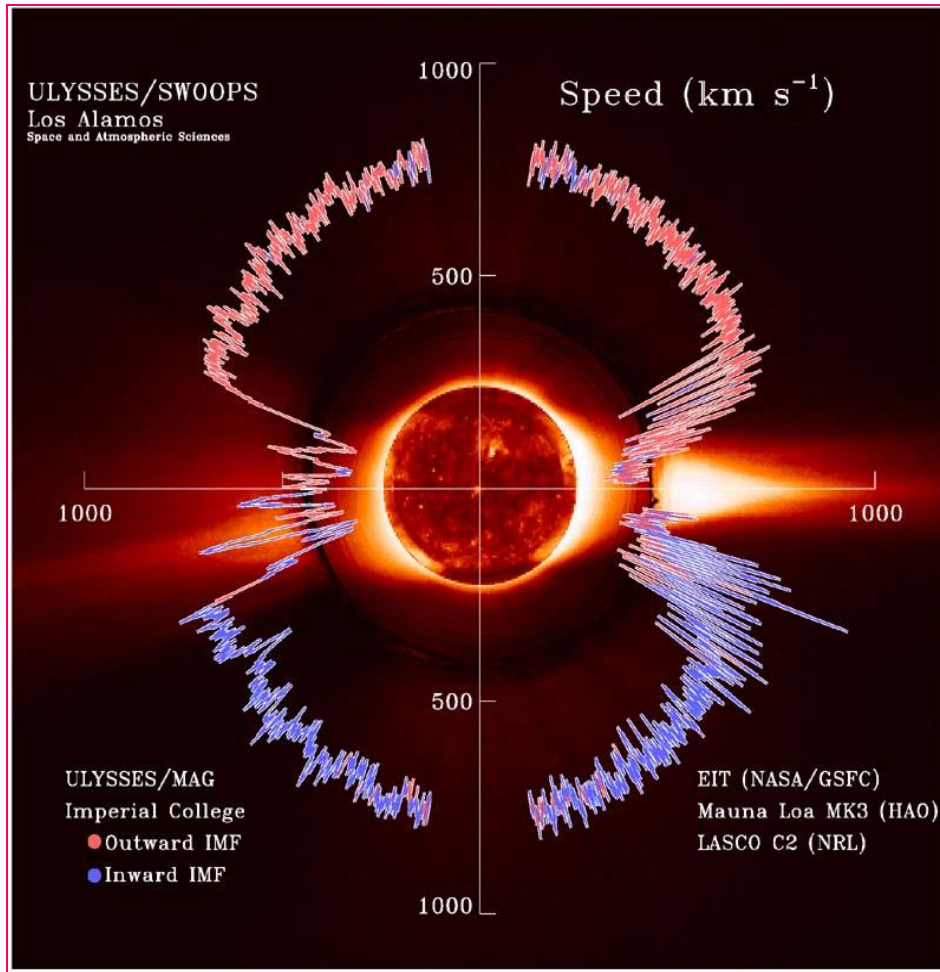
487

488 Figure 7. A large coronal hole (the dark region) near the north pole of the Sun. The figure was  
489 taken by the soft X-ray telescope (STX) onboard the Yohkoh satellite in 1992.

490

491 Figure 7 shows a polar coronal hole at the north pole of the Sun. This image was taken by the soft  
492 x-ray telescope (STX) onboard the Yohkoh satellite  
493 ([http://www.spaceweathercenter.org/swop/Gallery/Solar\\_pics/yohkoh\\_060892.html](http://www.spaceweathercenter.org/swop/Gallery/Solar_pics/yohkoh_060892.html)). The dark  
494 (low temperature) region at the pole is the coronal hole. Large polar coronal holes occur typically  
495 in the declining phase of the solar cycle (Bravo and Otaola, 1989; Bravo and Stewart, 1997; Zhang  
496 et al., 2005).

497



498

499 Figure 8. High speed solar wind streams emanating from coronal holes in the north and south  
500 solar poles. The figure was taken from Phillips et al. (1995) and McComas et al. (2002).

501

502 Figure 8 gives a “dial plot” of the solar wind speed for the first traversal of the Ulysses spacecraft  
503 over the Sun’s poles. The radius from the center of the Sun to the trace indicates the solar wind  
504 speed. The magnetic field polarity is indicated by the color of the trace, red for outward IMFs and  
505 blue for inward IMFs. A SOHO EIT soft x-ray image of the Sun is placed at the center of the figure  
506 and a High Altitude Observatory Mauna Loa coronagraph image [shows the inner corona at that](#)  
507 [time. The outer corona is an image taken by the SOHO C2 coronagraph.](#)

508

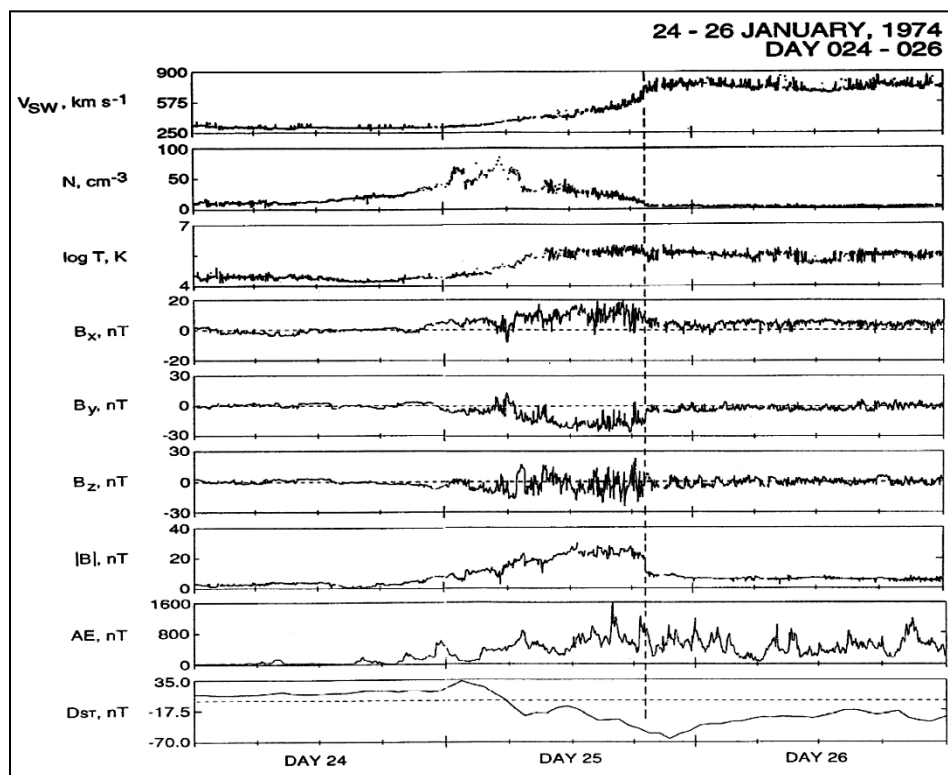
509 Two large polar coronal holes are detected at the Sun, one at the north pole and the other at the  
510 south pole. It is noted that HSSs of  $\sim 750$  to  $800$   $\text{km/s}$  are detected at Ulysses when over the polar  
511 coronal hole regions. When Ulysses was near the solar equatorial region where helmet streamers

512 are present, the solar wind speeds are of the slow solar wind variety,  $V_{sw} \sim 400$  km/s. The reader  
 513 should note that it took years for Ulysses to make this polar orbit while the solar and coronal  
 514 images were taken at one point in time. However this composite figure is useful to illustrate the  
 515 main points about the origins of HSSs.

516

### 517 3.2.2 High speed solar wind streams and the formation of CIRs

518



519

520 Figure 9. A high speed solar wind stream-slow solar wind interaction and the formation of a CIR  
 521 during January 1974. The format is the same as in Figure 4 except that the AE index is given in  
 522 the next to bottom panel. The figure is taken from Tsurutani et al. (2006b).

523

524 Figure 9 shows a HSS-slow speed stream interaction during January 1974. The right portion of the  
 525 top panel on day 26 shows a HSS with speeds of 750-800 km/s at 1 AU. On day 24, the top panel  
 526 left indicates a solar wind speed of  $\sim 300$  km/s, or the slow solar wind. The effects of the stream-  
 527 stream interaction occurs on day 25. This is best seen in the IMF magnitude panel, 7<sup>th</sup> from the  
 528 top. The stream-stream interaction creates intense magnetic fields of  $\sim 25$  nT. The 6<sup>th</sup> from the top  
 529 panel is the IMF  $B_z$  component (in GSM coordinates). The  $B_z$  is highly fluctuating. Magnetic

530 reconnection between the IMF southward components and the magnetopause magnetic fields leads  
531 to the irregularly shaped storm main phase shown in the bottom (Dst) panel.

532

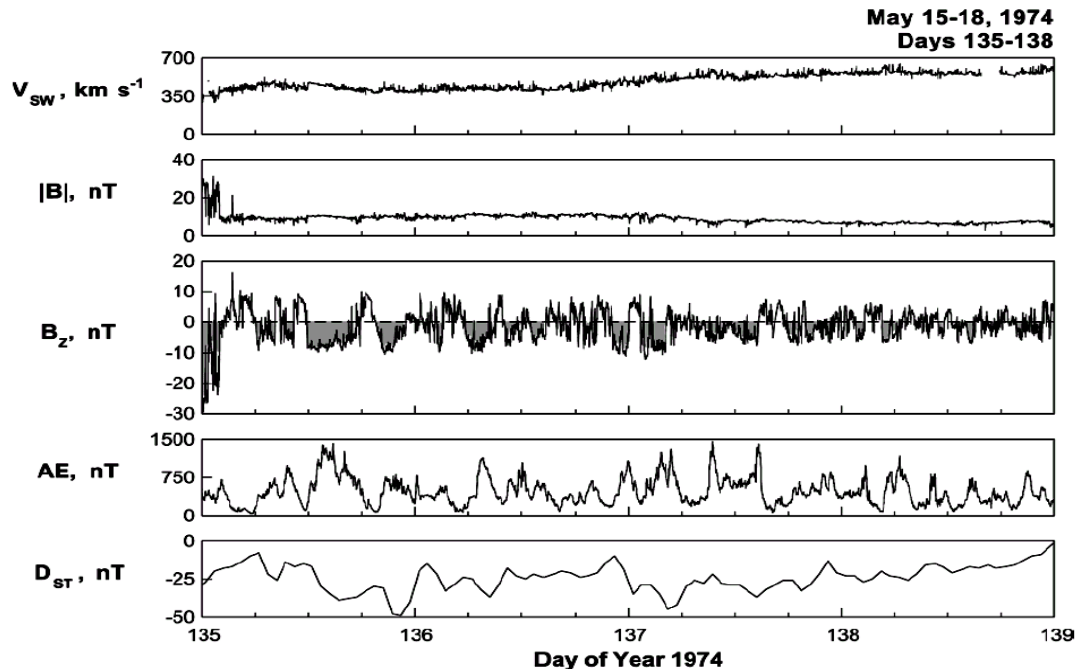
533 To be able to forecast a CIR magnetic storm, one would have to first understand the sources of the  
534 IMF Bz fields. For example are they compressed upstream Alfvén waves (Tsurutani et al. 1995,  
535 2006c)? Or could they be waves generated by the shock interaction with upstream waves in the  
536 slow solar wind? That would be only the first step for forecasting, of course. Then with knowledge  
537 of the properties of the slow speed stream, the details of the wave compression/interaction would  
538 then have to be calculated/modeled.

539

540 Another approach would be to determine if there is an underlying southward component of the  
541 IMF within the CIR. This would most likely be caused by the geometry of the HSS-slow speed  
542 stream interaction and may be predictable from MHD modeling. If this is correct, then the wave  
543 fluctuations can be modeled as being superposed on top of these DC magnetic fields. In (rare)  
544 cases of radial alignment, Solar Probe closest to the Sun could characterize sheath fields. The  
545 evolution of those fields would be detected by Solar Orbiter. Simulation of further evolution could  
546 be applied and predictions of the fields at 1 AU could be tested by ACE data. If there are waves  
547 generated by the shock, then the above scenario would not work as well as expected, or at least  
548 would be more complicated to apply in a useful manner.

549

550 **3.2.3. High speed solar wind streams, Alfvén waves and HILDCAAs**



551  
 552 Figure 10. A high-intensity, long-duration continuous AE activity (HILDCAA) event [during 1974](#).  
 553 Taken from Tsurutani et al. (2006c).

554  
 555 The schematic in Figure 6 showed a long “recovery phase” that trails the CIR magnetic storm main  
 556 phase (see Tsurutani and Gonzalez, 1987). However we now know that the storm wasn’t  
 557 “recovering” as in the case of an MC magnetic storm [recovery](#) but that something else was  
 558 occurring. This “recovery” can last from days to weeks. Thus processes of charge exchange,  
 559 Coulomb collisions, etc. for [ring current](#) particle losses are not tenable to explain such long  
 560 “recoveries”.

561  
 562 Figure 10 shows the interplanetary cause of this extended geomagnetic activity. It occurs primarily  
 563 during HSSs independent of whether a CIR magnetic storm occurred prior to it or not (Tsurutani  
 564 and Gonzalez, 1987; Tsurutani et al., 1995, 2006b; Kozyra et al. 2006b; Turner et al. 2006; Hajra  
 565 et al. 2013, 2014a, 2014b, 2014c, 2017). From top to bottom are the solar wind speed, the IMF  
 566 magnitude, the IMF Bz component (in GSM coordinates) and the auroral electrojet (AE) index.  
 567 The bottom panel is the Dst index.

568



569 The interplanetary data were taken from the IMP-8 spacecraft, an Earth orbiting satellite that was  
570 located upstream of the magnetosphere in the solar wind at this time. The location was inside 40  
571 Re, where an Re is an Earth radius. The magnetic Bz fluctuations have been shown to be Alfvén  
572 waves which are of large nonlinear amplitudes in HSSs (Belcher and Davis, 1971; Tsurutani and  
573 Gonzalez, 1987; Tsurutani et al., 2018b). What is apparent from this figure is that every time the  
574 IMF Bz is negative (southward), there is an AE increase and a Dst decrease. This has been  
575 interpreted as being due to magnetic reconnection between the southward components of the  
576 Alfvén waves and the Earth magnetopause. The AE is enhanced by the same magnetic  
577 reconnection process that occurs during substorms, and a small parcel of plasmashet plasma is  
578 injected into the nightside magnetosphere causing the Dst index to decrease slightly. It is noted  
579 that there are many southward IMF Bz dips in this four day interval of data shown in Figure 10.  
580 There are also many corresponding AE increases and Dst decreases. Thus the interpretation of the  
581 constant/average Dst value of  $\sim -25$  nT for four days is that continuous plasma injection and decay  
582 is occurring. This is clearly not a “recovery phase” where the ring current particles are simply  
583 lost, it only appears as a recovery from the Dst trace. Soraas et al. (2004) have shown that particles  
584 are injected during these events but only to L values of 4 and greater (The L =4 magnetic field line  
585 is the dipole magnetic field that crosses the magnetic equator a distance 4 Earth radii from the  
586 center of the Earth). These are shallow injections as suggested above.

587  
588 These geomagnetic activity events have been named High-Intensity, Long-Duration Continuous  
589 AE events or HILDCAAs (Tsurutani and Gonzalez, 1987). This name is simply a description of  
590 the events without an interpretation. In 2004 when a detailed examination using Polar EUV auroral  
591 imaging was applied, it was found that many phenomena besides simple isolated substorms  
592 occurred (Guarnieri, 2006; Guarnieri et al., 2006). Although substorms occur during HILDCAA  
593 events, there are AE increases (injection events?) that are not well-correlated with substorm onsets  
594 (Tsurutani et al., 2004b). The full extent of HILCAAs is not well understood (see also Souza et  
595 al., 2016, 2018; Mendes et al., 2017). By using IMAGE auroral observations and geomagnetic  
596 indices to identify convection events which are not classical Akasofu (1964) substorms, the fields  
597 and particle data from SWARM, MMS and Arase could be used to characterize the physics  
598 properties of these “convection” events.

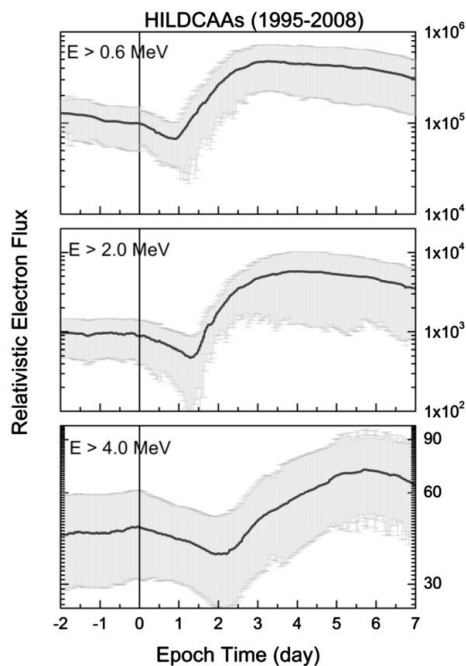
599

600 There is also the question of the origin of the interplanetary Alfvén waves? Do they originate at  
 601 the Sun caused by supergranular circulation, or is that mechanism untenable as argued by Hollweg  
 602 (2006)? Could the waves be generated locally between the Sun and Earth as speculated by Matteini  
 603 et al. (2006, 2007) and Hellinger and Travnicek (2008)? [Parker Solar Probe could identify Alfvén](#)  
 604 [waves within high speed streams and Solar Orbiter \(when radially aligned\) could determine the](#)  
 605 [wave evolution.](#)

606  
 607 The original requirement for identifying a HILCAA event was quite strict. The event had to occur  
 608 outside of a magnetic storm main phase (Dst was required to be  $> -50$  nT: Gonzalez et al. 1994),  
 609 the peak AE intensity had to be greater than 1,000 nT (high-intensity), the event had to last longer  
 610 than 2 days (long-duration), and there could not be any dips in AE less than 200 nT for longer than  
 611 two [hours](#) (continuous). Clearly there are [events](#) with the same interplanetary causes and  
 612 geomagnetic effects as for the strict definition. However the strict definition is useful for further  
 613 studies using different data sets.

614

### 615 3.2.4. HILDCAAs and the Acceleration of Relativistic Magnetospheric Electrons



616  
 617 Figure 11. The relationship between HILDCAAs and relativistic electron acceleration. The figure  
 618 is [taken](#) from Hajra et al. (2015a).

619

620 One of the consequences of HSSs and HILDCAAs is the acceleration of relativistic (~MeV)  
621 electrons. These energetic particles can damage orbiting satellite electronic components (Wrenn,  
622 1995), and thus are known as “killer electrons”. Figure 11 shows the relationship between the onset  
623 of HILCAA events (vertical line) and relativistic electron fluxes. From top to bottom are the  $E >$   
624 0.6 MeV, the  $E >$  2.0 MeV and the  $E >$  4.0 MeV electron fluxes detected by the GOES-8 and  
625 GOES-12 satellites located at  $L = 6.6$ . This figure is a superposed epoch analysis (Chree, 1913)  
626 result of 35 HILDCAA events in solar cycle 23, from 1995 to 2008, which are not preceded by  
627 magnetic storms. This was done to avoid contamination by storm-time particle acceleration (by  
628 intense convection/compression). The zero epoch time (vertical line) corresponds to the  
629 HILDCAA onset time. Here the “strict” definition of HILDCAAs was used to define the onset  
630 times.

631

632 The figure shows that the flux enhancement of  $E >$  0.6 MeV electrons is statistically delayed by  
633 ~1.0 day from the onset of the HILDCAAs. The  $E >$  4.0 MeV electrons are statistically delayed  
634 by ~2.0 days from the HILDCAA onset. It is thus possible that HILCAAs may be used to forecast  
635 relativistic electron flux enhancements in the magnetosphere (see Hajra et al., 2015b; Tsurutani et  
636 al., 2016a; Hajra and Tsurutani, 2018a; Guarnieri et al., 2018). This however has not been done  
637 yet and could be implemented by scientists today.

638

639 The physics for electron acceleration to relativistic (~MeV) energies has been well-developed by  
640 magnetospheric scientists. Two competing acceleration mechanisms have been developed. In one  
641 mechanism, with each injection of plasmashet particles on the nightside magnetosphere, the  
642 anisotropic ~10 to 100 keV electrons generate electromagnetic whistler mode chorus waves  
643 (Tsurutani and Smith, 1974; Meredith et al. 2002) by the loss cone/temperature anisotropy  
644 instability (Brice, 1964; Kennel and Petschek, 1966; Tsurutani et al., 1979; Tsurutani and Lakhina,  
645 1997). The chorus then interacts with the ~100 keV injected electrons to energize them to ~0.6  
646 MeV energies (Inan et al., 1978; Horne and Thorne, 1998; Thorne et al., 2005, 2013; Summers et  
647 al., 2007; Tsurutani et al., 2010; Reeves et al., 2013; Boyd et al., 2014). The lower-frequency part  
648 of the chorus in turn interact with the ~0.6 MeV electrons to accelerate them to ~2.0 MeV energies,  
649 etc. This bootstrapping mechanism has been suggested by several authors (Baker et al., 1979,

650 1998; Li et al., 2005; Turner and Li, 2008; Boyd et al., 2014, 2016; Reeves et al., 2016) and has  
651 been confirmed by Hajra et al. (2015a) during HILDCAA events.

652

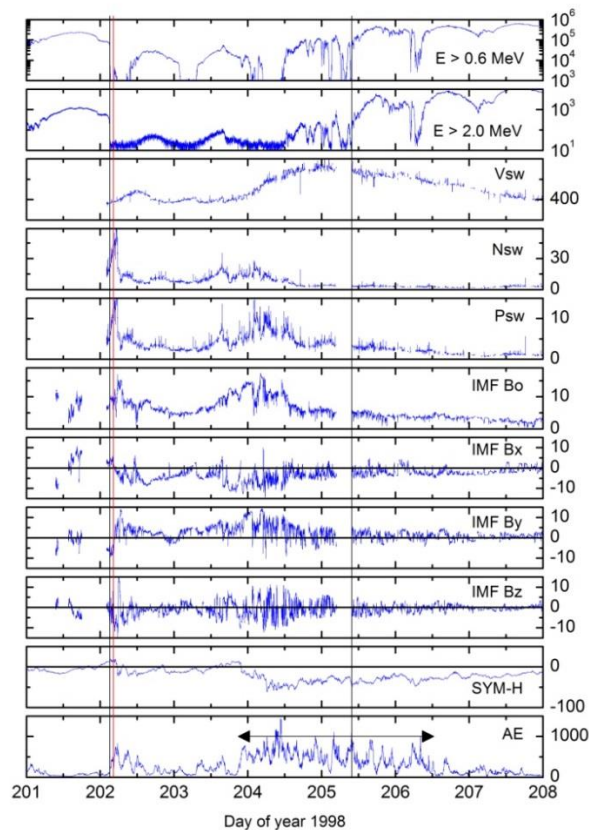
653 An alternative scenario is that relativistic electrons are created through particle radial diffusion  
654 driven by micropulsations (Elkington et al., 1999, 2003; Hudson et al., 1999; Li et al., 2001,  
655 O'Brien et al., 2001; Mann et al., 2004; Miyoshi et al., 2004). However the same general scenario  
656 would hold as for chorus acceleration. The substorms and convection events within HILDCAAs  
657 would be the sources for the micropulsations and the micropulsations would last from days to  
658 weeks in duration. Bootstrapping of energy would still take place.

659

660 A few important questions for researchers to ask are: “How high can the relativistic  
661 magnetospheric electron energy get?”. If there are two HSSs, one from the south pole and another  
662 from the north pole so that Earth’s magnetosphere is bathed in HSSs for years, as happened during  
663 1973-1975 (Sheeley et al., 1976, 1977; Gosling et al. 1976; Tsurutani et al. 1995), will the energies  
664 go above ~10 MeV? What will physically limit the energy range? This answer is important for  
665 keeping Earth-orbiting satellites safe during such events.

666

667 **3.2.5. Solar wind ram pressure pulses and the loss of relativistic electrons**



668  
 669 Figure 12. A relativistic electron decrease (RED) event and later acceleration. Taken from  
 670 Tsurutani et al. (2016b).

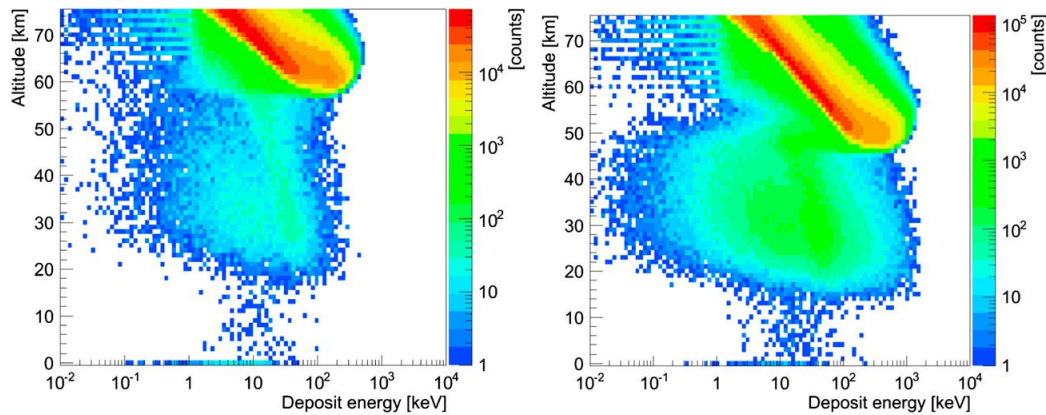
671  
 672 Figure 12 shows a relativistic electron decrease (RED) event [occurring during 1998](#). From top to  
 673 bottom are the  $E > 0.6$  MeV electron fluxes, the  $E > 2.0$  MeV electron fluxes, the solar wind speed,  
 674 density and ram pressure, and the IMF magnitude, Bx, By and Bz component in the GSM  
 675 coordinate system. The bottom two panels are the 1 min SYM-H index (a high time resolution  
 676 Dst index) and the AE index. The relativistic electron measurements were taken at  $L = 6.6$ .

677  
 678 At the beginning of day 202, a vertical black line indicates the onset of a high density HPS [crossing](#)  
 679 [\(Winterhalter et al., 1994\)](#) that is identified in the fourth panel from the top. The HPS is by  
 680 definition located adjacent to the HCS (Smith et al. 1978). The HCS is noted by the reversal in the  
 681 signs of the IMF Bx and By components (seventh and eighth panels from the top). The onset of  
 682 the HPS is followed within one [hour](#) by the vertical red line, the sudden disappearance of the  $E >$   
 683  $0.6$  MeV (first panel) and  $E > 2.0$  MeV (second panel) relativistic electron [fluxes](#). Tsurutani et al.

684 (2016b) has shown that for 8 relativistic electron [flux](#) disappearance events during solar cycle 23  
685 all of the disappearances were associated with HPS impingements onto the magnetosphere.

686  
687 Where have the relativistic electrons gone? There are two primary possibilities. One is that the  
688 energetic electrons have gradient drifted out of the magnetosphere through the dayside  
689 magnetopause, a feature that has been called “magnetopause shadowing” by West et al. (1972).  
690 However a second possible mechanism is electron pitch angle scattering by electromagnetic ion  
691 cyclotron (EMIC) waves. We think that this second possibility is more intriguing and has far more  
692 interesting consequences, if correct. One might ask where the EMIC waves come from and why is  
693 pitch angle scattering particularly important? It has been shown by Remya et al. (2015) that when  
694 the magnetosphere is compressed, both electromagnetic chorus (electron) waves (Thorne et al.,  
695 1974; Tsurutani and Smith, 1974; Meredith et al. 2002) and EMIC (ion) waves (Cornwall, 1965;  
696 Kennel and Petschek, 1966; Olsen and Lee, 1983; Anderson and Hamilton, 1993; Engebretson et  
697 al., 2002; Halford et al. 2010; Usanova, 2012; Saikin, 2016) are generated. The compression of  
698 the magnetosphere causes betatron acceleration of remnant ~10 to 100 keV electrons and protons,  
699 and thus plasma instabilities associated with both particle populations occur. What is particularly  
700 important is that the EMIC waves are coherent (Remya et al., 2015), leading to extremely rapid  
701 pitch angle scattering of ~ 1 MeV electrons by the waves. The scattering rate has been shown to  
702 be three orders of magnitude faster than that with incoherent waves (Tsurutani et al., 2016b).

703  
704 Another possible loss mechanism is associated with possible generation of PC waves by the HPS  
705 impingement followed by radial diffusion of the relativistic electrons. Wygant et al. (1998) and  
706 Halford et al. (2015) have mentioned that larger loss cone sizes at lower L could be a source of  
707 loss to the ionosphere. [Rae et al. \(2018\)](#) has shown that superposition of compressional PC waves  
708 and the conservation of the first two adiabatic invariants could enhance particle losses. However  
709 one should mention that there are not observations of PC wave generation during HPS  
710 impingements and this needs to be tested. It is also uncertain how rapidly the relativistic electrons  
711 would be lost by the above processes. It has been shown that the total loss of L >6.6 relativistic  
712 electrons occurs in ~1 [hour](#) (Tsurutani et al., 2016b).



713  
 714 Figure 13. The GEANT4 code run results for the precipitation of  $E > 0.6$  MeV electrons (left  
 715 panel) and  $E > 2.0$  MeV electrons (right panel). The vertical scale is altitude above the ground and  
 716 the horizontal scale is energy deposition. The color scheme (legend on the right) gives the amount  
 717 of counts. Taken from Tsurutani et al. (2016b).

718  
 719 Why can the loss of relativistic electrons to the atmosphere be important? Figure 13 shows the  
 720 results of the GEometry ANd Tracking 4 (GEANT4) code developed by the European  
 721 Organization for Nuclear Research (Agostinelli et al., 2003) applied to the relativistic electron  
 722 disappearance problem. The GEANT4 code takes into account Rayleigh scattering, Compton  
 723 scattering, photon absorption, gamma ray pair production, multiple scattering, ionization,  
 724 bremsstrahlung for electrons and positrons and annihilation of positrons (positron formation is not  
 725 germane for these “low energy” relativistic particles, but the code includes it anyway). A standard  
 726 atmosphere was used.

727  
 728 Figure 13 shows the GEANT4 Monte Carlo results for the electron shower for  $E > 0.6$  MeV  
 729 electrons on the left and for  $E > 2.0$  MeV electrons on the right. Two important features should be  
 730 noticed. First the bulk of energy deposition (the red areas) descends down to  $\sim 60$  km for the  $E >$   
 731  $0.6$  MeV electron simulation and down to  $\sim 50$  km for the  $E > 2.0$  MeV electron simulation. This  
 732 portion of the energy from the incident electrons is due to direct ionization and particle energy  
 733 cascading. However there is a second region which might be extremely important. That is the  
 734 blue-green area that goes down to  $\sim 20$  km for the  $E > 0.6$  MeV simulation and  $\sim 16$  km for the  $E >$   
 735  $2.0$  MeV simulation. There are also “hits” seen on the ground. This lower altitude energy  
 736 deposition is due to the relativistic electrons interacting with atmospheric atomic and molecular

737 nuclei creating bremsstrahlung X-rays and  $\gamma$ -rays. X-rays and  $\gamma$ -rays have very large mean free  
738 paths and thus can freely propagate through the dense atmosphere without interactions. They  
739 propagate to much lower altitudes where they interact and [continue the energy cascading process](#)  
740 [further](#).

741  
742 The reason why this process may be quite an important [Space Weather](#) topic is that it might relate  
743 to atmospheric weather as well. Wilcox et al. (1973) discovered a correlation between  
744 interplanetary HCS crossings and high atmospheric vorticity winds at 300 mb altitude. Over the  
745 years a number of different explanations for the physics of the trigger has been offered (Tinsley  
746 and Deen, 1991; Lam et al., 2013). Tsurutani et al. (2016b) presented the above relativistic  
747 electron [precipitation](#) scenario (instead of HCS crossings) for the possible triggers of high  
748 atmospheric vorticity winds. Quantitative estimates of potential energy deposition at different  
749 atmospheric altitudes were provided in the original paper.

750  
751 It is noted that the energy deposition should occur in a limited spatial region of the globe (just  
752 inside the auroral zone and a small region of the dayside atmosphere) which is more geoeffective  
753 than either cosmic ray energy or solar flare particle deposition. The fact that it is [relativistic](#)  
754 electron precipitation gives an additional advantage that substantial energy is deposited at quite  
755 low altitudes.

756  
757 Advances to this problem can be made in a number of different ways. Simultaneous ground-  
758 detected EMIC waves,  $\gamma$ -rays and atmospheric heating/[cooling](#) could be sought. Correlation with  
759 such events with solar wind pressure pulses like the HPSs or interplanetary shocks (see Hajra and  
760 Tsurutani, 2018b) would advance our knowledge of the details of such events.

761  
762 Atmospheric heating events known as Sudden Stratospheric Warmings (SSWs) (Scherhag, 1960;  
763 Harada et al., 2010) occur at subauroral latitudes by unknown causes. They are known to be related  
764 to atmospheric wind system changes, perhaps the same phenomenon as the Wilcox et al. (1973)  
765 effect. Atmospheric scientists generally assume that SSWs are created by gravity waves  
766 propagating from lower atmosphere upward, but so far no one-to-one correlated case has been  
767 found. Thus it would be quite interesting to see if [Space Weather](#) can have a major impact on

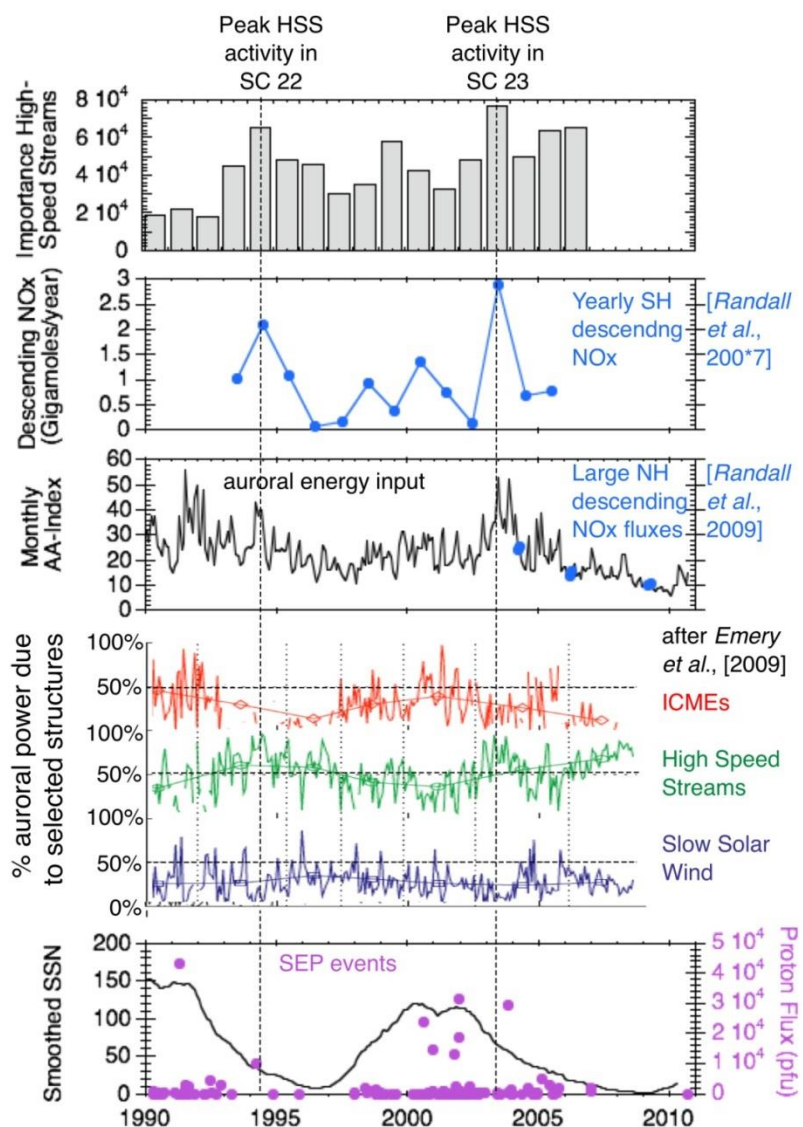


768 atmospheric weather. The connection between these two disciplines **could** be quite interesting for  
 769 the next generation of **Space Weather** scientists.

770

### 771 3.2.6. Energetic particle precipitation and ozone depletion

772



773

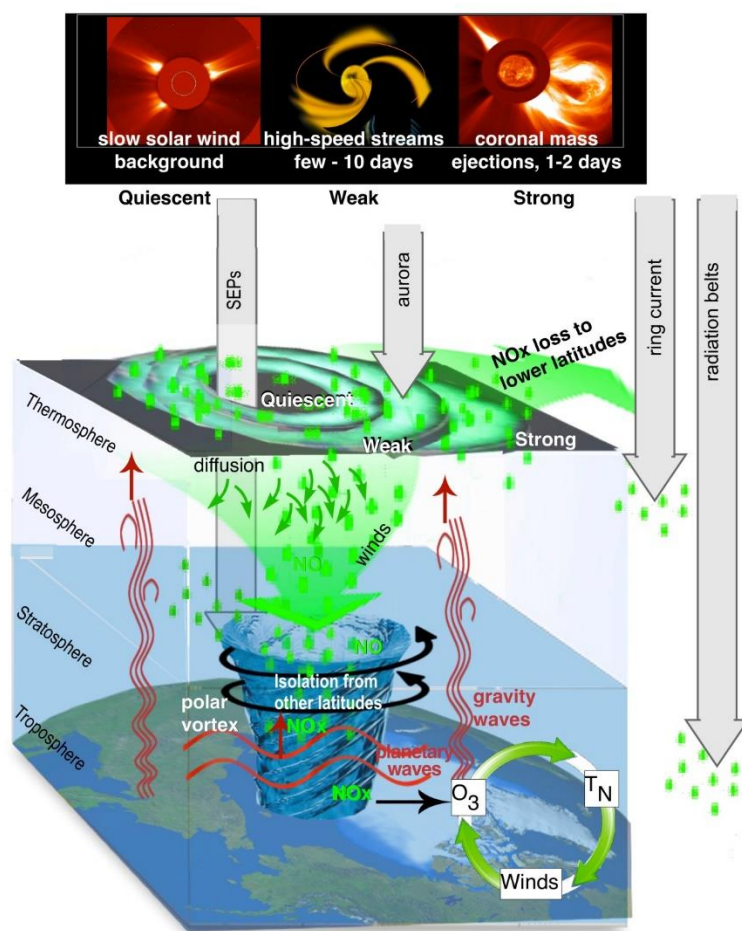
774 Figure 14. The dashed vertical lines show the peaks in solar wind high speed streams during SC  
 775 22 and SC23. These are coincident with the peaks in auroral energy input and the peaks in yearly  
 776 NOx descent. **The authors** thank J.U. Kozyra for **providing** this unpublished figure.

777

778 Figure 14 shows two solar cycles of data, SC22 and SC23. From top to bottom are the  
 779 “importance” of high speed streams, the descending NO<sub>x</sub>, the monthly AA index, the percent  
 780 auroral power due to three types of solar wind phenomena (ICMEs, HSSs and slow solar wind),  
 781 and the bottom panel solid line trace is the sunspot number (SSN). Also shown in the bottom panel  
 782 is the solar energetic particle (SEP) flux.

783  
 784 There are two vertical dashed lines. They correspond to the peaks in HSS activity for SC22 and  
 785 SC23 (top panel), peaks in auroral energy input (third panel from the top), and peaks in the yearly  
 786 descending NO<sub>x</sub> (second panel from the top). It is noted that all three peaks are aligned in time.  
 787 The bottom panel shows that both dashed vertical lines correspond to times in the descending  
 788 phase of the solar cycle.

789



790

791 Figure 15. The scenario for polar cap ozone destruction using the observations shown in Figure  
792 14. The authors thank J.U. Kozyra and her colleagues (personal communication, 2019) for this  
793 unpublished figure.

794  
795 Figure 15 shows the Kozyra et al. (2019) scenario for ozone destruction over the polar cap. The  
796 top of the Figure shows the various types of solar wind (and associated energetic particles) that  
797 can affect atmospheric ozone. The quiet solar wind will lead to quiescence. HSSs lasting a few to  
798 ten days have weak effects and ICMEs (and of course shock acceleration of energy particles) can  
799 have much stronger effects.

800  
801 Energetic particles from different sources will precipitate in different regions of the ionosphere.  
802 The energetic particles associated with interplanetary CME shock acceleration will be deposited  
803 in the polar regions of the both the north and south ionospheres. If the particles are energetic  
804 enough with sufficient gyroradii, they can reach to as low latitudes as  $\sim 50^\circ$  magnetic latitude.  
805 Precipitating substorm/HILDCAA  $\sim 10$ - $100$  keV magnetospheric charged particles will deposit  
806 their energy on closed auroral zone ( $\sim 60^\circ$  to  $70^\circ$ ) magnetic field lines.

807  
808 The energetic particle entering the atmosphere lose a portion of their energy in the dissociation of  
809  $N^2$  into  $N + N$ . The nitrogen atoms will attach to oxygen atoms to form  $NO_x$ . Auroral HILDCAA  
810  $\sim 10$  - $100$  keV energy particles will only penetrate to depths of  $\sim 75$  km above the surface of the  
811 Earth. Solar energetic particles with greater kinetic energies can penetrate lower into the  
812 atmosphere to  $\sim 50$  to  $60$  km. If there is a polar vortex, this vortex can “entrain” the  $NO_x$  molecules  
813 and atmospheric diffusion can bring them down to lower altitudes over months time duration. The  
814  $NO_x$  can act as a catalyst in the destruction of ozone.

815  
816 One interesting consequence of extreme ICME shocks is that one would expect extreme Mach  
817 numbers to lead to both extreme SEP fluences and also extremely high energies. The former will  
818 lead to greater production of  $NO_x$  at the polar regions and the latter to deeper penetration and thus  
819 less loss of  $NO_x$  as they diffuse downward. Alternatively there is a scenario where radiation belt  
820 “killer” relativistic electrons can play an important role. If there are large solar polar coronal holes  
821 like in 1973-1975, HSSs could produce extremely intense and energetic relativistic electrons.

822 Shocks and HPS impingements on the magnetosphere could cause loss of the electrons to the lower  
 823 atmosphere. This magnetospheric energy pumping and dumping may have important  
 824 consequences for NO<sub>x</sub> production. The topic of shock acceleration of energetic particles will be  
 825 discussed in more details in Section 4.1.

826

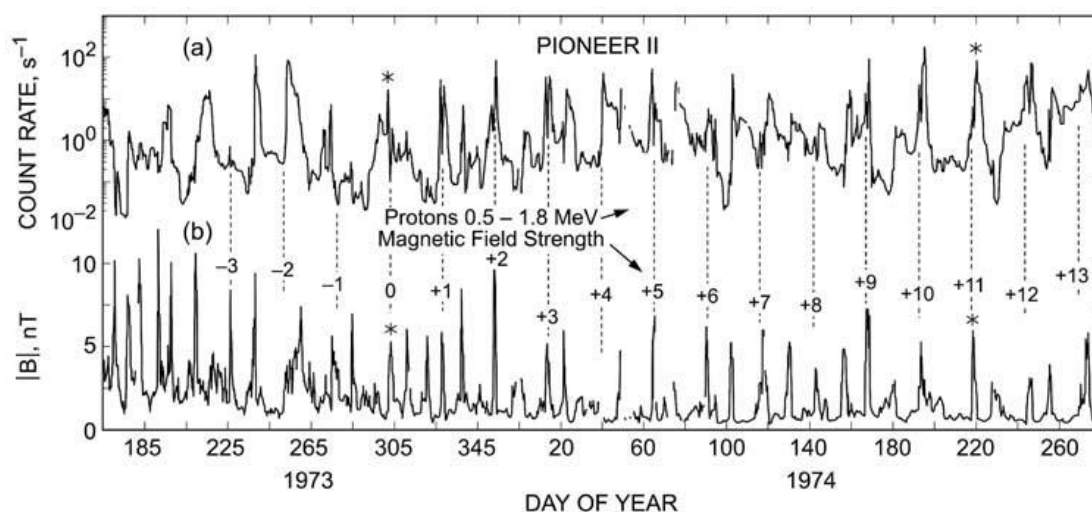
## 827 **4.0. RESULTS: Interplanetary Shocks**

### 828 **4.1. Interplanetary Shocks and Energetic Charged Particle Acceleration**

829

830 Interplanetary shocks have a variety of effects both in interplanetary space and to the Earth's  
 831 magnetosphere. It is important for the reader to note that these Space Weather phenomena can  
 832 occur with or without the occurrence of magnetic storms. Shock and magnetic storm intensities  
 833 are related but only in a loose sense. The physical mechanism for energy transfer for different  
 834 phenomena is different. As one example, interplanetary shock acceleration of energetic charged  
 835 particles (called "solar cosmic rays") are due to an ICME ram energy driving the fast shocks which  
 836 then transfers energy to the charged particles. Solar cosmic ray events can occur with or without  
 837 magnetic storms (Halford et al. 2015, 2016; Mays et al., 2015; Foster et al. 2015). Some of the  
 838 major extreme Space Weather topics will be addressed below.

839



840

841 Figure 16. Energetic ~0.5 to 1.8 MeV protons accelerated by interplanetary fast forward and fast  
 842 reverse shocks. Taken from Tsurutani et al. (1982).

843

844 Acceleration of energetic particles in deep space was discovered by Pioneer 11 energetic particle  
845 scientists (McDonald et al., 1976; Barnes and Simpson, 1976; Pesses et al., 1978, 1979; Van  
846 Hollebeke et al., 1978; Christon and Simpson, 1979). As the Pioneer 11 spacecraft traveled away  
847 from the Sun, it was found that the particle fluences kept increasing, contrary to the concept of  
848 adiabatic deceleration. The interplanetary magnetic field magnitude decreases with increasing  
849 distance from the Sun, so one would expect energetic particle deceleration with distance. Thus it  
850 was clear to scientists that something must be accelerating these particles in the interplanetary  
851 medium. Figure 16 shows one channel of the Pioneer 11 energetic proton count rate, ~0.5 to 1.8  
852 MeV (see Simpson et al., 1974). The bottom panel is the Pioneer 11 magnetic field (Smith et al.,  
853 1975). Some of the peak magnetic fields are numbered, corresponding to a ~25 day recurrence of  
854 these magnetic structures. The magnetic magnitude structures are identified as well-developed  
855 CIRs (see Smith and Wolfe, 1976), bounded by fast forward and fast reverse shocks.

856  
857 Tsurutani et al. (1982) identified the shocks and showed statistically that both forward and reverse  
858 shocks were related to proton peak count rates. One of the results, which still remains to be solved,  
859 is that the proton peaks were generally higher at the reverse shocks. What is the mechanism for  
860 greater particle acceleration at fast reverse shocks? This has received little attention and should be  
861 addressed in the future.

862  
863 Reames (1999) has argued that fast forward shocks upstream (anti-solarward) of ICMEs are the  
864 most important [phenomenon for the acceleration of](#) “solar flare” particle events. Particle  
865 acceleration occurs throughout interplanetary space from near the Sun (where the shocks first  
866 form) to 1 AU and beyond as the shocks propagate through the heliosphere. Studies of this  
867 acceleration as a function of longitudinal distance away from magnetic connection to the flare site  
868 (this gives the variations in the shock normal angle and thus dominant mechanism for  
869 acceleration—see Lee (2017) and references therein) have been done by Lario (2012). The  
870 features of the energetic particles in space have different characteristics depending on these  
871 distances and the portion [and characteristics](#) of the shock that the particles are being accelerated  
872 from.

873

874 Forecasting the solar flare/interplanetary shock features such as the fluence, energy, spectra and  
875 composition will require knowledge of the upstream seed population, upstream (and downstream)  
876 waves, and shock properties such as the magnetosonic Mach number and shock normal angle.  
877 This is a very difficult task since knowledge of the entire slow solar wind plasma from the Sun to  
878 1 AU will be required for accurate forecasting. But again, the Parker Solar Probe and Solar Orbiter  
879 may help in developing two points of measurements for modeling of specific events.

880  
881 A more fundamental problem is why [measured](#) interplanetary fast forward shock Mach numbers  
882 [at 1 AU are](#) so low? As previously mentioned, Tsurutani and Lin (1985) from ISEE-3  
883 measurements have found that at 1 AU, the measured magnetosonic Mach numbers were typically  
884 only 1 to 3. Tsurutani et al (2014) have identified a shock with Mach number  $\sim 9$  and Riley et al.  
885 (2016) has identified an event with magnetosonic Mach number  $\sim 28$ . The latter event was  
886 associated with the SOHO 2012 extreme ICME which did not impact the Earth's magnetosphere.  
887 The above are extreme events and little or no events have been detected with intermediate values.  
888 [A study that is needed is to determine shock Mach numbers at different distances from the Sun.](#)  
889 [These will give clues as to why 1 AU shock Mach numbers are so low. Is the acceleration of](#)  
890 [energetic particles causing the dissipation of shock energy as they propagate from the Sun to 1](#)  
891 [AU? Data from Parker Solar Probe, Solar Orbiter and ACE could be useful in this regard.](#)

892  
893 [In a related issue, the use of STEREO imaging and MHD modeling could be useful to determine](#)  
894 [the mass loading of ICME sheaths in causing the deceleration of the ICMEs. This deceleration](#)  
895 [will also lower the Mach number of the shocks.](#)

896  
897 **4.2. Extreme Interplanetary Shocks and Extreme Interplanetary Energetic Particle**  
898 **Acceleration**

899  
900 Tsurutani and Lakhina (2014) have shown from simple calculations that [for CMEs have extreme](#)  
901 [speeds of 3,000 km/s \(Yashiro et al., 2004; Gopalswamy, 2011\), shock Mach numbers of  \$\sim 45\$  are](#)  
902 [possible. These Mach numbers are getting close to \[expected\]\(#\) supernova shock \[values\]\(#\).](#) Why haven't  
903 such strong shocks been observed at 1 AU? If such events are possible, what would the energetic  
904 particle fluences be? Experts on shock particle acceleration will hopefully answer this complex

905 question. It is well known that such solar flare particles enter the polar regions of the Earth's  
906 atmosphere and cause radio blackouts. Will extreme solar flare particle fluence precipitation cause  
907 different ionospheric effects other than those known today? This latter question might be addressed  
908 by ionospheric modelers.

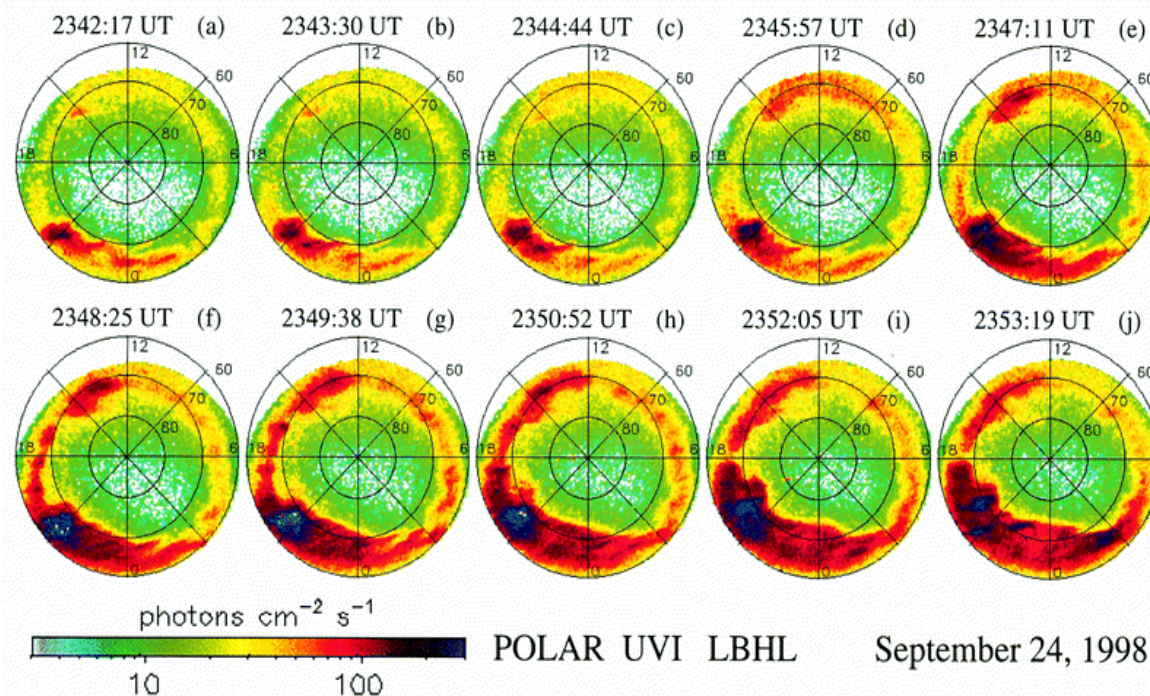
909  
910 It should be noted that although Space Weather is a chain of events/phenomena going from the  
911 Sun to interplanetary space to the magnetosphere, ionosphere and atmosphere, there is often not a  
912 direct link between different facets of Space Weather. Each feature of Space Weather should be  
913 examined separately and it should not be assumed that an extreme flare will cause extreme  
914 cascading Space Weather phenomena. We use solar flare particles as an example for the reader.  
915 The largest solar flare particle event in the space age occurred in August 1972 (Dryer et al., 1976  
916 and references therein). However there was no magnetic storm caused by the MC impact onto the  
917 Earth's magnetosphere (the MC field was directed almost entirely northward, leading to  
918 geomagnetic quiet: Tsurutani et al. 1992b). On the other hand, the largest magnetic storm on  
919 record is the "Carrington" storm. The storm intensity will be discussed further in Section 7.0.  
920 There is little or no evidence of large solar flare particle fluences in Greenland ice core data from  
921 that event (Wolff et al., 2012; Schrijver et al., 2012). Usoskin and Kovfaltsov (2012) examining  
922 historical proxy data ( $^{14}\text{C}$  and  $^{10}\text{Be}$ ) also find a lack of any signature associated with the Carrington  
923 flare. Although this is an extreme example, it is useful to mention it to illustrate the point: **different**  
924 **facets of Space Weather may have only loose correlations with other facets.**

925  
926 An area that has received a lot of attention lately is ancient solar flares. Miyake et al. (2012)  
927 discovered an anomalous 12% rapid increase in  $^{14}\text{C}$  content from 774 to 775 AD in Japanese cedar  
928 tree rings. Usoskin et al. (2013) have argued that such an extreme radiation event could be  
929 associated with an extreme solar energetic particle event (or a sequence of events). The latter  
930 authors estimated that the fluence of  $> 30$  MeV particles was  $\sim 4.5 \times 10^{10} \text{ cm}^{-2}$ . Could such an  
931 extreme particle event be associated with an extremely strong interplanetary shock or **instead** series  
932 of **strong** shocks? Space Weather scientists are currently working on this problem.

933

### 934 **4.3. Interplanetary shocks, dayside aurora and nightside substorms**

935



936  
 937 Figure 17. Interplanetary shocks cause dayside auroras and trigger nightside substorms. [The](#)  
 938 [images show the](#) northern polar views of polar cap and auroral zones taken in UV wavelengths.  
 939 [Local noon is at the top in each image.](#) The Figure is taken from Zhou and Tsurutani (2001).

940  
 941 Interplanetary shocks can trigger the precipitation of energetic ~10 to 100 keV electrons into the  
 942 auroral ionosphere (Halford et al. 2015). In fact, low energy ( $E < 10$  keV) electron precipitation  
 943 can occur as well. Figure 17 shows interplanetary shock impingement auroral UV effects for an  
 944 event on September 23, 1998. Each image has the north pole at the center and  $60^\circ$  magnetic  
 945 latitude (MLAT) shown at the outer edge. Noon is at the top and dawn is at the right. The cadence  
 946 between images is ~1min 13 s. From ACE measurements and propagation calculations it is known  
 947 that the fast forward shock arrived the magnetosphere between the images c), 2344:44 UT and d),  
 948 2345:47 UT. What is apparent in panel d) is the sudden appearance of aurora on the dayside (Zhou  
 949 and Tsurutani et al., 1999). From further analyses of these shock auroral events, Zhou et al. (2003)  
 950 [have](#) shown that magnetospheric compression of preexisting ~10 to 100 keV electrons and protons  
 951 will generate both electromagnetic electron and proton plasma waves and diffuse auroras (as  
 952 discussed previously). Also noted were the generation of field-aligned dayside currents.  
 953 Compression of the magnetosphere will generate Alfvén waves (Haerendel, 1994) which will



954 propagate along the magnetic [field](#) lines down to the ionosphere. Wave damping could provide  
955 substantial ionospheric heating.

956  
957 The mechanism for energy transfer from the solar wind to the magnetosphere is the absorption of  
958 the solar wind ram energy. Dayside auroras occur with shock impingement irrespective of the  
959 interplanetary magnetic field Bz direction. Another possible mechanism for the dayside aurora  
960 not mentioned above are double layers above the ionosphere (Carlson et al., 1998) with the  
961 acceleration of ~1 to 10 keV electrons and the formation of discrete dayside auroras. What is the  
962 relative importance of these three different auroral energy mechanisms? This would be an  
963 excellent topic for the SWARM and Arase satellite missions. Coordinated ground measurements  
964 would be useful.

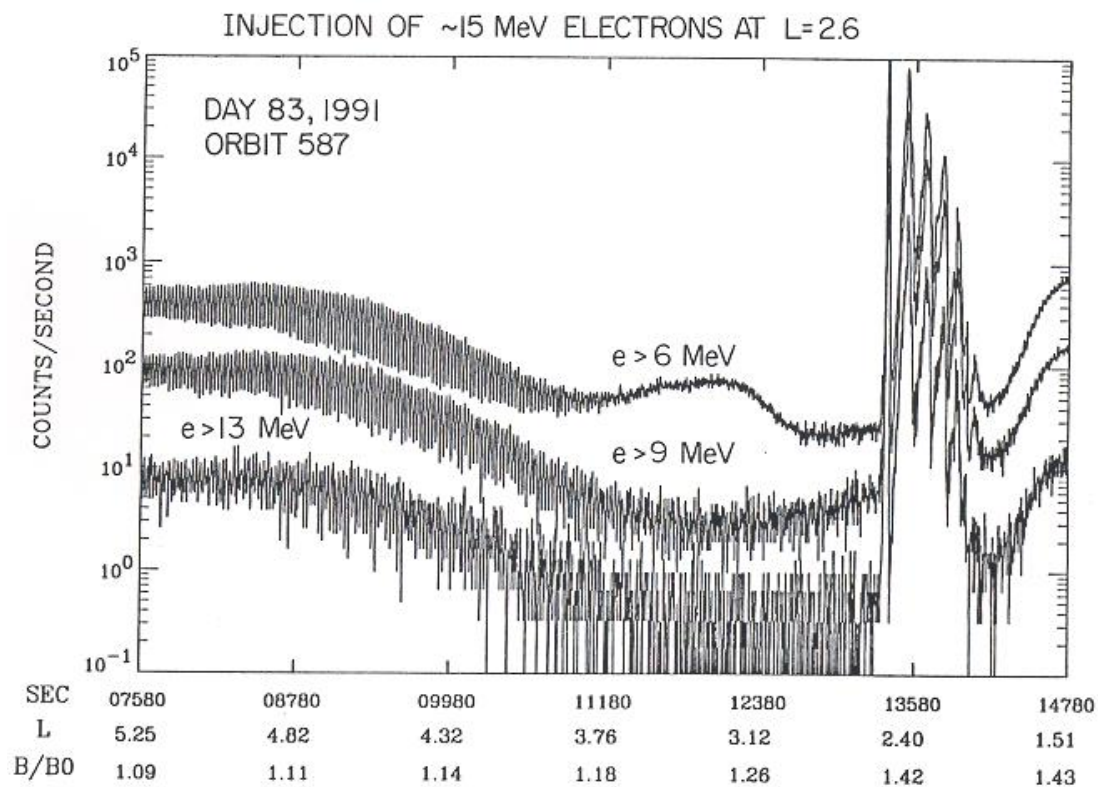
965  
966 Returning back to Figure 17 panel e) 2347:11UT, there is a substorm intensification centered at  
967 ~2100 magnetic local time (MLT). The substorm further intensification and expansion can be  
968 noted in the sequence of images. Interplanetary shock triggering of substorms has been known to  
969 occur before the advent of imaging polar orbiting spacecraft (Heppner, 1955; Akasofu and Chao,  
970 1980). The AE index had been used to identify these events.

971  
972 [An important fundamental question for substorm physics that has existed for a long time, is](#) where  
973 in the tail/magnetosphere does the substorm get initiated and by what physical mechanism? Is it  
974 reconnection or plasma instabilities (Akasofu, 1972; Hones, 1979; Lui et al., 1991; Lui, 1996;  
975 Baker et al., 1996; Lakhina, 2000)? Where does the energy come from, recent [percursor](#) solar  
976 wind inputs as suggested by Zhou and Tsurutani (1999), or stored tail energy or even possibly  
977 solar wind ram energy (see Hajra and Tsurutani, 2018b)? The rapid response of the magnetosphere  
978 to the shock should limit the downstream location of the substorm initiation point. It should be  
979 noted that there are probably several different mechanisms for causing substorms. Although this  
980 is only the shock triggering case, knowledge of this may help understand other cases, [if they are](#)  
981 [indeed different](#). The MMS mission will be ideally suited for addressing this question in the tail  
982 phase of the mission.

983

984 **4.4. Interplanetary shocks and the formation of new radiation belts**

985



986

987 Figure 18. Shock creation of a new [relativistic electron](#) radiation belt in the magnetosphere. [The](#)  
 988 [three energy channel plots](#) show an abrupt increase in flux at the same time. [Recurrence of the flux](#)  
 989 [with decreasing amplitude occurs at least 4 more times](#). Figure taken from Blake et al. (1992).

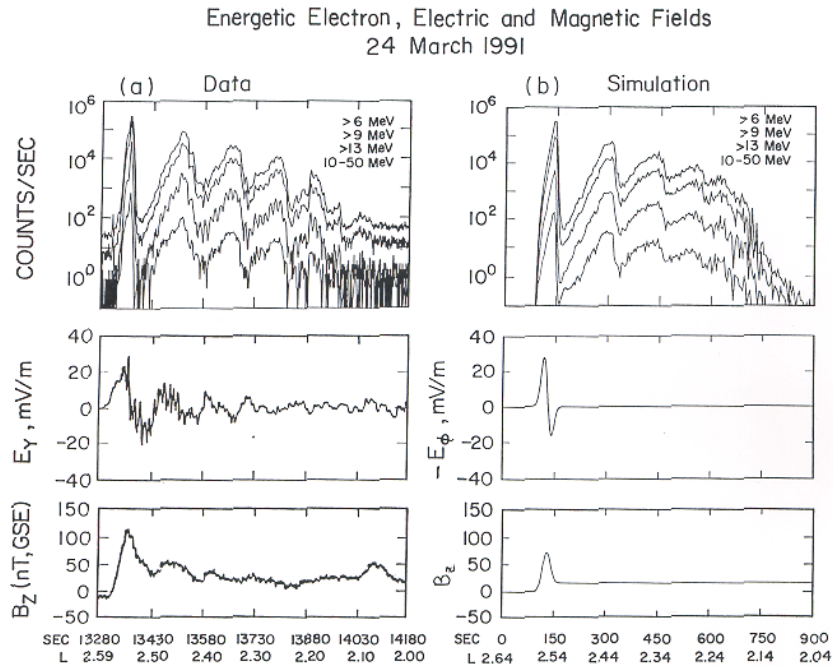
990

991 Figure 18 shows evidence of a new “radiation belt” triggered by a strong interplanetary shock. The  
 992 Figure shows three traces,  $E > 6$  MeV,  $> 9$  MeV and  $> 13$  MeV fluences. At the time of the strong  
 993 [and sudden](#) increase in all energy fluxes, the spacecraft was at  $L = 2.6$ . [This is time-coincident](#)  
 994 [with the shock impingement upon the magnetosphere \(not shown\)](#). With increasing time, a second,  
 995 then third, etc., [electron flux](#) pulse appear. These are “drift echoes” where the energetic electron  
 996 [“cloud” have gradient drifted](#) around the magnetosphere to return to the [satellite](#) location [once](#)  
 997 [again](#).

998

999 **4.4.1. What is the mechanism to create this new radiation belt?**

1000



1001  
1002 Figure 19. An expanded version of the relativistic electron pulse and measured magnetospheric  
1003 electric field and magnetic field  $B_z$  on the left and simulation results on the right. Taken from Li  
1004 et al. (1993).

1005  
1006 The left hand column of Figure 19 shows an expanded version of Figure 16 on the top with the  
1007 addition of the  $\sim 10$  to 50 MeV count rate channel included. Next is the d.c. electric field in the Y  
1008 direction, and magnetospheric  $B_z$  on the bottom. The right hand column bottom shows a magnetic  
1009 pulse input into the system. This generates a time varying azimuthal electric field (right middle)  
1010 and the relativistic electron flux at the top right.

1011  
1012 Using the input of a single magnetospheric magnetic pulse into the magnetosphere, Li et al. (1993)  
1013 simulated the acceleration and injection of  $E > 40$  MeV electrons. What is interesting is that the  
1014 origin of the electrons was  $L > 6$  with energies of only a few MeV. The reader should read Li et  
1015 al. (1993) for more details concerning the simulation and results. Related works on acceleration of  
1016 magnetospheric electrons by shock impact on the magnetosphere can be found in Wygant et al.  
1017 (1994), Kellerman and Shprits, 2012; Kellerman et al., 2014; Foster et al. (2015).

1018

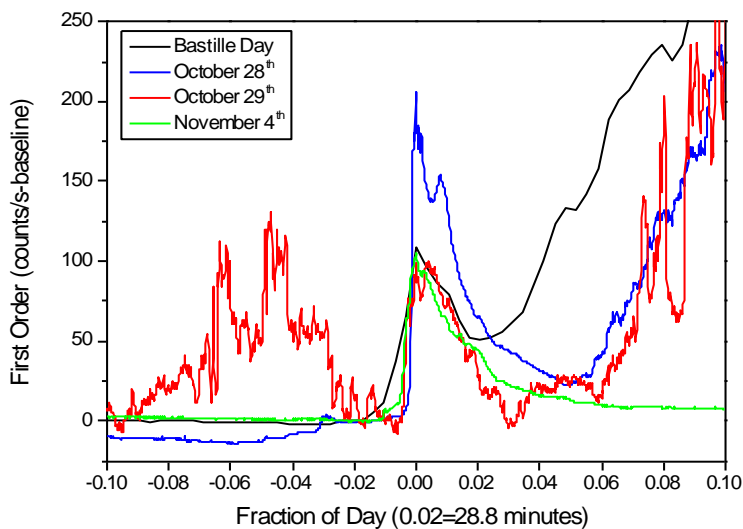
1019 How strong was the interplanetary shock? **There** were not any spacecraft upstream of the Earth at  
 1020 the time of the event, **so no measurements of shock strength can be made**. However Araki (2014)  
 1021 has noted that this shock caused a  $SI^+$  of magnitude 202 nT. This is the second largest  $SI^+$  in  
 1022 recorded history. In Tsurutani and Lakhina (2014) with the assumption of a 3,000 km/s CME and  
 1023 only a 10% deceleration from the Sun to 1 AU, they estimated a maximum  $SI^+$  of 234 nT under  
 1024 normal conditions. Could this 1991 shock **strength** have been close to the  $M = 45$  estimate  
 1025 mentioned earlier? **One** cannot really tell **for sure** because the shock **Mach** number strongly  
 1026 depends on the upstream plasma conditions, which can only be estimated **in this case**.

1027  
 1028 Tsurutani and Lakhina (2014) estimated a dB/dt six times larger than the one used in the Li et al.  
 1029 (1993) modeling. What would a maximum dB/dt cause in a new radiation belt formation? **How**  
 1030 **much greater could the relativistic electron energy and flux become?**

1031

## 1032 5.0. RESULTS: Solar Flares and Ionospheric Total Electron Content

1033



1034  
 1035 Figure 20. The largest solar EUV flare in recorded history, October 28, 2003. Taken from  
 1036 Tsurutani et al. (2005b).

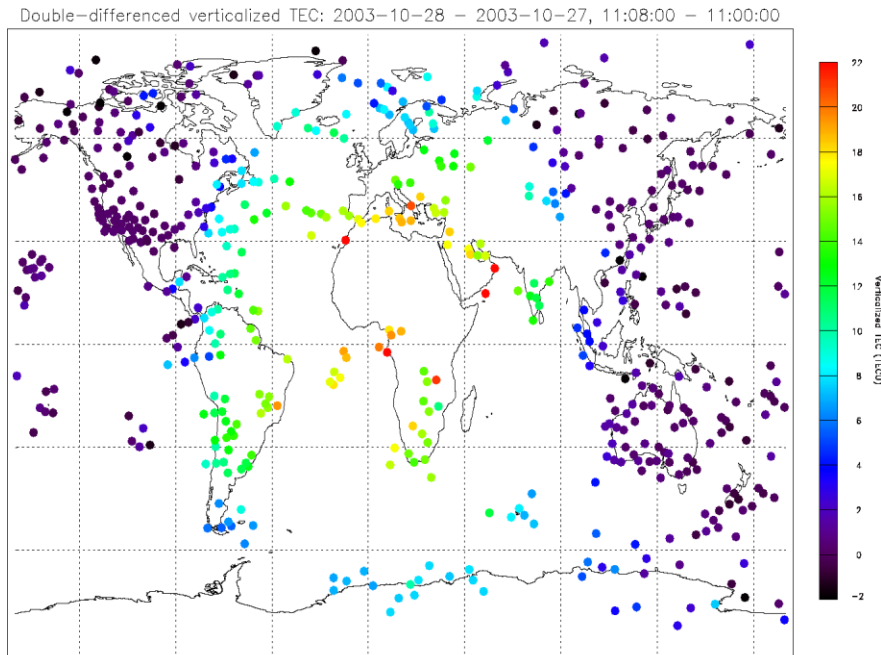
1037

1038 Figure 20 shows four well-known solar X-ray flare events taken in a narrow band 26-34 nm EUV  
1039 spectrum. The four flare events are the Bastille day (July 14, 2000) flare and three “Halloween”  
1040 flares occurring on October 28, 29 and November 4, 2003. The narrow band EUV spectrum is  
1041 shown because some of the flare X-ray and EUV fluxes were so intense that most spacecraft  
1042 detectors became saturated (all except the SOHO SEM narrowband EUV detector). The X-ray  
1043 flare intensities could only be estimated from fitting techniques for the saturated data. Here we  
1044 use the narrow band channel of the SOHO SEM detector where the four above mentioned flares  
1045 were not saturated. The four flare count rate profiles were aligned so that they start at time zero.  
1046 What is particularly remarkable is that the October 28, 2003 flare has the highest EUV peak  
1047 intensity of all four events and was greater by a factor of ~2. This is the most intense EUV solar  
1048 flare in recorded history.

1049  
1050 After each flare reached a peak intensity and then decreased in count rate, there was often a  
1051 following increase in count rate. This is particularly notable in the Bastille day (black trace) flare.  
1052 This increase is contamination due to delayed energetic electrons propagating through space along  
1053 interplanetary magnetic field lines reaching the spacecraft later in time. The November 4 flare  
1054 (green) did not have such contamination because it was a limb flare and presumably (magnetic)  
1055 connection from the flare site to the spacecraft did not occur.

1056  
1057 NOAA personnel have estimated the November 4 flare had an intensity of ~X28. This event  
1058 saturated the detector so this is a conservative estimate. Thomson et al. (2004) using a different  
1059 technique estimated a value of X45 for this event. NOAA has estimated that the October 28 flare  
1060 as ~X17. However in EUV fluxes, the October 28 flare was the most intense by far.

1061



1062

1063 Figure 21. The global TEC during the October 28, 2003 solar flare. The scale is given on the right.

1064 The figure is taken from Tsurutani et al. (2005b).

1065

1066 Figure 21 shows the global total electron content (TEC) in the ionosphere after the October 28,

1067 2003 solar flare. The map has been adjusted so Africa, the subsolar point, is in the center of the

1068 Figure. The top and bottom of the plot correspond to the [Earth's polar regions](#) and the left side

1069 and right side edges local midnight. The enhanced TEC area corresponds to the sunlit hemisphere.

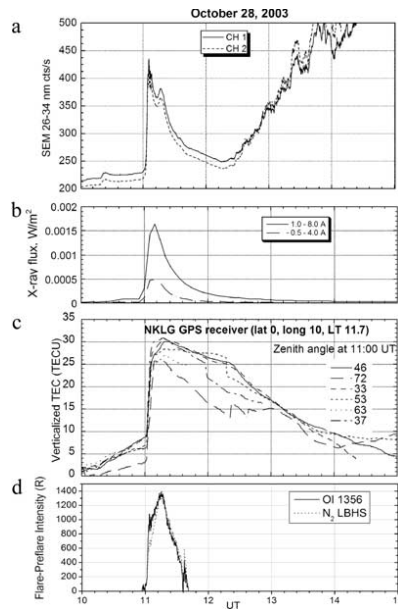
1070 [At the subsolar point the TEC enhancement was ~30%. This is the record for flare-induced](#)

1071 [ionospheric TEC \(Tsurutani et al., 2005b\).](#) The nightside hemisphere shows no TEC enhancement,

1072 as expected. The TEC enhancement is due to ionization by X-rays, EUV photons and UV photons,

1073 all part of the solar flare spectrum.

1074



1075  
1076 Figure 22. The ionospheric and atmospheric effects of the October 28, 2003 solar flare.

1077  
1078 Figure 22 shows the effects of the October 28 solar flare. From top to bottom are the SOHO SEM  
1079 EUV count rate, the GOES X-ray flux, the Libreville, Gabon TEC data and the GUVI O and N<sup>2</sup>  
1080 dayglow data. It is noted that the flare profiles in EUV and X-rays last ~tens of mins and are similar  
1081 in profile to each other. However the TEC over Libreville last hours. This is due to the EUV  
1082 portion of the solar flare. These photons deposit their energy at ~170 to 220 km altitude where the  
1083 recombination time scales are ~ 3 to 4 hours. Thus EUV photon ionization has longer lasting  
1084 ionospheric TEC effects. The X-ray portion of the solar flare spectrum deposit their energy in the  
1085 ~80 to 100 km altitude range where the recombination time scale is tens of min (Thomson et al.,  
1086 2005, and references therein). [This solar flare example is one where solar energy goes directly](#)  
1087 [from the Sun to the Earth's ionosphere. There is no transfer of energy to interplanetary space and](#)  
1088 [then to the magnetosphere.](#)

1089  
1090 Some future [Space Weather](#) problems are to understand if the solar flare [photon](#) spectrum varies  
1091 [often](#) and why this happens? We have indicated that the 28 October 2003 and the 4 November  
1092 2003 flares were significantly different [spectra-wise](#). The question is why and how often does this  
1093 happen? Ionospheric satellites like the Constellation Observing System for Meteorology,  
1094 Ionosphere and Climate-2 (COSMIC II) and SWARM can probe for detailed altitude dependence  
1095 of ionization to work backwards to attempt to identify what spectrum would cause the layered

1096 ionization detected. Solar flare data taken by instrumentation onboard the *SORCE* and *TIMED*  
 1097 spacecraft would be useful to understand the details of flare spectral differences but solar physicists  
 1098 are needed to explain what the causes are. Other questions are how large can X-ray and EUV  
 1099 flares become? What will their ionospheric effects be?

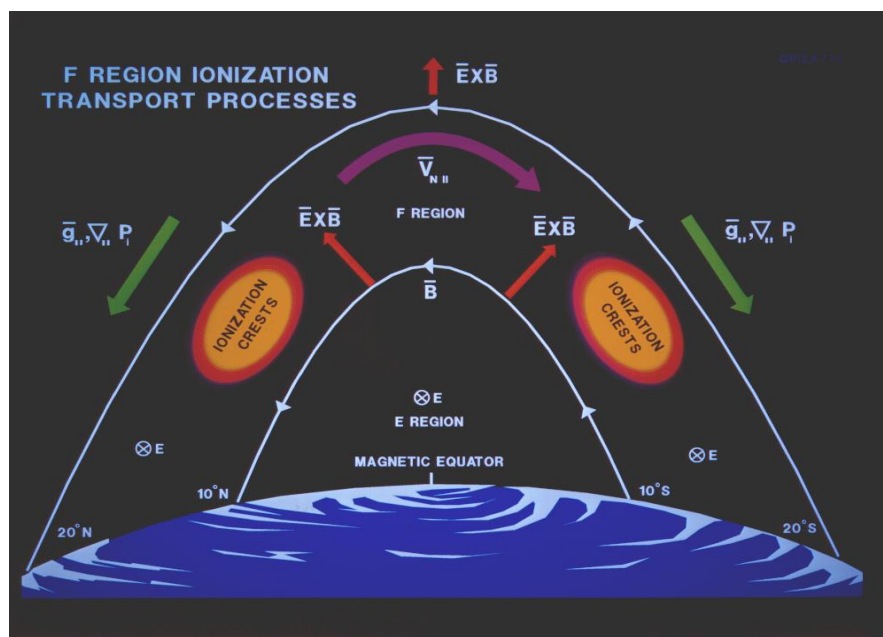
1100

## 1101 **6.0. RESULTS: Magnetic Storms and Prompt Penetrating Electric Fields** 1102 **(PPEFs)**

1103

1104 For substorms, PPEFs occurring in the ionosphere have been known for a long time, [since the](#)  
 1105 [beginning of the space age](#) (Nishida and Jacobs, 1962; Obayashi, 1967; Nishida, 1968; Kelley et  
 1106 al. 1979, 2003). In the last 10 years lots of work [has been](#) done on PPEFs during magnetic storms.  
 1107 Why didn't people look at storms earlier? Because it was theoretically predicted that the PPEFs  
 1108 would be shielded out. Why doesn't shielding happen? This is a very good question for [workers](#)  
 1109 [in the field](#). [Right now we don't know the answer.](#)

1110



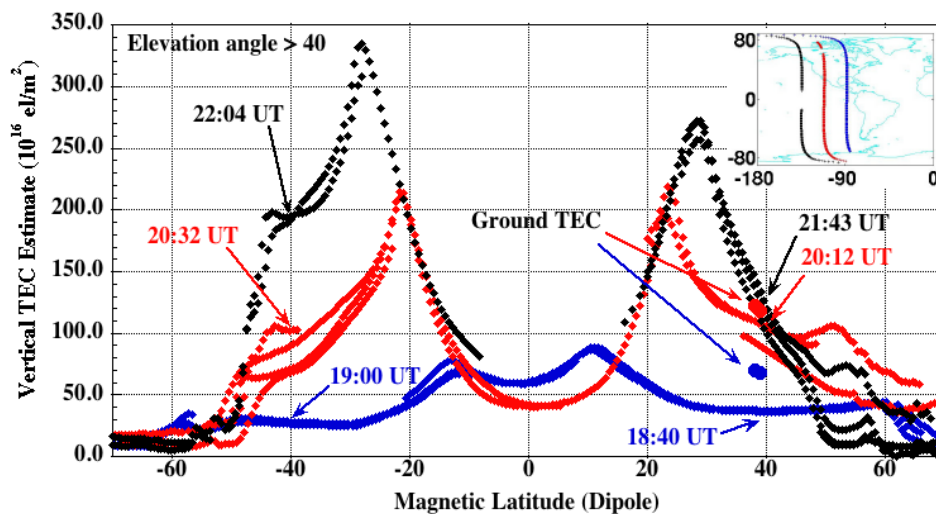
1111

1112 Figure 23. Dayside (near) equatorial ionization anomalies (EIAs) located  $\sim \pm 10^\circ$  on both sides of  
 1113 the magnetic equator. The local Earth magnetic field is shown in this schematic. The figure is  
 1114 taken from Anderson et al. (1996).

1115



1116 Figure 23 show the geometry of the Earth’s magnetic field near the magnetic equator. It is parallel  
 1117 to the Earth’s surface at the equator but where the equatorial ionization anomalies (EIAs) are  
 1118 located, the magnetic field is slanted. The EIAs are standardly located at  $\sim\pm 10^\circ$  MLAT in the  
 1119 dayside [ionosphere](#). With red arrows, the figure also shows the direction of  $E \times B$  convection. At  
 1120 exactly the magnetic equator,  $E \times B$  is in a purely upward direction. At the positions of the EIAs,  
 1121 the  $E \times B$  direction is both upward and to higher [absolute](#) magnetic latitudes.  
 1122



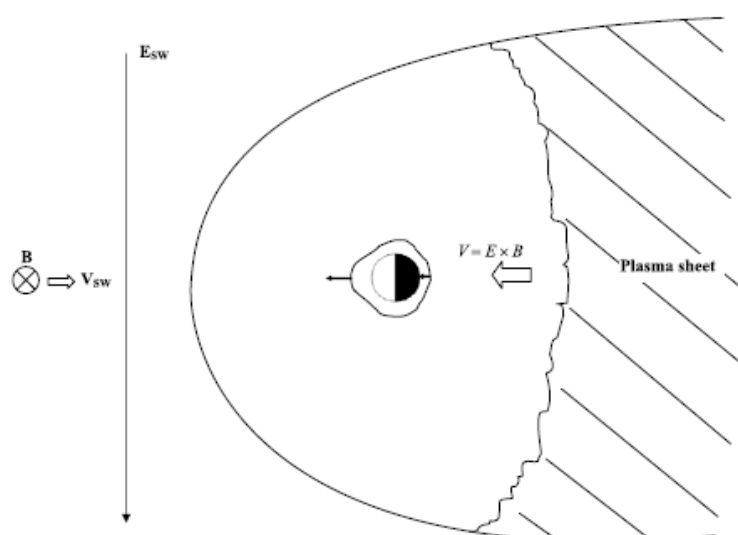
1123  
 1124 Figure 24. Three passes of the CHAMP satellite measuring the near equatorial and midlatitude  
 1125 TEC during October 30, 2003. CHAMP was at an altitude of  $\sim 430$  km, so the TEC measured was  
 1126 the [total](#) thermal electron [column density](#) above that altitude. The figure is taken from Mannucci  
 1127 et al. (2005).  
 1128

1129 Figure 24 shows three passes of the CHAMP satellite in polar orbit with an altitude of  $\sim 430$  km at  
 1130 the near equatorial crossings. The three orbits are given in the upper right hand portion of the  
 1131 Figure. The first TEC trace shown in blue is before the onset of the October 30-31 magnetic storm.  
 1132 The two EIAs are identified by the TEC enhancements at  $\sim \pm 10^\circ$  with peak intensities of  $\sim 80$  TEC  
 1133 units. In the next pass (red trace), the EIAs are located at  $\sim \pm 21^\circ$  MLAT and the peak intensities  
 1134 are  $\sim 210$  TEC units. During the next satellite pass, the EIAs are located near  $\pm 30^\circ$  and the TEC  
 1135 values become as high as  $\sim 330$  TEC units. This “movement” of the EIAs to higher magnetic

1136 latitudes can be explained by a convective electric field (PPEF) in the east-west direction causing  
 1137 an uplift to both EIAs by  $E \times B$  convection as explained earlier associated with Figure 23. One  
 1138 might ask why does the TEC increase to such high values?

1139  
 1140 The answer is as the PPEF removes the plasma from the ionospheric lower F region and brings it  
 1141 to higher altitudes where the recombination time scale is longer (hours), the Sun's EUV photons  
 1142 replace the plasma by photoionization of the upper atmosphere, replacing the lost plasma and thus  
 1143 increasing the "total electron content" of the ionosphere. This is one cause of a "positive  
 1144 ionospheric storm".

1145



1146  
 1147 Figure 25. The interplanetary, magnetospheric and equatorial ionospheric electric fields during a  
 1148 PPEF event. The Figure is taken from Tsurutani et al. (2004c; 2008b).

1149  
 1150 Figure 25 shows the interplanetary motional electric field for southward interplanetary  $B_z$ . The  
 1151 electric field will be in the dawn-to-dusk direction. When magnetic reconnection takes place in  
 1152 the nightside plasmashet, the convective electric field will be in the same direction but with a  
 1153 reduced amplitude. This electric field brings the plasmashet plasma into the nightside low L  
 1154 region magnetosphere during magnetic storms. The PPEFs penetrate into the dayside equatorial  
 1155 ionosphere (shown in Figure 24) and also the nightside equatorial ionosphere. However  
 1156 significantly different from the dayside case, the  $E \times B$  convection on the nightside will bring the  
 1157 ionospheric plasma to lower altitudes, leading to recombination and reduction in TEC. This is one

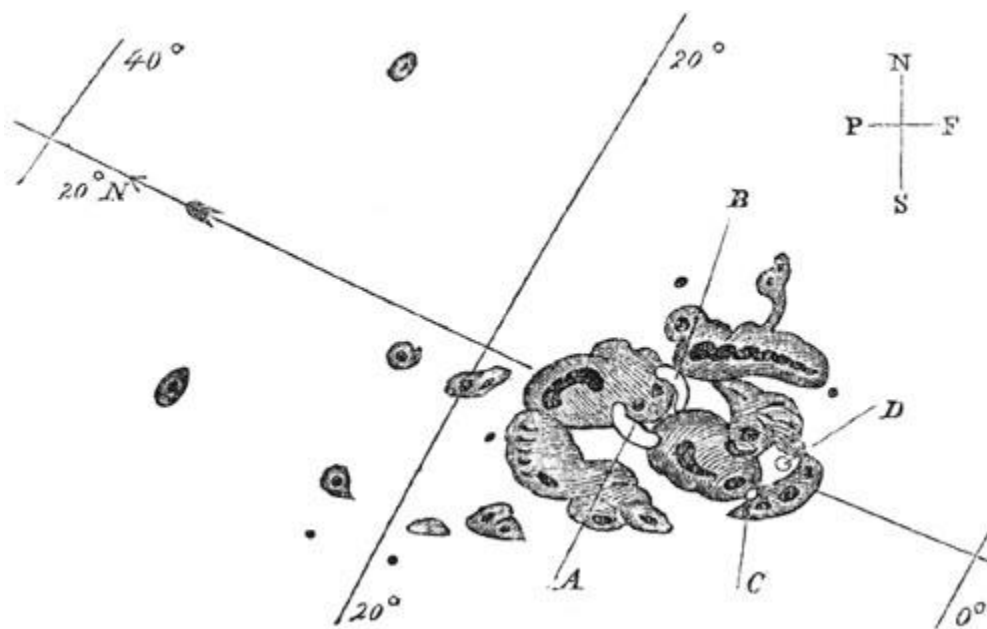
1158 form of a “negative ionospheric storm”. See Mannucci et al. (2005, 2008) for discussions of  
 1159 positive and negative ionospheric storms.

1160  
 1161 There are many important questions about PPEFs which are almost always present during major  
 1162 magnetic storms. As previously mentioned, “why aren’t the electric fields shielded out?” What is  
 1163 the mechanism for generating PPEFs, wave propagation from the polar ionosphere as suggested  
 1164 by Kikuchi and Hashimoto (2016) or a more global picture as Figure 25 and Nishida and Jacobs  
 1165 (1962) suggest? Figure 25 is a simple schematic. What are the real local time dependences of the  
 1166 PPEF? Does this vary from storm to storm, and if so, why? Why does the [relative](#) PPEF magnitude  
 1167 vary from one storm to the next? Again future spacecraft and ground based studies will be able to  
 1168 help answer these questions.

1169

## 1170 7.0 RESULTS: The Carrington Storm

1171



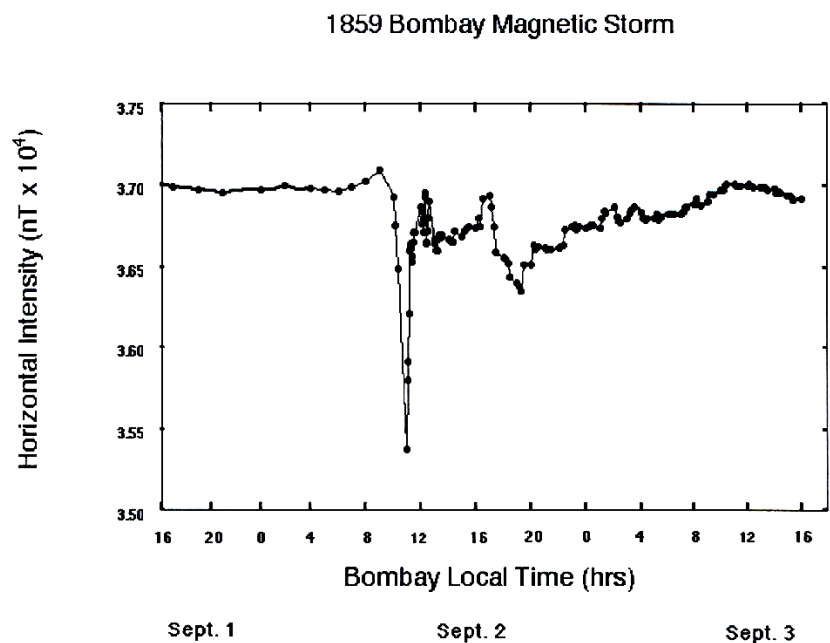
1172  
 1173 Figure 26. The solar active region during the Carrington 1 September 1859 optical solar flare. The  
 1174 figure is taken from Carrington (1859).

1175

1176 Figure 26 is the active region (AR) that was hand-drawn by Richard Carrington. This was the  
 1177 source of the optical solar flare that he and Hodgson (1859) saw and reported on 1 September

1178 1859. See Cliver (2006) for a nice accounting of the observational activity taken during 1859 flare  
 1179 interval and Kimball (1960) for an accounting of the aurora during the storm. The optical part of  
 1180 the flare lasted only  $\sim 5$  min. Some  $\sim 17$  hr 40 min later a magnetic storm occurred at Earth  
 1181 (Carrington, 1859).

1182



1183

1184 Figure 27. The Carrington storm detected in the Colaba, India magnetometer. The Figure is taken  
 1185 from Tsurutani et al. 2003 and Lakhina et al. 2012.

1186

1187 Figure 27 shows the H-component magnetic field taken by the Colaba magnetic observatory during  
 1188 the “Carrington” magnetic storm. The  $SI^+$  is estimated to be  $\sim 110$  nT and the magnetic decrease  
 1189  $\sim 1600$  nT at Colaba (Mumbai, India). The  $SI^+$  and storm main phase has been recently shown to  
 1190 be most likely caused by an upstream solar wind density of  $5$  particles  $\text{cm}^{-3}$  and a MC with intensity  
 1191  $\sim 90$  nT (pointed totally southward) by Tsurutani et al. (2018a). No particularly unusual solar wind  
 1192 conditions are believed to have been necessary (in contrast to the [original](#) conclusions of Ngwira  
 1193 et al., 2014). [Ngwira et al. \(2018\) is now in accord with this more recent assessment of a normal](#)  
 1194 [upstream solar wind.](#)

1195

1196 The intensity of the “Carrington” storm was estimated as  $Dst = -1760$  nT (Tsurutani et al., 2003)  
 1197 based on observations of the lowest latitude of red auroras being at  $\pm 23^\circ$  (Kimball, 1960). The

1198 storm intensity was calculated using recent theoretical expressions of magnetospheric potentials  
1199 needed to convect plasma into such low latitudes. Siscoe (1979) basing his estimate on a model  
1200 that treats the pressure as a constant along the magnetic flux tube came up with a value of Dst = -  
1201 2000 nT.

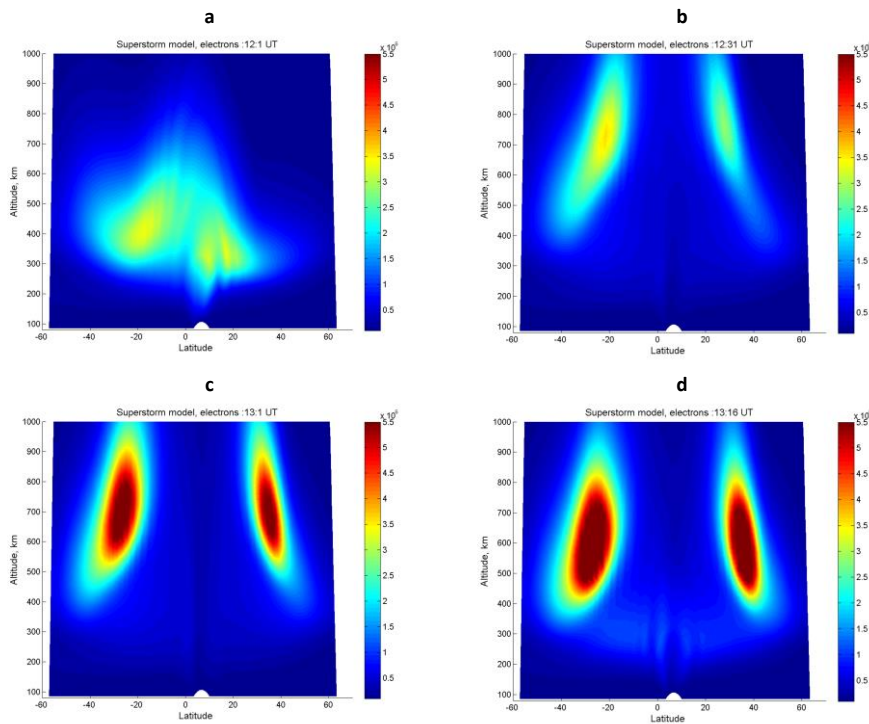
1202  
1203 It should be mentioned that some researchers have taken exception with the Colaba magnetogram  
1204 as an indication of ring current effects (see Comment by Akasofu and Kamide (2005) and Reply  
1205 by Tsurutani et al. (2005a)). The Colaba magnetic profile is unlike those of ICME magnetic storms  
1206 discussed in Sections 2.3, 2.4 and 3.1 of this paper. Several researchers have estimated the storm  
1207 intensity based on the Colaba magnetogram (see articles in a special journal edited by Clauer and  
1208 Siscoe, 2006; Acero et al. 2018). The Colaba data clearly show that the storm had exceptionally  
1209 large geomagnetic effects, irregardless of the interpretation of the Colaba data. Possible  
1210 interpretations of the Colaba profile will be discussed later in the paper.

1211  
1212 The most accurate method of estimating a magnetic storm intensity is by using the latitude of the  
1213 aurora. Red auroras (Stable Auroral Red or SAR arcs) are presumably an indication of the location  
1214 of the plasmopause (R.M. Thorne, private communication, 2002). Kimball (1960) noted that “red  
1215 glows” were detected at  $\pm 23^\circ$  from the geomagnetic equator during the Carrington event. In 1960  
1216 the term “SAR arc” was not in use, but we can assume that this was what he was reporting. At the  
1217 present time, this is the most equatorward SAR arcs that have been observed (thus the most intense  
1218 magnetic storm). That is until researchers find records of even lower latitude red auroras!

1219  
1220 Comments on the short duration of the recovery phase has been made by Li et al. (2006). A high  
1221 density filament was used to explain this unusual feature of the magnetic storm profile. Tsurutani  
1222 et al. (2018a) have recently proposed another possibility. During extreme events when the storm  
1223 time convection brings the plasmashet into very low L, all of the standard ring current loss process  
1224 rates will be enhanced. There will be greater Coulomb scattering, greater charge exchange loss  
1225 rates and greater plasma wave growth with consequential greater wave-particle pitch angle  
1226 scattering and losses to the atmosphere. In Tsurutani et al. (2018a) the authors focused particularly  
1227 on wave-particle interactions because the size of the loss cone will increase dramatically with  
1228 decreasing L. This, plus greater energetic particle compression due to the extreme inward

1229 convection, will lead to stronger loss cone/temperature anisotropy instabilities, greater wave  
 1230 growth and thus greater losses. This hypothesis can be easily tested by magnetospheric spacecraft  
 1231 observations during large magnetic storms and by magnetospheric modeling perhaps bringing  
 1232 some light to the unusual Colaba magnetic signature.

1233



1234

1235 Figure 28. A model of the PPEF effects of the Carrington 1859 storm on the dayside ionosphere.  
 1236 The input electric field was taken from Tsurutani et al. (2003) and the simulation was performed  
 1237 using the Huba et al. (2000, 2002) SAMI2 code. The figure is taken from Tsurutani et al. (2012).

1238

### 1239 7.1. The Carrington PPEF

1240

1241 One of the concerns for extreme Space Weather in the ionosphere are extremely intense PPEFs  
 1242 and the daytime superfountain effect on the uplift of  $O^+$  ions (positive ionospheric storms). Higher  
 1243 ion densities in the exosphere will lead to the possibility of enhanced low altitude satellite drag.  
 1244 In Tsurutani et al. (2003), the authors used modern theories of the electric magnetospheric potential  
 1245 given by Volland (1973), Stern (1975) and Nishida (1978) to determine the electric field during

1246 the Carrington storm main phase. The former authors obtained an estimate of  $\sim 20$  mV/m. They  
1247 then applied this electric field in the SAMI2 model with the results shown in Figure 28.

1248  
1249 Figure 28 shows the SAMI2 results of the modeled dayside ionosphere with a  $\sim 20$  mV/m added  
1250 to the diurnal variation electric field. The quiet ionosphere is shown at the upper left. The uplift  
1251 of the  $O^+$  ions both in altitude and MLAT after  $\sim 30$  min is given on the upper right panel. The  
1252 maximum time that the electric field was applied was 1 hr. The ionosphere at that time is shown  
1253 on the lower left. The storm time equatorial ionospheric anomalies (EIAs) are located at  $|MLAT|$   
1254  $\sim 30^\circ$  to  $40^\circ$  and an altitude of  $\sim 550$  to  $900$  km for the most dense portion of the EIAs. The bottom  
1255 right panel shows that the EIAs have come down in altitude but to higher latitudes  $\sim 15$  min after  
1256 the termination of the PPEF application. Parts of the still intense EIAs are now beyond  $|MLAT| >$   
1257  $40^\circ$  and now the bulk of the maximum density portion is at  $\sim 400$  to  $800$  km altitude.

1258  
1259 It was found that at altitudes of  $\sim 700$  to  $1,000$  km, the  $O^+$  densities are predicted to be  $\sim 300$  times  
1260 that of the quiet time neutral densities. It has been also been shown by Tsurutani and Lakhina  
1261 (2014) that in extreme cases, the magnetospheric/ionospheric electric field can be twice as large  
1262 as the Carrington storm and six times as large as the 1991 event. Even if the magnetospheric  
1263 radiation belt is saturated (there are other scientific papers that state that magnetospheric beta can  
1264 be greater than one: Chan et al. 1994; Saitoh et al. 2014; Nishiura et al., 2015), this is a different  
1265 facet of Space Weather and the electric field may not be saturated. What will be the ionospheric  
1266 effects of these even larger electric fields?

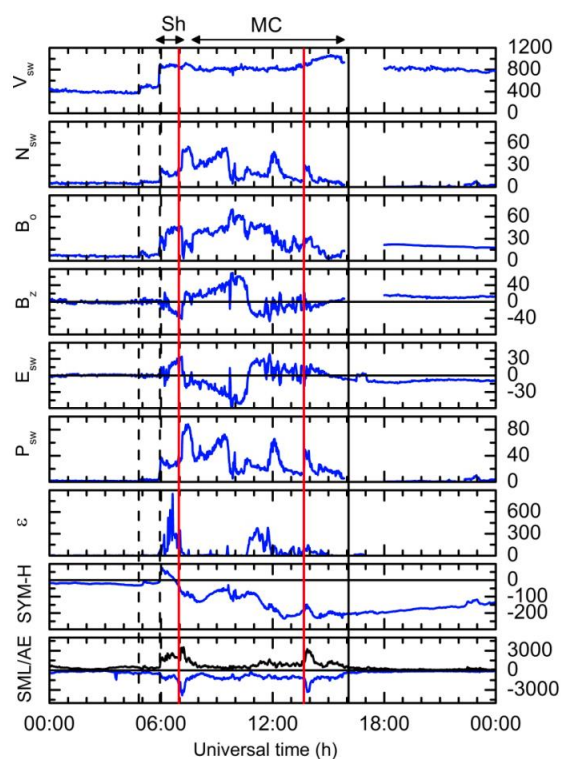
1267  
1268 A fundamental question for the future is “can the upward  $O^+$  ion flow drag sufficient numbers of  
1269 oxygen neutrals upward so that the oxygen ions plus neutral densities are even higher still?” A  
1270 short time interval analytic calculation done by Lakhina and Tsurutani (2017) and a mini-  
1271 Carrington event modeled by Deng et al. (2018) have indicated that the answer is “yes”. However  
1272 a full code needs to be developed and run to answer this question quantitatively. This is an  
1273 interesting future problem for computer modelers.

1274

## 1275 **8.0 RESULTS: Supersubstorms**

1276

1277 **Super intense** substorms (supersubstorms: SSSs) appear to be externally (solar wind) triggered.  
 1278 Why are they important? They might be the feature within extreme magnetic storms that cause  
 1279 geomagnetically induced currents (GICs)/power outages. This hypothesis needs to be tested.  
 1280



1281  
 1282 Figure 29. Two supersubstorms (SSSs) that occur during a two-phase magnetic storm on 20  
 1283 November 2001. The onsets of the supersubstorms are indicated by the vertical red lines. The  
 1284 figure is taken from Tsurutani et al. (2015).

1285  
 1286 Figure 29 shows the solar wind data during an intense magnetic storm and two SSSs. From top to  
 1287 bottom are the solar wind speed and density, the magnetic field magnitude and Bz component, and  
 1288 the interplanetary motional electric field, ram pressure and Akasofu epsilon parameter (Perreault  
 1289 and Akasofu, 1978). The bottom two parameters are the SYM-H index and the SML index (blue)  
 1290 and AE index (black). An initial forward shock is indicated by a vertical dashed line at ~0500 UT,  
 1291 a second shock at ~0600 UT, and the two SSS onsets by red vertical lines. The criterion for a SSS  
 1292 event was a SML peak value  $< -2500$  nT (an arbitrary number, but chosen to be an extremely high  
 1293 value). At the top of the diagram, the sheath region is indicated by a “Sh” and the magnetic cloud  
 1294 region by “MC”. The first storm main phase is caused by southward Bz in the sheath and the



1295 second, more intense main phase by southward Bz in the MC. The interplanetary magnetic field  
1296 measurement cadence is 1 min. It has been noted that the magnetosphere typically reacts to  
1297 southward Bz with durations > 10 to 15 min (Tsurutani et al., 1990), so this high rate of cadence  
1298 is sufficient to identify any causes of geomagnetic response.

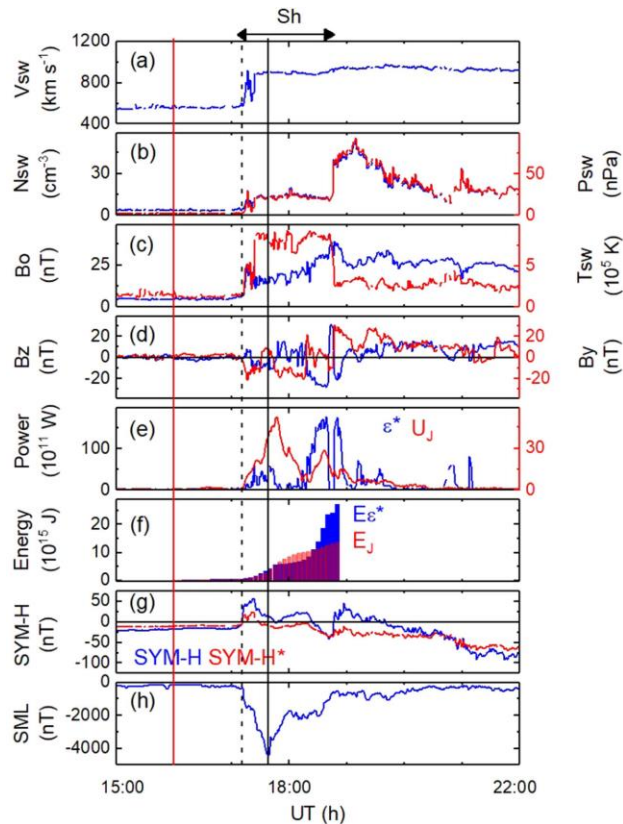
1299

1300 It is noted that the SSS events in this case are not triggered at either of the two shocks nor do they  
1301 occur during the peak negative SYM-H values of the storm main phases. However the first SSS  
1302 event is collocated with a peak Esw and a peak southward Bz of the sheath plasma. The SSS event  
1303 is also collocated with a large solar wind pressure pulse which is caused by an intense solar wind  
1304 density feature. The second SSS event occurred in the recovery phase of the second magnetic  
1305 storm. The IMF Bz was ~0 nT. The second SSS event was associated with a solar wind pressure  
1306 pulse associated with a small density enhancement.

1307

1308 A study of SSSs from 1981 to 2012 was conducted by Hajra et al. (2016). In that study a variety  
1309 of solar wind features were found to be associated with SSS onsets. In that survey it was noted  
1310 that two SSS events were triggered by fast forward shocks. One of these events will be discussed  
1311 below.

1312



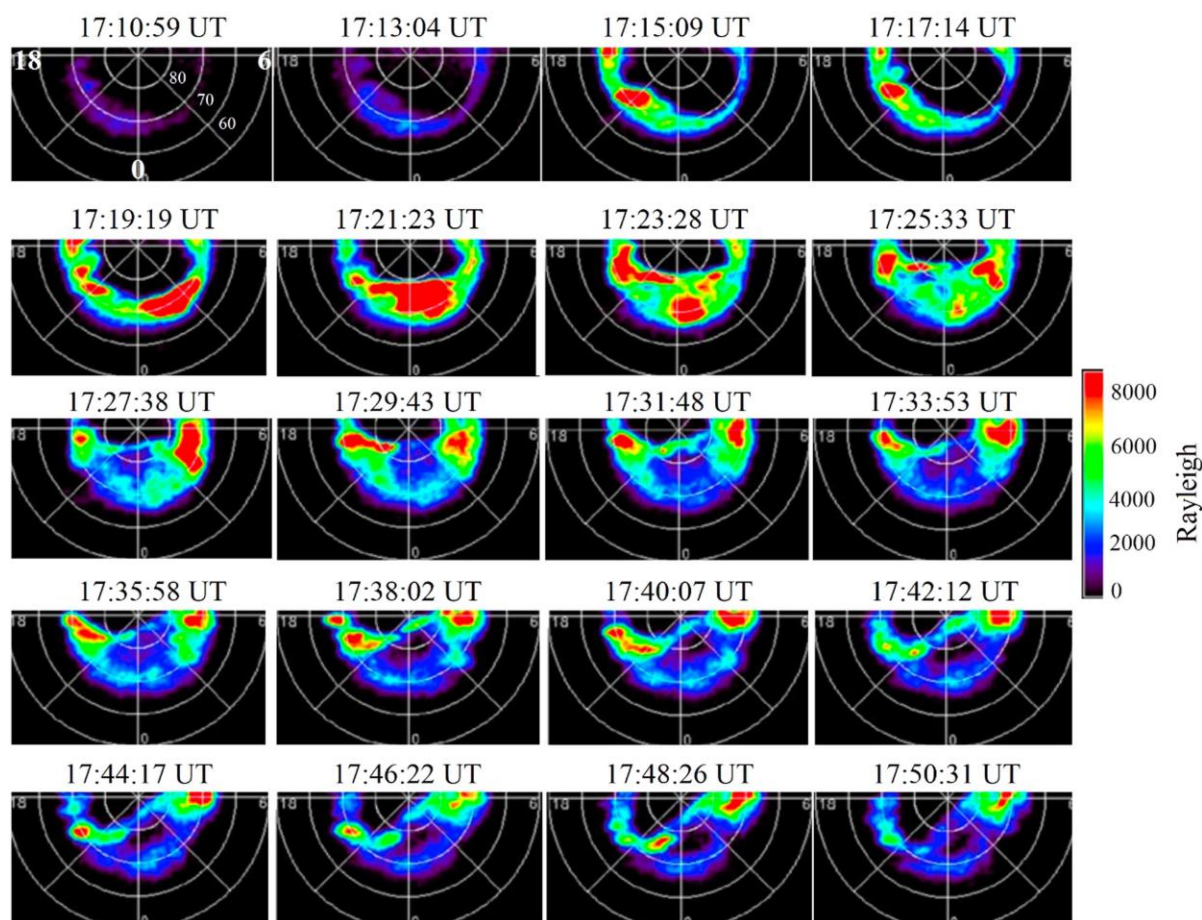
1313  
 1314 Figure 30. A SSS triggered by an interplanetary shock on 21 January 2005. The dashed vertical  
 1315 line indicates a fast forward shock and the solid black line the peak intensity of the SSS event. The  
 1316 figure is taken from Hajra and Tsurutani (2018b).

1317  
 1318 Figure 30 shows solar wind/interplanetary parameters and geomagnetic parameters during a SSS  
 1319 event on 21 January 2005. From top to bottom are the solar wind speed, density and ram pressure,  
 1320 the magnetic field magnitude and solar wind temperature (in the same panel), the IMF Bz and By  
 1321 components (GSM coordinates), Joule energy and the Akasofu epsilon pressure corrected  
 1322 parameter  $\epsilon^*$ , the time-integrated energy input into the magnetosphere and time-integrated joule  
 1323 energy. The next to the bottom panel contains the [SYM-H index](#) and the pressure corrected SYM-  
 1324 H index ([SYM-H\\*](#)). The bottom panel is the SML index. A dashed vertical line denotes the  
 1325 occurrence of a fast forward shock. A vertical solid line indicates the peak of the SSS event.

1326  
 1327 The SSS event onset at 1711 UT coincided with a shock with magnetosonic Mach number of  $\sim 5.5$   
 1328 with a shock normal angle of  $81^\circ$ . The high density sheath sunward of the shock causes a  $SI^+$  of  
 1329  $\sim 57$  nT. The solar feature associated with this event was an X7 class flare that occurred at  $\sim 0700$

1330 UT January 20 (Bombardieri et al., 2008; Saldanha et al., 2008; Pérez-Peraza et al., 2009; Wang  
 1331 et al., 2009; Firoz et al., 2012; Bieber et al., 2013; Tan, 2013). The IMF Bz turned abruptly  
 1332 southward at the time of the shock so this is part of the energy driving the event. When the IMF  
 1333 Bz turned abruptly northward at ~1738 UT, the SSS began a recovery phase. This was followed  
 1334 by an interplanetary solar filament (Kozyra et al., 2013), but the latter was not geoeffective in this  
 1335 case. This high plasma density, high magnetic field intensity feature was interpreted by Kozyra et  
 1336 al. (2013) as the interplanetary manifestation of the Illing and Hundhausen (1986) most sunward  
 1337 portion of the 3 parts of a CME discussed earlier.

1338



1339  
 1340 Figure 31. IMAGE-FUV images taken from ~1711 UT to ~1751 UT on January 21, 2005. These  
 1341 selected auroral images correspond to the SSS event in Figure 30.

1342  
 1343 Figure 31 contains the Imager for Magnetopause-to-Aurora global Exploration (IMAGE) far  
 1344 ultraviolet images for the SSS event in Figure 30. At ~1713 UT there was a small brightening at

1345 ~68° MLAT, which was a very small substorm or pseudobreakup (Elvey, 1957; Tsurutani et al.,  
1346 1998; Aikio et al., 1999). At ~1715 UT, 2 min later there was a ~2100 MLT premidnight  
1347 brightening of the aurora at ~68° to 75°. At ~1719 UT the most intense aurora was located at ~68°  
1348 to 72° in the postmidnight/morning sector, ~0000 to 0400 MLT. The aurora moved from a  
1349 dominant premidnight location to a postmidnight location in ~4 min.

1350  
1351 By ~1726 UT there was almost no aurora of significant intensity at local midnight. At the peak of  
1352 the SML value at ~1738 UT until ~1751, there were both intense premidnight and postmidnight  
1353 auroras.

1354  
1355 The SSS event did not exhibit the Akasofu (1964) standard model of a substorm with an  
1356 intensification at midnight and then expansion to the west, east and north. The changes in the  
1357 location of intense auroras were too rapid to track with the IMAGE cadence of ~2 min.

1358  
1359 The SSS events display rapid auroral movements which may entail the appearance of sudden local  
1360 field-aligned currents. Even smooth motion of auroral forms will cause strong dB/dt effects over  
1361 local ground stations. SSS events may be features that can cause GIC effects that have been  
1362 attributed to “magnetic storms”. Thus it might be the SSS events within magnetic storms which  
1363 are the real cause. SWARM satellites are excellently instrumented spacecraft that can study the  
1364 SSS events in detail and possible resultant GIC effects. However as noted in the auroral images,  
1365 there is a need for even higher time resolution global images than is present today. **Therefore, it is**  
1366 **important to development and fly auroral UV imagers that can be operated at ~1 s cadence in**  
1367 **intense auroral substorm events.**

1368  
1369 **8.0. CONCLUSIONS: The Physics of Space Weather and Possible Forecasting**

1370  
1371 We have discussed the current knowledge about various facets of **the physics of Space Weather**.  
1372 There are others which we have not touched upon because of limited time and knowledge. The  
1373 reader should know that other areas of **Space Weather** exist which may be equally important.

1374

1375 The most critical area for forecasting magnetic storms, either during solar maximum or the  
1376 declining phase of the solar cycle is the prediction of the magnetic field  $B_z$  and the speed of the  
1377 convected fields at 1 AU. For CME/MC storms (primarily during solar maximum), this is  
1378 identifying MC  $B_z$  fields near the Sun and understanding the evolution of the MC as it propagates  
1379 from the Sun to Earth. This major challenge will be applicable for the prediction of extreme  
1380 magnetic storms and hopefully great progress will be made in the next 5 to 10 years. It was shown  
1381 that for simple MCs for extreme storms one need to focus on events where the transit time from  
1382 the Sun to the Earth is less than  $\sim 24$  hours.

1383  
1384 For sheaths upstream of ICMEs during solar maximum and CIRs during the declining phase (CIRs  
1385 are double sheath structures), the problem is different. Detailed knowledge of the slow solar wind  
1386 in the space between the Sun and Earth are needed to accurately describe and predict the IMF  $B_z$   
1387 that impacts the Earth. So far little work has been applied towards predicting the slow solar wind  
1388 (plus verification). Effort needs to be placed in this area to be able to forecast intense to moderate  
1389 magnetic storms. It was shown that sheath magnetic fields are extremely important for the  
1390 generation of super intense ( $Dst < -250$  nT) magnetic storms (Meng et al., 2019b).

1391  
1392 A great deal of knowledge presently exists for establishing SEP events, those energetic particles  
1393 associated with acceleration at ICME shock fronts (see Luhmann et al., 2017). What is needed for  
1394 better forecasting is to understand the Mach number of the shocks, the shock normal angles and  
1395 possibly upstream “seed” particles. The upstream seed particle population is similar to the sheath  
1396  $B_z$  problem in that this component of the slow solar wind needs to be modeled carefully and  
1397 accurately. Three spacecraft in the solar wind at different distances from the Sun should help a  
1398 lot.

1399  
1400 The appearance of HSSs at 1 AU is a very tractable problem. That is if the coronal hole boundaries  
1401 in the photosphere can be established firmly and the HSS propagation to 1 AU can be done  
1402 accurately. However the most difficult task again is the IMF  $B_z$ . If Alfvén waves are generated  
1403 in the interplanetary medium, this will make the task even more difficult. One solution is to  
1404 measure the interplanetary magnetic field at 1 AU and use filtering techniques (Guarnieri et al.  
1405 2018) or again have large apogee Earth orbiters like the IMP-8 spacecraft again. Another

1406 possibility is developing some type of statistical IMF Bz generator. Of course this technique will  
1407 only give a ~30 min to 1 hour advanced warning.

1408  
1409 Predicting the interplanetary shock Mach numbers and ram pressure jumps will allow  
1410 foreknowledge of new radiation belt formation, SI<sup>+</sup> effects and magnetospheric and ionospheric  
1411 dB/dt effects. Dayside auroral intensities and nightside substorm triggering will also be enhanced  
1412 by predicting incoming shocks.

1413  
1414 Several spacecraft missions have been mentioned in relationship to some forecasting problems.  
1415 However the reader should note that the missions and/or their data alone will not solve these  
1416 problems. It will be the scientists either on these missions or perhaps totally independent scientists  
1417 who will make the most progress on these problems. An example is magnetic storms caused by  
1418 interplanetary shocks/sheaths and CIRs. How long will it take scientists to be able to accurately  
1419 forecast the time of occurrence of the storm (the easiest part) and the intensity (the hardest part)?  
1420 Here we will not make an estimate of how long this will take. Shock acceleration of solar flare  
1421 particles is clearly a fundamental part of Space Weather. How long will it scientists to be able to  
1422 predict the fluence and spectral shape at a variety of distances away from the Sun? This is a  
1423 fundamental problem which space agencies are not currently directly addressing.

1424

## 1425 **Final Comments**

1426

1427 A great amount of effort has been put into developing Space Weather models with the appropriate  
1428 physics and chemistry included. Some models even use solar and solar wind data and geomagnetic  
1429 indices that might be useful for short time-duration predictions (Gopalswamy et al., 2001;  
1430 Srivastava, 2005; Cho et al., 2010; Kim et al., 2010; Kim et al., 2014; Schrijver et al., 2015; Savani  
1431 et al., 2015). However in most cases, the usefulness of such models for predictive purposes has  
1432 not been independently and objectively tested. This needs to be done so that missing physics and  
1433 chemistry can be applied. When done (testing), surprises might result. Meng et al. (2019b) have  
1434 tested the applicability of two well-known ionospheric codes to predict ionospheric TEC. It was  
1435 found that the predictability was not so good, even though interplanetary plasma and field data,  
1436 the solar F10.7 flux, and the geomagnetic Kp indices were used. The causes of this lack of good

1437 representation of the ionospheric TEC data is not understood at this time. It is now being realized  
1438 that not only the predictability of various models need improvement, but also the level of  
1439 uncertainty of prediction needs to be assessed as well (Knipp et al., 2018; Savani et al., 2017).

1440  
1441 CME propagation through the interplanetary medium using ENLIL-based codes are making good  
1442 progress in estimating arrival times of ICMEs at 1 AU and have had varying success in predicting  
1443 the solar wind parameters as well (Falkenberg et al., 2010; Davis et al., 2011; Pizzo et al. 2015;  
1444 Jackson et al., 2015; Jian et al. 2015, 2016). However the fundamental issue of space weather  
1445 prediction for magnetic storms is the direction and intensity of the magnetic field both in the MC  
1446 and upstream sheath. These topics still remain a challenge.

1447  
1448 Another new approach, the application of machine learning algorithms, is quite hopeful. For this  
1449 application, the physics and chemistry need not be known to be applied. Rather the reverse, finding  
1450 good correlations between solar and interplanetary parameters and magnetospheric observations  
1451 (for magnetic storms as an example) could lead to the understanding of the physics, the topic of  
1452 this paper. But again one should test these approaches and carefully and objectively assess their  
1453 accuracy and reliability in making predictions (see Wing et al., 2005, 2016; Reikard, 2015, 2018).

1454  
1455 We have one final comment on a third type of approach at predicting Space Weather. For  
1456 atmospheric weather forecasts, the experts downselect to ~25 of their best codes, and run each of  
1457 the codes with the same input data. The codes produce ~25 different predictions. The weather  
1458 service uses the average of the values. Why this scheme works reasonably well is not understood.  
1459 This may be the final path of Space Weather forecasting.

1460  
1461 Our hope is that the paper is stimulating to the reader in a positive sense: that they will be energized  
1462 to attack some of the interesting problems in our field of Space Weather. On the other hand if the  
1463 reader finds statements/topics that they disagree with, please send us email comments and we will  
1464 try to answer them the best that we can. And if you have disagreements that should see print,  
1465 Nonlinear Processes in Geophysics has a “Comment” and “Reply” format for discussions of this  
1466 type.

1467

## 10.0 GLOSSARY

1468

1469 **Partially taken from:** “*From the Sun: Auroras, Magnetic Storms, Solar Flares, Cosmic*  
1470 *Rays*” (Suess and Tsurutani, 1998, AGU Press)

1471

1472 **Adiabatic Invariant:** In a nearly collisionless, ionized gas, electrically charged particles orbit  
1473 around magnetic lines of force. Certain physical quantities are approximately constant for  
1474 slow (adiabatic) changes of the magnetic field in time or in space and these quantities are  
1475 called *adiabatic invariants*. For example, the magnetic moment of a charged particle,  
1476  $\mu = mV_{\perp}^2 / (2B)$ , is such a constant where  $V_{\perp}$  is the velocity of the particle perpendicular to  
1477 the magnetic field, B is the magnetic field strength, and m is the particle mass. In a  
1478 converging field such as in approaching the pole of a dipole magnetic, the field strength  
1479 increases and therefore  $V_{\perp}$  increases as well because  $\mu$  has to remain constant.

1480 **Aeronomy:** The science of the (upper) regions of atmospheres, those regions where dissociation  
1481 of molecules and ionization are present.

1482 **Alfvén Wave** (magnetohydrodynamic shear wave): A transverse wave in magnetized plasma  
1483 characterized by a change of direction of the magnetic field with no change in either the  
1484 intensity of the field or the plasma density.

1485 **Anisotropic Plasma:** A Plasma whose properties vary with direction relative to the ambient  
1486 magnetic field direction. This can be due, for example, to the presence of a magnetic or  
1487 electric field. See also Isotropic Plasma; Plasma.

1488 **Arase satellite, formerly called Exploration of energization and Radiation in Geospace** or  
1489 **ERG:** a scientific satellite developed by the Institute of Space and Astronautical Science  
1490 (ISAS) of the Japanese Aerospace Exploration Agency (JAXA) to study the Van Allen  
1491 radiation belts.

1492 **Astronomical Unit (AU):** The mean radius of the Earth's orbit,  $1.496 \times 10^{13}$  cm.

1493 **Aurora:** A visual phenomenon that occurs mainly in the high-latitude night sky. Auroras occur  
1494 within a band of latitudes known as the auroral oval, the location of which is dependent



1495 on the intensity of geomagnetic activity. Auroras are a result of collisions between  
 1496 precipitating charged particles (mostly electrons) and atmospheric atoms and molecules,  
 1497 exciting the atmospheric constituents. The charged particles come from the outer parts of  
 1498 the magnetosphere and guided by the geomagnetic field. Each gas (oxygen and nitrogen  
 1499 molecules and atoms) emits its own characteristic radiation when bombarded by the  
 1500 precipitating particles. Since the atmospheric composition varies with altitude, and the  
 1501 faster precipitating particles penetrate deeper into the atmosphere, certain auroral colors  
 1502 originate preferentially from certain heights in the sky. The auroral altitude range is 80 to  
 1503 500 km, but typical auroras occur 90 to 250 km above the ground. The color of the  
 1504 typical aurora is yellow-green, from a specific transition line of atomic oxygen. Auroral  
 1505 light from lower levels in the atmosphere is dominated by blue and red bands from  
 1506 molecular nitrogen and molecular oxygen. Above 250 km, auroral light is characterized  
 1507 by a red spectral line of atomic oxygen. To an observer on the ground, the combined light  
 1508 of these three fluctuating, primary colors produces an extraordinary visual display.  
 1509 Auroras in the Northern Hemisphere are called the aurora borealis or “northern lights”.  
 1510 Auroras in the Southern Hemisphere are called aurora australis. The patterns and forms of  
 1511 the aurora include quiescent “arcs”, rapidly moving “rays” and “curtains,” “patches,” and  
 1512 “veils.”

1513 **Auroral Electrojet (AE):** See Electrojet.

1514 **Auroral Oval:** An elliptical band around each geomagnetic pole ranging from about 75 degrees  
 1515 magnetic latitude at local noon to about 67 degrees magnetic latitude at midnight under  
 1516 average conditions. It is the locus of those locations of the maximum occurrence of  
 1517 auroras, and widens to both higher and lower latitudes during the expansion phase of a  
 1518 magnetic substorm.

1519 **Beta** (e.g., low-beta plasma): The ratio of the thermal pressure to the magnetic ‘pressure’ in a  
 1520 plasma -  $p / (B^2 / (8\pi))$  in centimeter-gram-second (c.g.s.)

1521 **Bow Shock** (Earth, heliosphere): A collisionless shock wave in front of the magnetosphere  
 1522 arising from the interaction of the supersonic solar wind with the Earth's magnetic field.  
 1523 An analogous shock is the heliospheric bow shock which exists in front of the

1524 heliosphere and is due to the interaction of the interstellar wind with the solar wind and  
1525 the interplanetary magnetic field.

1526 **Charge Exchange:** An interaction between a charged particle and a neutral atom wherein the  
1527 charged particle becomes neutral and the neutral particle becomes charged through the  
1528 exchange of an electron.

1529 **Cloud** (magnetic): see Magnetic Cloud.

1530 **Collisional** (de-) **Excitation:** Excitation of an atom or molecule to a higher energy state due to a  
1531 collision with another atom, molecule, or ion. The higher energy state generally refers to  
1532 electrons in higher energy around atoms. Deexcitation is the reduction of a higher  
1533 electron energy state to a lower one, usually accomplished by a collision with another  
1534 atom, molecule or ion.

1535 **Convection** (magnetospheric, plasma, thermal): The bulk transport of plasma (or gas) from one  
1536 place to another, in response to mechanical forces (for example, viscous interaction with  
1537 the solar wind) or electromagnetic forces. Thermal convection, due to heating from below  
1538 and the gravitational field, is what drives convection inside the Sun. Magnetospheric  
1539 convection is driven by the dragging of the Earth's magnetic field and plasma together by  
1540 the solar wind when the magnetic field becomes attached to the magnetic field in the  
1541 solar wind.

1542 **Coriolis Force:** In the frame of a rotating body (such as the Earth), a force due to the bodily  
1543 rotation. All bodies that are not acted upon by some force have the tendency to remain in  
1544 a state of rest or of uniform rectilinear motion (Newton's First Law) so that this force is  
1545 called a "fictitious" forces. It is a consequence of the continuous acceleration which must  
1546 be applied to keep a body at rest in a rotating frame of reference.

1547 **Corona:** The outermost layer of the solar atmosphere, characterized by low densities ( $<10^9 \text{ cm}^{-3}$   
1548 or  $10^{15} \text{ m}^{-3}$ ) and high temperatures ( $>10^6 \text{ K}$ ).

1549 **Coronal Hole:** An extended region of the solar corona characterized by exceptionally low  
1550 density and in a unipolar photospheric magnetic field having "open" magnetic field  
1551 topology. Coronal holes are largest and most stable at or near the solar poles, and are a

1552 source of high speed (700-800 km/s) solar wind. Coronal holes are visible in several  
1553 wavelengths, most notably solar x-rays visible only from space, but also in the He 1083  
1554 nm line which is detectable from the surface of the Earth. In soft x-ray images (photon  
1555 energy of ~0.1-1.0 keV or a wavelength of 10-100 Å), these regions are dark, thus the  
1556 name "holes".

1557 **Coronal Mass Ejection (CME):** A transient outflow of plasma from or through the solar  
1558 corona. CMEs are often but not always associated with erupting prominences,  
1559 disappearing solar filaments, and flares.

1560 **Corotation** (with the Earth): A plasma in the magnetosphere of the Earth is said to be corotating  
1561 with the Earth if the magnetic field drags the plasma with it and together they have a 24  
1562 hour rotation period.

1563 **Cosmic Ray** (galactic, solar): Extremely energetic (relativistic) charged particles or  
1564 electromagnetic radiation, primarily originating outside of the Earth's magnetosphere.  
1565 Cosmic rays usually interact with the atoms and molecules of the atmosphere before  
1566 reaching the surface of the Earth. The nuclear interactions lead to formation of daughter  
1567 products, and they in turn to granddaughter products, etc. Thus there is a chain of  
1568 reactions and a "cosmic ray shower". Some cosmic rays come from outside the solar  
1569 system while others are emitted from the Sun in solar flares. See also Anomalous Cosmic  
1570 Ray; Energetic Particle; Solar Energetic Particle (SEP) Event.

1571 **Constellation Observing System for Meteorology, Ionosphere and Climate-2 (COSMIC II):**  
1572 A joint Taiwan National Space Organization (NSPO)-U.S. National Oceanic and Atmospheric  
1573 Administration (NOAA) mission of six satellites in low-inclination orbit to study the Earth's  
1574 ionosphere.

1575

1576 **Corotating Interaction Region (CIR):** An interplanetary region of high magnetic fields and  
1577 plasma densities created by the interaction of a high speed solar wind stream with the upstream  
1578 slow solar wind. The antisunward portion of the CIR is compressed slow solar wind plasma and  
1579 magnetic fields, and the sunward portion is compressed fast solar wind plasma and magnetic  
1580 fields. The two regions of the CIR are separated by a tangential discontinuity.

- 1581
- 1582 **Cyclotron Frequency:** When a particle of charge  $q$  moves in a magnetic field  $B$ , the particle  
1583 orbits, or gyrates around the magnetic field lines. The cyclotron frequency is the  
1584 frequency of this gyration, and is given by  $\omega_c = q|B|/mc$ , where  $m$  is the mass of the  
1585 particle, and  $c$  is the velocity of light (in centimeter-gram-second (c.g.s.) units).
- 1586 **Cyclotron Resonance:** The frequency at which a charged particle experiences a Doppler-shifted  
1587 wave at the particle's cyclotron frequency. Because the particle and wave may be  
1588 traveling at different speeds and in different directions, there is usually a Doppler shift  
1589 involved.
- 1590 **D Region:** A daytime region of the Earth's ionosphere beginning at approximately 40 km,  
1591 extending to 90 km altitude. Radio wave absorption in this region can be significantly  
1592 increased due to increasing ionization associated with the precipitation of solar energetic  
1593 particles through the magnetosphere and into the ionosphere.
- 1594 **Diffusion:** The slow, stochastic motion of particles.
- 1595 **Diffusive Shock Acceleration:** Charged particle acceleration at a collisionless shock due to  
1596 stochastic scattering processes caused by waves and plasma turbulence. See also Shock  
1597 Wave (collisionless).
- 1598 **Dipole Magnetic Field:** A magnetic field whose intensity decreases as the cube of the distance  
1599 from the source. A bar magnet's field and the magnetic field originating in the Earth's  
1600 core are both approximately dipole magnetic fields.
- 1601 **Drift** (of ions/electrons): As particles gyrate around magnetic field lines, their orbits may "drift"  
1602 perpendicular to the local direction of the magnetic field. This occurs if there is a force  
1603 also perpendicular to the field - e.g. an electric field, curvature in the magnetic field  
1604 direction, or gravity.
- 1605 **Driver Gas:** A mass of plasma and entrained magnetic field that is ejected from the Sun, that has  
1606 a velocity higher than the upstream plasma, and which "drives" a (usually collisionless)  
1607 shock wave ahead of itself. The magnetic cloud within an ICME is the same thing as a  
1608 driver gas.

- 1609 **Dst Index:** A measure of variation in the geomagnetic field due to the equatorial ring current. It  
1610 is computed from the H-components at approximately four near-equatorial stations at  
1611 hourly intervals. At a given time, the Dst index is the average of variation over all  
1612 longitudes; the reference level is set so that Dst is statistically zero on internationally  
1613 designated quiet days. An index of -50 nT (nanoTesla) or less indicates a storm-level  
1614 disturbance, and an index of -200 nT or less is associated with middle- latitude auroras.  
1615 Dst is determined by the World Data Center C2 for Geomagnetism, Kyoto University,  
1616 Kyoto, Japan.
- 1617 **Dynamo** (solar magnetospheric): The conversion of mechanical energy (rotation in the case of  
1618 the Sun) into electrical current. This is the process by which magnetic fields are amplified  
1619 by the induction of plasmas being forced to move perpendicular to the magnetic field  
1620 lines. See also Mean Field Electro-Dynamics.
- 1621 **E-Region:** A daytime region of the Earth's ionosphere roughly between the altitudes of 90 and  
1622 160 km. The E-region characteristics (electron density, height, etc.) depend on the solar  
1623 zenith angle and the solar activity. The ionization in the E layer is caused mainly by x-  
1624 rays in the range 0.8 to 10.4 nm coming from the Sun.
- 1625 **Ecliptic Plane:** The plane of the Earth's orbit about the Sun. It is also the Sun's apparent annual  
1626 path, or orbit, across the celestial sphere.
- 1627 **Electrically Charged Particle:** Electrons and protons, for example, or any atom from which  
1628 electrons have been removed to make it into a positively charged ion. The elemental  
1629 charge of particles is  $4.8 \times 10^{-10}$  esu. An electron and proton have this charge. Combined (a  
1630 hydrogen atom), the charge is zero. Ions have multiples of this charge, depending on the  
1631 number of electrons which have been removed (or added).
- 1632 **Electrojet:** (1) Auroral Electrojet (AE): A current that flows in the ionosphere at a height of  
1633 ~100 km in the auroral zone. (2) Equatorial Electrojet: A thin electric current layer in the  
1634 ionosphere over the dip equator at about 100 to 115 km altitude.
- 1635 **Electron Plasma Frequency/Wave:** The natural frequency of oscillation of electrons in a  
1636 neutral plasma (e.g., equal numbers of electrons and protons).

- 1637 **Electron Volt (eV):** The kinetic energy gained by an electron or proton being accelerated in a  
 1638 potential drop of one Volt.
- 1639 **ESA:** European Space Agency
- 1640 **Extreme Ultraviolet (EUV):** A portion of the electromagnetic spectrum from approximately 10  
 1641 to 100 nm.
- 1642 **Extremely Low Frequency (ELF):** That portion of the radio frequency spectrum from 30 to  
 1643 3000 Hz.
- 1644 **Fast Mode (wave/speed):** In magnetohydrodynamics, the fastest wave speed possible.  
 1645 Numerically, this is equal to the square root of the sum of the squares of the Alfvén speed  
 1646 and plasma sound speed.
- 1647 **Field Aligned Current:** A current flowing along (or opposite to) the magnetic field direction.
- 1648 **Filament:** A mass of gas suspended over the chromosphere by magnetic fields and seen as dark  
 1649 ribbons threaded over the solar disk. A filament on the limb of the Sun seen in emission  
 1650 against the dark sky is called a prominence. Filaments occur directly over magnetic-  
 1651 polarity inversion lines, unless they are active.
- 1652 **Flare:** A sudden eruption of energy in the solar atmosphere lasting minutes to hours, from which  
 1653 radiation and energetic charged particles are emitted. Flares are classified on the basis of  
 1654 area at the time of maximum brightness in H alpha.
- 1655 Importance 0 (Subflare): < 2.0 hemispheric square degrees
- 1656 Importance 1: 2.1-5.1 square degrees
- 1657 Importance 2: 5.2-12.4 square degrees
- 1658 Importance 3: 12.5-24.7 square degrees
- 1659 Importance 4:  $\geq$  24.8 square degrees
- 1660 [One square degree is equal to  $(1.214 \times 10^4 \text{ km})^2 = 48.5$  millionths of the  
 1661 visible solar hemisphere.] A brightness qualifier F, N, or B is generally appended

1662 to the importance character to indicate faint, normal, or brilliant (for example,  
1663 2B).

1664 **Flux Rope:** A magnetic phenomenon which has a force-free field configuration.

1665 **Force Free Field:** A magnetic field which exerts no force on the surrounding plasma. This can  
1666 either be a field with no flowing electrical currents or a field in which the electrical  
1667 currents all flow parallel to the field.

1668 **Free Energy** (of a plasma): When an electron or ion distribution is either non-Maxwellian or  
1669 anisotropic, they are said to have free energy" from which plasma waves can be  
1670 generated via instabilities. The waves scatter the particles so they become more isotropic,  
1671 reducing the free energy.

1672 **Frozen-in Field:** In a tenuous, collisionless plasma, the weak magnetic fields embedded in the  
1673 plasma are convected with the plasma. i.e., they are "frozen in."

1674 **Galactic Cosmic Ray (GCR):** See Cosmic Ray.

1675 **Gamma Ray:** Electromagnetic radiation at frequencies higher than x-rays.

1676 **Geomagnetic Storm:** A worldwide disturbance of the Earth's magnetic field, distinct from  
1677 regular diurnal variations. A storm is precisely defined as occurring when  $D_{ST}$  becomes  
1678 less than -50 nT (See geomagnetic activity).

1679 Main Phase: Of a geomagnetic storm, that period when the horizontal magnetic field at  
1680 middle latitudes decreases, owing to the effects of an increasing magnetospheric ring  
1681 current. The main phase can last for hours, but typically lasts less than 1 day.

1682 Recovery Phase: Of a geomagnetic storm, that period when the depressed northward field  
1683 component returns to normal levels. Recovery is typically complete in one to two days.

1684 **Geomagnetically Induced Currents (GICs):** Currents flowing along electric power  
1685 transmission systems and other electrically conducting infrastructures are produced by  
1686 naturally induce geoelectric fields during geomagnetic disturbances.

1687 **Geosynchronous Orbit:** Term applied to any equatorial satellite with an orbital velocity equal to  
1688 the rotational velocity of the Earth. The geosynchronous altitude is near 6.6 Earth radii

1689 (approximately 36,000 km above the Earth's surface). To be geostationary as well, the  
1690 satellite must satisfy the additional restriction that its orbital inclination be exactly zero  
1691 degrees. The net effect is that a geostationary satellite is virtually motionless with respect  
1692 to an observer on the ground.

1693 **GeV:**  $10^9$  electron Volts (Giga-electron Volt).

1694 **Global Navigation Satellite System (GNSS):** GNSS receivers use the orbiting satellite Global  
1695 Positioning System (GPS) transmitted signals to obtain the geographic location of a  
1696 user's receiver anywhere in the world.

1697 **Global Positioning System (GPS):** is a global navigation satellite system that provides  
1698 geolocation and time information to a GPS receiver anywhere on or near the Earth where  
1699 there is an unobstructed line of sight to four or more GPS satellites.

1700 **Global-scale Observations of the Limb and Disk (GOLD):** a NASA mission to “ investigate  
1701 the dynamic intermingling of space and Earth's uppermost atmosphere”

1702 **Heliosphere:** The magnetic cavity surrounding the Sun, carved out of the galaxy by the solar  
1703 wind.

1704 **Heliospheric Current Sheet (HCS):** This is the surface dividing the northern and southern  
1705 magnetic field hemispheres in the solar wind. The magnetic field is generally one polarity  
1706 in the north and the opposite in the south so just one surface divides the two polarities.  
1707 However, the Sun's magnetic field changes over the 11-year solar sunspot cycle and  
1708 reverses polarity at solar maximum. The same thing happens in the magnetic field carried  
1709 away from the Sun by the solar wind so the HCS only lies in the equator near solar  
1710 minimum. It is called a "current sheet" because it carries an electrical current to balance  
1711 the oppositely directed field on either side of the surface. It is very thin on the scale of the  
1712 solar system - usually only a few proton gyroradii, or less than 100,000 km.

1713 **Helmet Streamer:** See Streamer.

1714 **High Frequency (HF):** That portion of the radio frequency spectrum between 3 and 30 MHz.

1715 **Heliospheric Plasma Sheet (HPS):** A high density slow solar wind region that is located  
1716 adjacent to the heliospheric current sheet (HCS).



- 1717 **High Speed Solar Wind (HSS):** A solar wind with speeds of 750 to 800 km/s emanating from  
1718 solar coronal holes. The HSS is characterized by embedded, particularly large amplitude  
1719 Alfvén waves. At the edges of HSSs, the velocities can be less due to superradial  
1720 expansion effects.
- 1721 **Instability:** When an electron or ion distribution is sufficiently anisotropic, it becomes unstable  
1722 (instability), generating plasma waves. The anisotropic distribution provides a source of  
1723 free energy for the instability. A simple analog is a stick, which if stood on end is  
1724 "unstable," but which if laid on its side is "stable." In this analog, gravity pulls on the  
1725 stick and provides a source of free energy when the stick is stood on end.
- 1726 **Interplanetary Magnetic Field (IMF, Parker spiral):** The magnetic field carried with the solar  
1727 wind and twisted into an Archimedean spiral by the Sun's rotation.
- 1728 **Interplanetary Medium:** The volume of space in the solar system that lies between the Sun and  
1729 the planets. The solar wind flows in the interplanetary medium.
- 1730 **Interplanetary Coronal Mass Ejection (ICME):** The evolutionary part of a CME as it propagates  
1731 through interplanetary space. Typically after the CME has propagated 1 AU from the Sun,  
1732 the ICME only contains the magnetic cloud (MC) portion of the initial three parts of a  
1733 CME. The MC may also have been compressed/expanded or rotated by the time it reaches  
1734 1 AU.
- 1735 **Interplanetary Shock:** A fast forward shock is characterized by a sharp increase in solar wind  
1736 speed, plasma density, plasma temperature and magnetic field magnitude. The shock  
1737 reduces the upstream plasma from a supermagnetosonic state to a subsonic state, much as  
1738 an airplane wing sonic shock reduces the relative flow of air from a supersonic speed  
1739 (relative to the airplane) to a subsonic speed. A fast (magnetosonic) forward (propagating  
1740 in the direction of the "piston", in this case the propagation of the ICME in the antisolar  
1741 direction) shock is detected upstream (antisolarward) of fast ICMEs. A reverse shock  
1742 propagates in the direction of the Sun. Planetary bow shocks are reverse shocks. There  
1743 are other types of shocks not discussed in this paper: slow shocks and intermediate shocks.

- 1744 **Interstellar** (gas, neutral gas, ions, cosmic rays, wind, magnetic field, etc.) Literally, between  
1745 the stars. In practical terms, it is anything beyond the outer boundary of the solar wind  
1746 (the "heliopause") yet within the Milky Way.
- 1747 **Ion:** (1). An electrically charged atom or molecule. (2). An atom or molecular fragment that has  
1748 a positive electrical charge due to the loss of one or more electrons; the simplest ion is the  
1749 hydrogen nucleus, a single proton.
- 1750 **Ionization State:** The number of electrons missing from an atom.
- 1751 **Ionosphere:** The region of the Earth's upper atmosphere containing free (not bound to an atom  
1752 or molecule) electrons and ions. This ionization is produced from the neutral atmosphere  
1753 by solar ultraviolet radiation at very short wavelengths (<100 nm) and also by  
1754 precipitating energetic particles.
- 1755 **Ionospheric Storm:** A positive ionospheric storm is where the ionospheric total electron content  
1756 (TEC) increases. A negative ionospheric storm is an event where the ionospheric TEC  
1757 decreases.
- 1758 **Ionospheric Connection Explorer (ICON):** is a NASA 2-year mission that will give new views  
1759 of the boundary between our atmosphere and space, where planetary weather and **Space**  
1760 **Weather** meet.
- 1761 **Irradiance:** Radiant energy flux density on a given surface (e. g.  $\text{ergs cm}^{-2}\text{s}^{-1}$ ).
- 1762 **keV:** 1000 electron Volts (kiloelectron Volt). See electron Volt. See also Anisotropic Plasma;  
1763 Plasma.
- 1764 **L value:** For a dipole magnetic field, the field line that crosses the magnetic equator at a L value  
1765 equal to the number in Earth radii.
- 1766 **Loop** (solar-loop prominence system): A magnetic loop is the flux tube which crosses from one  
1767 polarity to another. A loop prominence bridges a magnetic inversion line across which  
1768 the magnetic field changes direction. See also Magnetic Foot Point; Prominence.
- 1769 **Loss Cone:** A small cone angle about the ambient magnetic field direction where  
1770 magnetospheric charged particles with velocity vectors within the cone will mirror at

1771 sufficiently low altitudes such that the particle will have collisions with atmospheric  
 1772 atoms and molecules and will be “lost” from returning to the magnetosphere.

1773 **Loss Cone Instability:** An instability generated by a plasma anisotropy where the temperature  
 1774 perpendicular to the magnetic field is greater than the temperature parallel to the field.  
 1775 This instability gets its name because this condition exists in the Earth's magnetosphere  
 1776 and the "loss cone" particles are those that are lost into the upper atmosphere.

1777 **Magnetic Cloud:** A region in the solar wind of about 0.25 AU or more in radial extent in which  
 1778 the magnetic field strength is high and the direction of one component of the magnetic  
 1779 field changes appreciably by means of a rotation nearly parallel to a plane. Magnetic  
 1780 clouds may be parts of the driver gases (coronal mass ejections) in the interplanetary  
 1781 medium.

1782 **Magnetic Foot Point:** For the Earth’s magnetic field lines, where the magnetic field enters the  
 1783 surface of the Earth.

1784 **Magnetic Mirror:** Char particles moving into a region of converging magnetic flux (as at the  
 1785 pole of a magnet) will experience "Lorentz" forces that slow the particles and "mirror"  
 1786 them by eventually reversing their direction if the particles are initially moving slowly  
 1787 enough along the field line. See also Mirror Point.

1788 **Magnetic Reconnection:** The act of interconnection between oppositely directed magnetic field  
 1789 lines. [Magnetic reconnection is recognized as a basic plasma process, which converts](#)  
 1790 [magnetic energy into plasma kinetic energy accompanied by topological changes in the](#)  
 1791 [magnetic field configuration. It does not allow an excessive buildup of magnetic energy](#)  
 1792 [in the current sheets.](#)

1793 **Magnetic Storm:** see Geomagnetic Storm.

1794 **Magnetopause:** The boundary surface between the solar wind and magnetosphere, where the  
 1795 pressure of the magnetic field of the object effectively equals the ram pressure of the  
 1796 solar wind plasma.

1797 **Magnetosheath:** The region between the bow shock and the magnetopause, characterized by  
 1798 very turbulent plasma. This plasma has been heated (shocked) and slowed as it passed

1799 through the bow shock. For the Earth, along the Sun-Earth axis, the magnetosheath is  
1800 about 3 Earth radii thick.

1801 **Magnetosonic Speed** (acoustic speed): The speed of the fastest low frequency magnetic waves  
1802 in a magnetized plasma. It is the equivalent of the sound speed in a neutral gas or non-  
1803 magnetized plasma.

1804 **Magnetosphere**: The magnetic cavity surrounding a magnetized planet, carved out of the  
1805 passing solar wind by virtue of the planetary magnetic field, which prevents, or at least  
1806 impedes, the direct entry of the solar wind plasma into the cavity.

1807 **Magnetospheric Multiscale Mission (MMS)**: A NASA mission designed to spend extensive  
1808 periods in locations where magnetic reconnection at the magnetopause/magnetotail is  
1809 expected to occur. The critical electron diffusion region will be studied. The mission  
1810 consists of 4 spacecraft flown in a tetrahedron configuration.

1811 **Magnetotail**: The extension of the magnetosphere in the anti-sunward direction as a result of  
1812 interaction with the solar wind. In the inner magnetotail, the field lines maintain a  
1813 roughly dipolar configuration. But at greater distances in the anti-sunward direction, the  
1814 field lines are stretched into northern and southern lobes, separated by a plasmashet.  
1815 There is observational evidence for traces of the Earth's magnetotail as far as 1000 Earth  
1816 radii downstream, in the anti-solar direction.

1817 **Maxwellian Distribution**: The minimum energy particle distribution for a given temperature. It  
1818 is also the equilibrium distribution in the absence of losses due to radiation, collisions,  
1819 etc.

1820 **Mean Free Path**: The statistically most probably distance a particle travels before undergoing a  
1821 collision with another particle or interacting with a wave.

1822 **Mesosphere**: The region of the Earth's atmosphere between the upper limit of the stratosphere  
1823 (approximately 30 km altitude) and the lower limit of the thermosphere (approximately  
1824 80 km altitude).

1825 **MeV**: One million electron Volts (Megaelectron Volt). See also Electron Volt.

1826 **Mirror Point:** The point where the charged particles reverse direction (mirrors). At this point, all  
1827 of the particle motion is perpendicular to the local ambient magnetic field. See also  
1828 Magnetic Mirror.

1829 **Parker Solar Probe:** a NASA robotic spacecraft to probe the outer corona of the Sun. It will  
1830 approach to within 9.9 solar radii (6.9 million kilometers or 4.3 million miles from the  
1831 center of the Sun and will travel, at closest approach, as fast as 690,000 km/h  
1832 (430,000 mph).

1833 **Photosphere:** The lowest visible layer of the solar atmosphere; corresponds to the solar surface  
1834 viewed in white light. Sunspots and faculae are observed in the photosphere.

1835 **Pickup Ion:** An ion which has entered the solar system as a neutral particle and then becomes  
1836 ionized either through charge exchange or photoionization. It is called a pickup ion  
1837 because as soon as the neutral atom is ionized, it becomes attached to the magnetic field  
1838 carried by the solar wind and so is "picked up" by the solar wind.

1839 **Pitch Angle:** In a plasma, the angle between the instantaneous velocity vector of a charged  
1840 particle and the direction of the ambient magnetic field.

1841 **Plasma** (ions, electrons): A gas that is sufficiently ionized so as to affect its dynamical behavior.  
1842 A plasma is a good electrical conductor and is strongly affected by magnetic fields. See  
1843 also Anisotropic Plasma; Isotropic Plasma.

1844 **Plasma Instability** (ion, electron): When a plasma is sufficiently anisotropic, plasma waves  
1845 grow, which in turn alter the distribution via wave-particle interactions. The plasma is  
1846 "unstable."

1847 **Plasma Sheet:** A region in the center of the magnetotail between the north and south lobes. The  
1848 plasma sheet is characterized by hot, dense plasma and is a high beta plasma region, in  
1849 contrast to the low beta lobes. The plasma sheet bounds the neutral sheet where the  
1850 magnetic field direction reverses from Earthward (north lobe direction) to anti-Earthward  
1851 (south lobe direction).

1852 **Plasma Wave** (electrostatic/electromagnetic): A wave generated by plasma instabilities or other  
1853 unstable modes of oscillation allowable in a plasma. "Chorus" and "Plasmasheric Hiss"

1854 are whistler wave modes. These are electromagnetic waves with frequencies below the  
1855 electron cyclotron frequency. Electromagnetic ion cyclotron (EMIC) waves are ion  
1856 cyclotron waves with frequencies below the proton cyclotron frequency.

1857 **Polar Cap Absorption Event (PCA):** An anomalous condition of the polar ionosphere whereby  
1858 HF and VHF (3-300 MHz) radio waves are absorbed, and LF and VLF (3-300 kHz) radio  
1859 waves are reflected at lower altitudes than normal. The cause is energetic particle  
1860 precipitation into the ionosphere/atmosphere. The enhanced ionization caused by this  
1861 precipitation leads to cosmic radio noise absorption and attenuation of that noise at the  
1862 surface of the Earth. PCAs generally originate with major solar flares, beginning within a  
1863 few hours of the event (after the flare particles have propagated to the Earth) and  
1864 maximizing within a day or two after onset. As measured by a riometer (relative  
1865 ionospheric opacity meter), the PCA event threshold is 2 dB of absorption at 30 MHz for  
1866 daytime and 0.5 dB at night. In practice, the absorption is inferred from the proton flux at  
1867 energies greater than 10 MeV, so that PCAs and proton events are simultaneous.  
1868 However, the transpolar radio paths may still be disturbed for days, up to weeks,  
1869 following the end of a proton event, and there is some ambiguity about the operational  
1870 use of the term PCA.

1871 **Prominence:** A term identifying cloud-like features in the solar atmosphere. The features appear  
1872 as bright structures in the corona above the solar limb and as dark filaments when seen  
1873 projected against the solar disk. Prominences are further classified by their shape (for  
1874 example, mound prominence, coronal rain) and activity. They are most clearly and most  
1875 often observed in H alpha. See also Loop.

1876 **Radiation Belt:** Regions of the magnetosphere roughly 1.2 to 6 Earth radii above the equator in  
1877 which charged particles are stably trapped by closed geomagnetic field lines. There are  
1878 two belts. The inner belt's maximum proton density lies near 5000 km above the Earth's  
1879 surface. Inner belt protons (10s of MeV) and electrons (100s of keV) and originate from  
1880 the decay of secondary neutrons created during collisions between cosmic rays and upper  
1881 atmospheric particles. The outer belt extends on to the magnetopause on the sunward side  
1882 (10 Earth radii under normal quiet conditions) and to about 6 Earth radii on the nightside.  
1883 The altitude of maximum proton density is near 16,000-20,000 km. Outer belt protons

1884 and electrons are lower energy (about 200 eV to 1 MeV). The origin of the particles  
1885 (before they are energized to these high energies) is a mixture of the solar wind and the  
1886 ionosphere. The outer belt is also characterized by highly variable fluxes of energetic  
1887 electrons. The radiation belts are often called the “Van Allen radiation belts” because  
1888 they were discovered in 1958 by a research group at the University of Iowa led by  
1889 Professor J. A. Van Allen. See also Trapped Particle.

1890 **Ram Pressure:** Sometimes called “dynamic pressure”. The pressure exerted by a streaming  
1891 plasma upon a blunt object.

1892 **Reconnection:** A process by which differently directed field lines link up allowing topological  
1893 changes of the magnetic field to occur, determining patterns of plasma flow, and resulting  
1894 in conversion of magnetic energy to kinetic and thermal energy of the plasma.  
1895 Reconnection is invoked to explain the energization and acceleration of the  
1896 plasmas/energetic particles that are observed in solar flares, magnetic substorms and  
1897 storms, and elsewhere in the solar system.

1898 **Relativistic:** Charged particles (ions or electrons) which have speeds comparable to the speed of  
1899 light.

1900 **Ring Current:** In the magnetosphere, a region of current that flows near the geomagnetic  
1901 equator in the outer belt of the two Van Allen radiation belts. The current is produced by  
1902 the gradient and curvature drift of the trapped charged particles of energies of 10 to 300  
1903 keV. The ring current is greatly augmented during magnetic storms because of the hot  
1904 plasma injected from the magnetotail and upwelling oxygen ions from the ionosphere.  
1905 Further acceleration processes bring these ions and electrons up to ring current energies.  
1906 The ring current (which is a diamagnetic current) causes a worldwide depression of the  
1907 horizontal geomagnetic field during a magnetic storm.

1908 **Solar Energetic Particle (SEP):** An energetic particle of solar flare/interplanetary shock origin.

1909 **Sheath:** The plasma and magnetic fields in the downstream subsonic region after collisionless  
1910 shocks. See Shock Wave.

1911 **Shock Wave:** A shock wave is characterized by a discontinuous change in pressure, density,  
 1912 temperature, and particle streaming velocity, propagating through a compressible fluid or  
 1913 plasma. Fast collisionless shock waves occur in the solar wind when fast solar wind  
 1914 overtakes slow solar wind with the difference in speeds being greater than the  
 1915 magnetosonic speed. Collisionless shock thicknesses are determined by the proton and  
 1916 electron gyroradii rather than the collision lengths. See also Diffusive Shock  
 1917 Acceleration; Solar Wind Shock.

1918 **Solar Corona:** See Corona.

1919 **Solar Cycle:** The approximately 11 year quasi-periodic variation in the sunspot number. The  
 1920 polarity pattern of the magnetic field reverses with each cycle. Other solar phenomena,  
 1921 such as the 10.7-cm solar radio emission, exhibit similar cyclical behavior. The solar  
 1922 magnetic field reverses each sunspot cycle so there is a corresponding 22 year solar  
 1923 magnetic cycle.

1924 **Solar Energetic Particle (SEP) Event:** A high flux event of solar (low energy) cosmic rays.  
 1925 This is commonly generated by larger solar flares or CME shocks, and lasts, typically  
 1926 from minutes to days. See also Cosmic Ray.

1927 **Solar Flares:** Transient perturbations of the solar atmosphere as measured by enhanced x-ray  
 1928 emission (see x-ray flare class), typically associated with flares. Five standard terms are  
 1929 used to describe the activity observed or expected within a 24-h period:

1930           Very low - x-ray events less than C-class.

1931           Low - C-class x-ray events.

1932           Moderate - isolated (one to 4) M-class x-ray events.

1933           High - several (5 or more) M-class x-ray events, or isolated (one to 4).

1934           M5 or greater x-ray events.

1935           Very high - several (5 or more) M5 or greater x-ray events.

1936



- 1937 **Solar Maximum:** The month(s) during the sunspot cycle when the smoothed sunspot number  
1938 reaches a maximum.
- 1939 **Solar Minimum:** The month(s) during the sunspot cycle when the smoothed sunspot number  
1940 reaches a minimum.
- 1941 **Solar Orbiter:** A European Space Agency-led (ESA) mission intended to perform detailed  
1942 measurements of the inner heliosphere and nascent solar wind to answer the question "How does  
1943 the Sun create and control the heliosphere?" The mission will make observations of the Sun from  
1944 an eccentric orbit moving as close as ~60 solar radii ( $R_S$ ), or 0.284 astronomical units (AU) from  
1945 the Sun.
- 1946 **Solar Wind:** The outward flow of solar particles and magnetic fields from the Sun. Typically at  
1947 1 AU, solar wind velocities are 300-800 km/s and proton and electron densities of 3-7 per  
1948 cubic centimeter (roughly inversely correlated with velocity). The total intensity of the  
1949 interplanetary magnetic field is nominally 3-8 nT.
- 1950 **SORCE: Solar Radiation and Climate Experiment.** A NASA mission that measures  
1951 electromagnetic radiation produced by the Sun and the power per unit area of that energy  
1952 on the Earth's surface.
- 1953 **Space Weather:** Dynamic variations at the Sun, in interplanetary space, in the Earth's and  
1954 planetary magnetospheres, ionospheres and atmospheres associated with space  
1955 phenomena.
- 1956 **Stratosphere:** That region of the Earth's atmosphere between the troposphere and the  
1957 mesosphere. It begins at an altitude of temperature minimum at approximately 13 km and  
1958 defines a layer of increasing temperature up to about 30 km.
- 1959 **Streamer:** A feature of the white light solar corona (seen in eclipse or with a coronagraph) that  
1960 looks like a ray extending away from the Sun out to about 1 solar radius, having an arch-  
1961 like base containing a cavity usually occupied by a prominence.
- 1962 **Substorm:** A substorm corresponds to an injection of charged particles from the magnetotail into  
1963 the nightside magnetosphere. Plasma instabilities lead to the precipitation of the particles

1964 into the auroral zone ionosphere, producing intense aurorae. Potential drops along  
 1965 magnetic field lines lead to the acceleration of ~1 to 10 keV electrons with brilliant  
 1966 displays of aurora as the electrons impact the upper atmosphere. Enhanced ionospheric  
 1967 conductivity and externally imposed electric fields lead to the intensification of the  
 1968 auroral electrojets.

1969 **Sudden Impulse (SI):** An abrupt (10s of seconds) jump in the Earth's surface magnetic field.  
 1970 The positive sudden impulses (SI<sup>+</sup>s) are caused by fast forward shock impingement onto  
 1971 the magnetosphere.

1972 **Sunspot:** An area seen as a dark spot, in contrast with its surroundings, on the photosphere of the  
 1973 Sun. Sunspots are concentrations of magnetic flux, typically occurring in bipolar clusters  
 1974 or groups. They appear dark because they are cooler than the surrounding photosphere.  
 1975 Larger and darker sunspots sometimes are surrounded (completely or partially) by  
 1976 penumbrae. The dark centers are umbrae. The smallest, immature spots are sometimes  
 1977 called pores.

1978 **Supersubstorm:** Defined as an event with SML < -2500 nT. These auroral zone events appear  
 1979 to have different evolutionary properties than the standard (Akasofu, 1964) auroral  
 1980 substorms.

1981 **SWARM:** A European Space Agency (ESA) mission originally instrumented to study the Earth's  
 1982 magnetic field. The current goals are to study magnetospheric-ionospheric coupling and  
 1983 auroral Space Weather problems.

1984 **Telsa:** A unit of magnetic flux density (Weber/m<sup>2</sup>). A nanoTesla (nT) is 10<sup>-9</sup> Teslas.

1985 **Termination Shock:** The shock wave in the solar wind which is caused by the abrupt  
 1986 deceleration of the solar wind as it runs into the local interstellar medium (LISM). It is  
 1987 thought to lie somewhere between 70 and 150 AU from the Sun.

1988 **Thermal Speed** (ion, electron): The random velocity of a particle associated with its  
 1989 temperature.

1990 **Thermosphere:** That region of the Earth's atmosphere where the neutral temperature increases  
 1991 with height. It begins above the mesosphere at about 80-85 km and extends upward to the  
 1992 exosphere.

1993 **TIMED:** Thermosphere Ionosphere Mesosphere Energetics and Dynamics (TIMED). A NASA  
 1994 mission to investigate and understand the energetics of the Earth's mesosphere and lower  
 1995 thermosphere/ionosphere.

1996 **Total Electron Content (TEC):** The column density of electrons in the Earth's ionosphere.

1997 **Trapped Particle:** Particles gyrating about magnetic field lines (e.g., in the Earth's  
 1998 magnetosphere). See also Magnetic Mirror and Pitch Angle.

1999 **Troposphere:** The lowest layer of the Earth's atmosphere, extending from the ground to the  
 2000 stratosphere, approximately 13 km altitude. In the troposphere, temperature decreases  
 2001 with height.

2002 **Ultraviolet (UV):** That part of the electromagnetic spectrum between 5 and 400 nm.

2003 **Ultra Low Frequency (ULF):** 1 milliHertz to 1 Hertz.

2004 **Very High Frequency (VHF):** That portion of the radio frequency spectrum from 3 to 300  
 2005 MHz.

2006 **Very Low Frequency (VLF):** That portion of the radio frequency spectrum from 3 to 300 kHz.

2007 **Van Allen Radiation Belt:** See Radiation Belt.

2008

## 2009 REFERENCES

2010

2011 Acero, F.J., Vaquero, J.M., Gallego, M.C., and Garcia, J.A.: A limit for the values of the Dst  
 2012 geomagnetic index, *Geophys. Res. Lett.*, 45, doi.org/10.1029/2018GL079676, 2018.

2013 Agostinelli, S., et al.: GEANT4-A simulation toolkit, *Nucl. Instr. Meth. In Phys. Res. Sect. A*, 506,  
 2014 250, doi:10.1016/S0168-9002(03)01368-8, 2003.

2015 Aikio, A. T., Sergeev, V. A., Shukhtina, M. A., Vagina, L. I., Angelopoulos, V., and Reeves, G.  
 2016 D.: Characteristics of pseudobreakups and substorms observed in the ionosphere, at the

- 2017 geosynchronous orbit, and in the midtail, *J. Geophys. Res.*, *104*, 12263-12287, doi:  
2018 10.1029/1999JA900118, 1999.
- 2019 Akasofu, S.-I.: The development of the auroral substorm, *Plan. Spa. Phys.*, *12*, 273-282, 1964.
- 2020 Akasofu, S.-I.: Magnetospheric substorms, a model, in *Solar Terrestrial Physics, Part III*, edited  
2021 by D. Dyer, p. 131, D. Reidel Publ., Norwell, Mass, 1972.
- 2022 Akasofu, S.-I., and Chao, J. K.: Interplanetary shock waves and magnetospheric substorms,  
2023 *Planetary and Space Science*, *28*, 381-385, 1980.
- 2024 Akasofu, S.-I., and Kamide, Y.: Comment on “The extreme magnetic storm of 1-2 September  
2025 1859” by B.T. Tsurutani, W.D. Gonzalez, G.S. Lakhina and S. Alex, *J. Geophys. Res.*, *110*,  
2026 A09226, doi:10.1029/2005JA011005, 2005.
- 2027 Alfvén, H.: *Cosmical Electrodynamics*, Oxford at the Clarendon Press, 1950.
- 2028 Anderson, B. J., and Hamilton, D.C.: Electromagnetic ion cyclotron waves stimulated by modest  
2029 magnetospheric compressions, *J. Geophys. Res.*, *98*, A7, 11369, 1993.
- 2030 Anderson, D. N., Decker, D. T., and Valladares, C. E.: Global theoretical ionospheric model  
2031 (GTIM) in *Solar-Terrestrial Energy Program: Handbook of Ionospheric Models*, Natl. Oceanic  
2032 and Atmos. Admin, Boulder, CO, 133-152, 1996.
- 2033 Araki, T., Tsunomura, S., and Kikuchi, T.: Local time variation of the amplitude of geomagnetic  
2034 sudden commencements (SC) and SC-associated polar cap potential, *Earth Plan. Spa.*, *61*, e13-  
2035 e16, 2009.
- 2036 Araki, T.: Historically largest geomagnetic sudden commencement (SC) since 1868, *Earth, Plan.*  
2037 *Spa.*, *66*:164, <http://www.earth-planets-space.com/66/1/164>, 2014.
- 2038 Baker, D.N., Higbie, P.R., Belian, R.D., and Hones Jr., E.W.: Do Jovian electrons influence the  
2039 terrestrial outer radiation zone?, *Geophys. Res. Lett.*, *6*, 531-534,  
2040 <https://doi.org/10.1029/GL006i006p00531>, 1979.
- 2041 Baker, D.N., Pulkkinen, T.I., Angelopoulos, V., Baumjohann, W., McPherron, R.L.: Neutral line  
2042 model of substorms: Past results and present view, *J. Geophys. Res.*, *101*, 12975-13010, 1996.
- 2043 Baker, D.N., Li, X., Blake, J.B., and Kanekal, S.: Strong electron acceleration in the Earth’s  
2044 magnetosphere, *Adv. Space Res.*, *21*, 609-613, 1998.
- 2045 Barnes, C.W., and Simpson, J.A.: Evidence for interplanetary acceleration of nucleons in  
2046 corotating interaction regions, *Astrophys. J.*, *210*, L91, 1976.

- 2047 Bartels, J.: Terrestrial-magnetic activity in the years 1931 and 1932, *Terrestrial Magnetism and*  
2048 *Atmospheric Electricity*, 39, 1-4, 1934.
- 2049 Belcher, J.W., and Davis Jr., L.: Large-amplitude Alfvén waves in the interplanetary medium, 2,  
2050 *J. Geophys. Res.*, 76, 16, 3534-3563, 1971.
- 2051 Bieber, J. W., Clem, J., Evenson, P., Pyle, R., Sáiz, A., and Ruffolo, D.: *Astrophys. J.*, 771, 92,  
2052 2013.
- 2053 Blake, J.B., Kolasinski, W.A., Filius, R.W., and Mullen, E.G.: Injection of electrons and protons  
2054 with energies of tens of MeV into  $L < 3$  on March 24, 1991, *Geophys. Res. Lett.*, 19, 821, 1992.
- 2055 Bombardieri, D. J., Duldig, M. L., Humble, J. E., and Michael, K. J.: An improved model for  
2056 relativistic solar proton acceleration applied to the 2005 January 20 and earlier events,  
2057 *Astrophysical J.*, 682, 1315-1327, 2008.
- 2058 Boyd, A.J., Spence, H.E., Claudepierre, S.G., Fennell, J.F., Blake, J.B., Baker, D.N., Reeves, G.D.,  
2059 and Turner, D.L.: Quantifying the radiation belt seed population in the March 17, 2013 electron  
2060 acceleration event, *Geophys. Res. Lett.*, 41, 2275-2281, <https://doi.org/10.1002/2014GL059626>,  
2061 2014.
- 2062 Boyd, A.J., Spence, H.E., Huang, C.L., Reeves, G.D., Baker, D.N., Turner, D.L., Claudepierre,  
2063 S.G., Fennell, J.F., Blake, J.B., and Shprits, Y.Y.: Statistical properties of the radiation belt seed  
2064 population, *J. Geophys. Res.* 121, 7636-7646, <https://doi.org/10.1002/2016JA022652>, 2016.
- 2065 Bravo, S., and Otaola, J.A.: Polar coronal holes and the sunspot cycle. A new method to predict  
2066 sunspot numbers, *Sol. Phys.* 122, 335. <https://doi.org/10.1007/BF00913000>, 1989.
- 2067 Bravo, S., and Stewart, G. A.: Fast and Slow Wind from Solar Coronal Holes, *Astrophys. J.* 489,  
2068 992-999. <https://doi.org/10.1086/304789>, 1997.
- 2069 Brice, N.: Fundamentals of very low frequency emission generation mechanisms, *J. Geophys. Res.*,  
2070 69, 4701, 1964.
- 2071 Buzulukova, N., *Extreme Events in Geospace, Origins, Predictability and Consequences*, Elsevier,  
2072 Wash. D.C., 2018.
- 2073 Burlaga, L., Sittler, E., Mariani, F., and Schwenn, R.: Magnetic loop behind an interplanetary  
2074 shock: Voyager, Helios and IMP 8 observations, *J. Geophys. Res.*, 86, A8, 6673-6684, 1981.
- 2075 Burlaga, L., Fitzenreiter, R., Lepping, R., et al.: A magnetic cloud containing prominence material:  
2076 January, 1997, *J. Geophys. Res.*, 103, A1, 77-285, 1998.

- 2077 Burton, R. K., McPherron, R. L., and Russell, C. T.: An empirical relationship between  
2078 interplanetary conditions and Dst, *J. Geophys. Res.*, *80*, 4204-4214, 1975.
- 2079 Carlson, C. W., McFadden, J. P., Ergun, R. E., Temerin, M., Peria, W., Mozer, F. S., Klumpar, D.  
2080 M., Shelley, E. G., Peterson, W. K., Moebius, E., Elphic, R., Strangeway, R., Cattell, C., and Pfaff,  
2081 R.: FAST observations in the downward auroral current region: Energetic upgoing electron beams,  
2082 parallel potential drops, and ion heating, *Geophys. Res. Lett.*, *25*, 2017-2020, 1998.
- 2083 Carrington, R.C: Description of a singular appearance seen in the Sun on September 1, 1859, *Mon.*  
2084 *Not. R. Astron. Soc.*, *XX*, 13, 1859.
- 2085 Chan, A.A., Xia, M., and Chen, L.: Anisotropic Alfvén-ballooning modes in Earth's  
2086 magnetosphere, *J. Geophys. Res.*, *99*, 17351-17366, 1994.
- 2087 Chapman, S., and Bartels, J.: *Geomagnetism*, vol. 1, Oxford Univ. Press, New York, 1940.
- 2088 [Cho, K.S., Bong, S.C., Moon, Y.J., Dryer, M., Lee, S.E. and Kim, K.H.: An empirical relationship](#)  
2089 [between coronal mass ejection initial speed and solar wind dynamic pressure, \*J. Geophys. Res.\*,](#)  
2090 [115, A10111, <https://doi.org/10.1029/2009JA015139>, 2010.](#)
- 2091 Choe, G.S., LaBelle-Hamer, N., Tsurutani, B.T., and Lee, L.C.: Identification of a driver gas  
2092 boundary layer, *EOS Trans. AGU*, *73*, 485, 1992.
- 2093 Chree, C.: Review of Maunder's recent investigations on the causes of magnetic disturbances,  
2094 *Terr. Mag.*, *10*, 9-14, 1905.
- 2095 Chree, C.: Some phenomena of sunspots and of terrestrial magnetism at Kew Observatory,  
2096 *Philosophical Transactions of the Royal Society A*, *212*, 75-116, 1913.
- 2097 Christon, S.P., and Simpson, J.A.: Separation of corotating nucleon fluxes from solar flare fluxes  
2098 by radial gradients and nuclear composition, *Astrophys. J. Lett.*, *227*, L49, 1979.
- 2099 [Clauer, C.R., and Siscoe, G.: The great historical geomagnetic storm of 1859: A modern look,](#)  
2100 [Adv. Space Res. \*38\*, 117-118. <https://doi.org/10.1016/j.asr.2006.09.001>, 2006.](#)
- 2101 Cliver, E.W.: The 1859 space weather event : Then and now, *Adv. Spa. Res.*, *38*, 119-129, 2006.
- 2102 Cornwall, J.M.: Cyclotron instabilities and electromagnetic emission in the ultra low frequency  
2103 and very low frequency ranges, *J. Geophys. Res.*, *70*, 61-69, doi:10.1029/JA0761004p00900,  
2104 1965.
- 2105 Daglis, I. A., Thorne, R.M., Baumjohann, W., and Orsini, S.: The terrestrial ring current: origin,  
2106 formation and decay, *Rev. Geophys.*, *37*, 4, 407-438, 1999.

- 2107 Dasso, S., Gómez, D., and Mandrini, C. H.: Ring current decay rates of magnetic storms: A  
2108 statistical study from 1957 to 1998, *J. Geophys. Res.*, 107(A5), 1059, doi:10.1029/2000JA000430,  
2109 2002.
- 2110 Davis, T. N., and Sugiura, M.: Auroral electrojet activity index AE and its universal time  
2111 variations, *Journal of Geophysical Research*, 71, 785-801,  
2112 <https://doi.org/10.1029/JZ071i003p00785>, 1966.
- 2113 Davis, C.J., de Koning, C.A., Davies, J.A., Biesecker, D., Milward, G., Dryer, M., Deehr, C.,  
2114 Webb, D.F., Schenk, K., Freeland, S.L., Mostl, C., Farrugia, C.J., and Odstreil, D.: A comparison  
2115 of space weather analysis techniques used to predict the arrival of the Earth-directed CME and its  
2116 shock wave launched on 8 April 2010, *Space Weather* 9, S01005,  
2117 <https://doi.org/10.1029/2010SW00620>, 2011.
- 2118 Deng, Y., Sheng, C., Tsurutani, B.T., and Mannucci, A.J.: Possible influence of extreme magnetic  
2119 storms on the thermosphere in the high latitudes, *Space Weather* 16,  
2120 <https://doi.org/10.1029/2018SW001847>, 2018.
- 2121 Dessler, A.J., and Parker, E.N.: Hydromagnetic theory of magnetic storms, *J. Geophys. Res.*, 64,  
2122 2239, 1959.
- 2123 Dryer, M., Smith, Z. K., Steinolfson, R. S., Mihalov, J. D., Wolfe, J. H., and Chao, J.-K.:  
2124 Interplanetary disturbances caused by the August 1972 solar flares as observed by Pioneer 9, *J.*  
2125 *Geophys. Res.*, 81, 4651-4663, doi: 10.1029/JA081i025p04651, 1976.
- 2126 Dungey, J.W.: Interplanetary magnetic field and the auroral zones, *Phys. Rev. Lett.*, 6, 47, 1961.
- 2127 Ebihara, Y., and Ejiri, M.: Modeling of solar wind control of the ring current buildup: A case study  
2128 of the magnetic storms in April 1997, *Geophys. Res. Lett.*, 25(20), 3751–3754,  
2129 doi:10.1029/1998GL900006, 1998.
- 2130 Echer, E., Gonzalez, W.D., Tsurutani, B.T., and Gonzalez, A.L.C.: Interplanetary conditions  
2131 causing intense geomagnetic storms ( $Dst \leq -100$  nT) during solar cycle 23 (1996-2006), *J.*  
2132 *Geophys. Res.*, 113, A05221, doi:10.1029/2007JA012744, 2008a.
- 2133 Echer, E., Gonzalez, W.D., and Tsurutani, B.T.: Interplanetary conditions leading to superintense  
2134 geomagnetic storms ( $Dst \leq -250$  nT) during solar cycle 23, *Geophys. Res. Lett.*, 35, L06S03,  
2135 doi:10.1029/2007GL031755, 2008b.
- 2136 Echer, E., Tsurutani, B.T., and Guarnieri, F.L.: Solar and interplanetary origins of the November  
2137 2004 superstorms, *Adv. Spa. Res.*, 44, 615-620, 2009.

- 2138 Echer, E., Tsurutani, B.T., Guarnieri, F.L., and Kozyra, J.U.: Interplanetary fast forward shocks  
2139 and their geomagnetic effects: CAWSES events, *J. Atmosph. Sol.-Terr. Phys.*, 73, 1330-1338,  
2140 2011.
- 2141 Elkington, S.R., Hudson, M.K., and Chan, A.A.: Acceleration of relativistic electrons via drift-  
2142 resonant interaction with toroidal-mode Pc-5 ULF oscillations, *Geophys. Res. Lett.*, 26, 3273,  
2143 1999.
- 2144 Elkington, S.R., Hudson, M.K., and Chan, A.A.: Resonant acceleration and diffusion of outer zone  
2145 electrons in an asymmetric geomagnetic field, *J. Geophys. Res.*, 108, doi: 10.129/2001JA009202,  
2146 2003.
- 2147 Elvey, C. T.: Problems in auroral morphology, *Proceedings of the National Academy of Sciences*  
2148 *Jan 1957*, 43 (1) 63-75; DOI: 10.1073/pnas.43.1.63, 1957.
- 2149 Emery, B.A., Richardson, I.G., Evans, D.S., Rich, F.J.: Solar wind structure sources and  
2150 periodicities of auroral electron power over three solar cycles, *J. Atmos. Sol. Terr. Phys.* 71, 1157-  
2151 1175. <https://doi.org/10.1016/j.jastp.2008.08.005>, 2009.
- 2152 Engebretson, M.J., Peterson, W.K., Posch, J.L., Klatt, M.R., Anderson, B.J., Russell, C.T., Singer,  
2153 H.J., Arnoldy, R.L., and Fukunishi, H.: Observations of two types of Pc 1-2 pulsations in the outer  
2154 dayside magnetosphere, *J. Geophys. Res.* 107, A12, 1415, doi:10.1029/2001JA00198, 2002.
- 2155 Falkenberg, T.V., Vrsnak, B., Taktakishvili, A., Odstreil, D., MacNeice, P., Hesse, M.:  
2156 Investigations of the sensitivity of a coronal mass ejection model (ENLIL) to solar input  
2157 parameters, *Space Weather* 8, S06004. <https://doi.org/10.1029/2009SW000555>, 2010.
- 2158 Firoz, K. A., Gan, W. Q., Moon, Y.-J., and Li, C.: An interpretation of the possible mechanisms  
2159 of two ground-level enhancement events, *Astrophys. J.*, 758, 119, 2012.
- 2160 Foster, J.C., Wygant, J.R., Hudson, M.K., Boyd, A.J., Baker, D.N., Erikson, P.J., and Spence,  
2161 H.E.: Shock-induced prompt relativistic electron acceleration in the inner magnetosphere, *J.*  
2162 *Geophys. Res. Spa. Phys.*, 120, 1661-1674, doi:10.1002/2014JA020642, 2015.
- 2163 Gonzalez, W.D., and Tsurutani, B.T.: Criteria of interplanetary parameters causing intense  
2164 magnetic storms ( $Dst < -100$  nT), *Planet. Spa. Sci.*, 35, 1101, 1987.
- 2165 Gonzalez, W.D., Joselyn, J.A., Kamide, Y., Kroehl, H.W., Rostoker, G., Tsurutani, B.T., and  
2166 Vasyliunas, V.M.: What is a geomagnetic storm?, *J. Geophys. Res.*, 99, A4, 5571-5792, 1994.



- 2167 Gonzalez, W.D., Gonzalez, A.L.C., Dal Lago, A., Tsurutani, B.T., Arballo, J.K., Lakhina, G.S.,  
2168 Buti, B., Ho, C.M., and Wu, S.-T.: Magnetic cloud field intensities and solar wind velocities,  
2169 *Geophys. Res. Lett.*, 25, 963-966, 1998.
- 2170 [Gopalswamy, N., Lara, A., Yashiro, S., Kaiser, M., and Howard, R.A.: Predicting the 1-AU arrival](#)  
2171 [times of coronal mass ejections, \*J. Geophys. Res.\* 106, 29207-29217, 2001.](#)
- 2172 Gopalswamy, N.: Coronal mass ejections and their heliospheric consequences, in First Asia-  
2173 Pacific Sol. Phys. Meet, vol. 2, edited by A. Choudhuri and D. Banerjee, *Astron. Soc. India Conf.*  
2174 *Series*, pp. 241–258, 21024 Mrach, Bengaluru, India, 2011.
- 2175 Gosling, J.T., Bame, S.J., and Feldman, W.C.: Solar wind speed variations: 1962, *J. Geophys.*  
2176 *Res.*, 81, 5061, 1976.
- 2177 Guarnieri, F. L.: The nature of auroras during high-intensity long-duration continuous AE activity  
2178 (HILDCAA) events: 1998–2001, in *Recurrent Magnetic Storms: Corotating Solar Wind Streams*,  
2179 *Geophys. Monogr. Ser.*, vol. 167, edited by B. T. Tsurutani et al., pp. 235–243, AGU, Washington,  
2180 D.C., 2006.
- 2181 Guarnieri, F. L., Tsurutani, B. T., Gonzalez, W. D., Echer, E., Gonzalez, A. L. C., Grande, M., and  
2182 Soraas, F.: ICME and CIR storms with particular emphasis on HILDCAA events, *ILWS Workshop*  
2183 2006, Goa, 2006.
- 2184 Guarnieri, F.L., Tsurutani, B.T., Vieira, L.E.A., Hajra, R., Echer, E., Mannucci, A.J., and  
2185 Gonzalez, W.D.: A correlation study regarding the AE index and ACE solar wind data for Alfvénic  
2186 intervals using wavelet decomposition and reconstruction, *Nonl. Proc. Geophys.* 25, 67-76,  
2187 <https://doi.org/10.5194/npg-25-67-2018>, 2018.
- 2188 Haerendel, G.: Acceleration from field-aligned potential drops, *Astrophys. J. Suppl. Ser.*, 90, 765,  
2189 1994.
- 2190 Hajra, R., Echer, E., Tsurutani, B.T., and Gonzalez, W.D.: Solar cycle dependence of high-  
2191 intensity long-duration continuous AE activity (HILDCAA) events, relativistic electron  
2192 predictors?, *J. Geophys. Res. Spa. Phys.*, 118, doi:10.1002/jgra.50530, 2013.
- 2193 Hajra, R., Echer, E., Tsurutani, B.T., and Gonzalez, W.D.: Solar wind-magnetosphere energy  
2194 coupling efficiency and partitioning: HILDCAAs and preceding CIR storms during solar cycle 23,  
2195 *J. Geophys. Res. Spa. Phys.*, 119, 2675-2690, 2014a.

- 2196 Hajra, R., Echer, E., Tsurutani, B. T., and Gonzalez, W. D.: Superposed epoch analyses of  
2197 HILDCAAs and their interplanetary drivers: solar cycle and seasonal dependences, *J. Atmos. Sol.*  
2198 *Ter. Phys.*, *121*, 24-31, 2014b.
- 2199 Hajra, R., Tsurutani, B. T., Echer, E., and Gonzalez, W. D.: Relativistic electron acceleration  
2200 during high-intensity, long-duration, continuous AE activity (HILDCAA) events: solar cycle  
2201 phase dependences, *Geophys. Res. Lett.*, *41*, 1876-1881, 2014c.
- 2202 Hajra, R., Tsurutani, B.T., Echer, E., Gonzalez, W.D., and Santolik, O.: Relativistic ( $E > 0.6$ ,  $> 2.0$ ,  
2203 and  $> 4.0$  MeV) electron acceleration at geosynchronous orbit during high-intensity long-duration  
2204 continuous AE activity (HILDCAA) events, *Ap. J.*, *799*:39, doi:10.1088/0004-637X/799/1/39,  
2205 2015a.
- 2206 Hajra, R., Tsurutani, B. T., Echer, E., Gonzalez, W. D., Brum, C. G. M., Vieira, L. E. A., and  
2207 Santolik, O.: Relativistic electron acceleration during HILDCAA events: are precursor CIR  
2208 magnetic storms important?, *Earth, Planets and Space*, *67*, 109, doi:10.1186/s40623-015-0280-5,  
2209 2015b.
- 2210 Hajra, R., Tsurutani, B.T., Echer, E., Gonzalez, W.D., and Gjerloev, J.W.: Supersubstorms (SML  
2211  $< -2500$  nT): Magnetic storm and solar cycle dependences, *J. Geophys. Res. Spa. Phys.*, *121*, 7805-  
2212 7816, doi:10.1002/2015JA021835, 2016.
- 2213 Hajra, R., Tsurutani, B. T., Brum, C. G. M., and Echer, E.: High-speed solar wind stream effects  
2214 on the topside ionosphere over Arecibo: a case study during solar minimum, *Geophys. Res. Lett.*,  
2215 *44*, 7607-7617, doi:10.1002/2017GL073805, 2017.
- 2216 Hajra, R., and Tsurutani, B. T.: Magnetospheric “killer” relativistic electron dropouts (REDs) and  
2217 repopulation: a cyclical process, in *Extreme Events in Geospace: Origins, Predictability, and*  
2218 *Consequences*, N. Buzulukova (Eds), pages 373-400, Elsevier, [https://doi.org/10.1016/B978-0-](https://doi.org/10.1016/B978-0-2219)  
2219 [12-812700-1.00014-5](https://doi.org/10.1016/B978-0-12-812700-1.00014-5), 2018a.
- 2220 Hajra, R., and Tsurutani, B. T.: Interplanetary shock inducing magnetospheric supersubstorms  
2221 (SML  $< -2500$  nT): Unusual auroral morphologies and energy flow, *Astrophys. J.*, *858*:123,  
2222 <https://doi.org/10.3847/1538-4357/aabaed>, 2018b.
- 2223 [Hajra, R., Tsurutani, B.T., and Lakhina, G.S.: The complex space weather events of September](#)  
2224 [2017, submitted to \*J. Geophys. Res.\*, 2019.](#)
- 2225 Hale, G.E.: The spectrohelioscope and its work Part III. Solar eruptions and their apparent  
2226 terrestrial effects, *Astrophys. J.*, *73*:379-412, 1931.

- 2227 Halford, A.J., Fraser, B.J., and Morley, S.K.: EMIC wave activity during geomagnetic storm and  
2228 nonstorm periods: CRRES results, *J. Geophys. Res.*, *115*, A12248, doi:10.1029/2010JA015716,  
2229 2010.
- 2230 Halford, A.J., McGregor, S.L., Murphy, K.R., Millan, R.M., Hudson, M.K., Woodger, L.A.,  
2231 Cattel, C.A., Breneman, A.W., Mann, I.R., Kurth, W.S., Hospodarsky, G.B., Gkioulidou, M., and  
2232 Fennel, J.F.: BARREL observations of an ICME-shock impact with the magnetosphere and the  
2233 resultant radiation belt electron loss, *J. Geophys. Res. Spa. Phys.*, *120*, 2557-2570, 2015.
- 2234 Halford, A.J., McGregor, S.L., Hudson, M.K., Milan, R.M., and Kress, B.T.: BARREL  
2235 observations of a solar energetic electron and solar energetic proton event, *J. Geophys. Res. Spa.*  
2236 *Phys.*, *121*, 4205-4216, doi:10.1002/2016JA022462, 2016.
- 2237 Hamilton, D. C., Gloeckler, G., Ipavich, F. M., Stüdemann, W., Wilken, B., and Kremser, G.: Ring  
2238 current development during the great geomagnetic storm of February 1986, *J. Geophys. Res.*,  
2239 *93*(A12), 14343-14355, doi:10.1029/JA093iA12p14343, 1988.
- 2240 [Hanslmeier, A., \*The Sun and Space Weather\* \(2007\), Springer Netherlands, edition 2.](https://doi.org/10.1007/978-1-4020-5604-8)  
2241 <https://doi.org/10.1007/978-1-4020-5604-8>.
- 2242 Harada, Y., Goto, A., Hasegawa, H., Fujikawa, N., Naoe, H., and Hirooka, T.: A major  
2243 stratospheric sudden warming event in January 2009, *J. Atmos. Sci.*, *67*, 2052,  
2244 doi:10.1175/2009JA53310.1, 2010.
- 2245 Hellinger, P., and Travnicek, P.M.: Oblique proton fire hose instability in the expanding solar  
2246 wind: Hybrid simulations, *J. Geophys. Res.*, *113*, A10109, <https://doi.org/10.1029/2008JA013416>,  
2247 2008.
- 2248 Heppner, J.P.: Note on the occurrence of world-wide SSCs during the onset of negative bays at  
2249 College, Alaska, *J. Geophys. Res.*, *60*, 29, 1955.
- 2250 Hodgson, R.: On a curious appearance seen in the Sun, *Mon. Not. R. Astron. Soc.*, *XX*, 15, 1859.
- 2251 Hollweg, J.V.: The solar wind: Then and now, in *Recurrent Magnetic Storms: Corotating Solar*  
2252 *Wind Streams* (Vol. 167, pp. 19-27), edited by B.T. Tsurutani, R.L. McPherron, W.D. Gonzalez,  
2253 G. Lu, J.H.A. Sobral and N. Gopalswamy, AGU Press, Wash D.C., 2006.
- 2254 Hones, E.W. Jr.: Transient phenomena in the magnetotail and their relation to substorms, *Spa. Sci.*  
2255 *Rev.*, *23*, 393-410, 1979.

- 2256 Horne, R. B., and Thorne, R. M.: Potential waves for relativistic electron scattering and stochastic  
2257 acceleration during magnetic storms, *Geophys. Res. Lett.*, 25, 3011-3014,  
2258 <https://doi.org/10.1029/98GL01002>, 1998.
- 2259 Huba, J.D., Joyce, G., and Fedder, J.A.: Sami2 is another model of the ionosphere (SAMI2): A  
2260 new low-latitude ionosphere model, *J. Geophys. Res.*, 105 (A10), 23035, 2000.
- 2261 Huba, J.D., Dymond, K.F., Joyce, G., Budzien, S.A., Thonnard, S.E., Fedder, J.A., and McCoy,  
2262 R.P.: Comparison of O<sup>+</sup> density from ARGOS LORAAS data analysis and SAMI2 model results,  
2263 *Geophys. Res. Lett.*, 29 (7), 6-1, doi:10.1029/2001GL013089, 2002.
- 2264 Hudson, M.K., Elkington, S.R., Lyon, J.G., Goodrich, C.C., and Rosenberg, T.J.: Simulations of  
2265 radiation belt dynamics driven by solar wind variations, in *Sun-Earth Plasma Connections*, edited  
2266 by J. Burch, R.L Carovillano, and S.K. Antiochos, Amer. Geophys. Un. Press, Wash. D.C., 171,  
2267 1999.
- 2268 Illing, R.M.E. and Hundhausen, A.J.: Disruption of a coronal streamer by an eruptive prominence  
2269 and coronal mass ejection, *J. Geophys. Res.*, 91, A10, 10,951-10,960, 1986.
- 2270 Inan, U.S., Bell, T.F., and Helliwell, R.A.: Nonlinear pitch angle scattering of energetic electrons  
2271 by coherent VLF waves in the magnetosphere, *J. Geophys. Res.*, 83, 3235-3253, 1978.
- 2272 Iyemori, T.: Storm-time magnetospheric currents inferred from midlatitude geomagnetic field  
2273 variations, *J. Geomag. Geoelectr.* 42, 1249, 1990.
- 2274 Jackson, B.V., Odstreil, D., Yu, H.S., Hick, P.P., Buffington, A., Mejia-Ambriz, J.C., Kim, J.,  
2275 Hong, S., Kim, Y., Han, J., and Tokumaru, M.: The UCSD kinematic IPS solar wind boundary  
2276 and its use in the ENLIL 3-D MHD prediction model, *Space Weather* 13, 104-115, 2015.
- 2277 Jian, L.K., MacNeice, P.J., Taktakishvili, A., Odstreil, D., Jackson, B., Yu, H.S., Riley, P.,  
2278 Sokolov, I.V., and Evans, R.M.: Validation of solar wind prediction at Earth: Comparison of  
2279 coronal and heliospheric models installed at the CCMC, *Space Weather* 13, 316-338, 2015.
- 2280 Jian, L.K., MacNeice, P.J., Mays, M.L., Taktakishvili, A., Odstreil, D., Jackson, B., Yu, H.S.,  
2281 Riley, P., and Sokolov, I.V.: Validation for global solar wind prediction using Ulysses comparison:  
2282 Multiple coronal and heliospheric models installed at the Community Coordinated Modeling  
2283 Center, *Space Weather* 14, 592-611, 2016.
- 2284 Jordanova, V. K., Farrugia, C.J., Janoo, L., Quinn, J.M., Torbert, R.B., Ogilvie, K.W., and Belian,  
2285 R.D.: October 1995 magnetic cloud and accompanying storm activity: Ring current evolution, *J.*  
2286 *Geophys. Res.*, 103, 79-92, <https://doi.org/10.1029/97JA02367>, 1998.

- 2287 Joselyn, J. A., and Tsurutani, B. T.: Geomagnetic sudden impulses and storm sudden  
2288 commencements, A note of terminology, *EOS*, 71, 47, 1808-1809, 1990.
- 2289 Kellerman, A.C., and Shprits, Y.Y.: On the influence of solar wind conditions on the outer-  
2290 electron radiation belts, *J. Geophys. Res.*, 117, A05127, doi:0.1029/2011JA017253, 2012.
- 2291 Kellerman, A.C., Shprits, Y.Y., Kondrashov, D., Subbotin, D., Makarevich, R.A., Donovan, E.,  
2292 and Nagal, T.: Three-dimensional data assimilation and reanalysis of radiation belt electrons:  
2293 Observations of a four-zone structure using five spacecraft and the VERB code, *J. Geophys. Res.*  
2294 *Spa. Phys.*, 119, doi:10.1002/2014JA020171, 2014.
- 2295 Kelley, M.C., Fejer, B.G., and Gonzales, C.A.: An explanation for anomalous equatorial  
2296 ionospheric electric field associated with a northward turning of the interplanetary magnetic field,  
2297 *Geophys. Res. Lett.*, 6(4), 301, 1979.
- 2298 Kelley, M.C., Makela, J.J., Chau, J.L., and Nicolls, M.J.: Penetration of the solar wind electric  
2299 field into the magnetosphere/ionosphere system, *Geophys. Res. Lett.*, 30(4), 1158,  
2300 doi:10.1029/2002GL016321, 2003.
- 2301 Kennel, C.F., and Petschek, H.E.: Limit of stably trapped particle fluxes, *J. Geophys. Res.* 71, 1-  
2302 28, 1966.
- 2303 Kennel, C.F., Edmiston, J.P., and Hada, T.: A quarter century of collisionless shock research in  
2304 Collisionless Shocks in the Heliosphere: A Tutorial Review, *Geophys. Mon. Ser.*, vol. 34, 1, AGU,  
2305 Wash. D.C., 1985.
- 2306 Kikuchi, T., and Hashimoto, K.K.: Transmission of the electric fields to the low latitude  
2307 ionosphere in the magnetosphere-ionosphere current circuit, *Geosc. Letts.*, 3:4,  
2308 doi:10.1186/s40562-016-0035-6, 2016.
- 2309 Kim, R.S., Cho, K.S., Moon, Y.J., Dryer, M., Lee, J., Yi, Y., Kim, K.H., Wang, H., Park, Y.D.,  
2310 and Kim, Y.H.: An empirical model for prediction of geomagnetic storms using initially observed  
2311 CME parameters at the Sun, *J. Geophys. Res.* 115, A12108,  
2312 <https://doi.org/10.1029/2010JA015322>, 2010.
- 2313 Kim, R.S., Moon, Y.J., Gopalswamy, N., Park, Y.D., and Kim, Y.H.: Two-step forecast of  
2314 geomagnetic storm using coronal mass ejection and solar wind condition, *Space Weather* 12, 246-  
2315 256. <https://doi.org/10.1002/2014SW001033>, 2014.
- 2316 Kimball, D.S.: A study of the aurora of 1859, *Sci. Rept.* 6, UAG-R109, Univ. of Alaska, Fairbanks,  
2317 Alaska, 1960.

- 2318 Klein, L.W., and Burlaga, L.F.: Interplanetary magnetic clouds at 1 AU, *J. Geophys. Res.*, 87, 613,  
2319 1982.
- 2320 Knipp, D. J., Hapgood, M.A., and Welling, D.: Communicating uncertainty and reliability in space  
2321 weather data, models, and applications. *Space Weather* 16, 1453-1454.  
2322 <https://doi.org/10.1029/2018SW002083>, 2018.
- 2323 Koskinen, H., *Physics of Space Storms: From the Solar Surface to the Earth* (2011), Springer-  
2324 Verlag, Berlin, Edition 1. <https://doi.org/10.1007/978-3-642-00319-6>.
- 2325 Kozyra, J.U., Jordanova, V.K., Horne, R.B., and Thorne, R.M.: Modeling of the contribution of  
2326 electromagnetic ion cyclotron (EMIC) waves to stormtime ring current erosion, in *Magnetic*  
2327 *Storms*, Geophys. Mon. Ser., 98, edited by B.T. Tsurutani et al., 187-202, 1997.
- 2328 Kozyra, J. U., Liemohn, M. W., Clauer, C. R., Ridley, A. J., Thomsen, M. F., Borovsky, J. E.,  
2329 Roeder, J. L., Jordanova, V. K., and Gonzalez, W. D.: Multistep Dst development and ring current  
2330 composition changes during the 4-6 June 1991 magnetic storm, *J. Geophys. Res.*, 107(A8), 1224,  
2331 doi:10.1029/2001JA000023, 2002.
- 2332 Kozyra, J.U., Nagy, A.F., Slater, D.W.: High-altitude energy source(s) for stable auroral red arcs,  
2333 *Rev. Geophys.*, 35, 155-190, 2006a.
- 2334 Kozyra, J. U., Crowley, G., Emery, B. A., Fang, X., Maris, G., Mlynczak, M. G., Niciejewski, R.  
2335 J., Palo, S. E., Paxton, L. J., Randal, C. E., Rong, P. P., III Russell, J. M., Skinner, W., Solomon,  
2336 S. C., Talaat, E. R., Wu, Q., and Yee, J. H.: Response of the upper/middle atmosphere to coronal  
2337 holes and powerful high-speed solar wind streams in 2003, in *Recurrent Magnetic Storms:*  
2338 *Corotating Solar Wind Streams*, Geophys. Monogr. Ser., vol. 167, edited by B. T. Tsurutani et al.,  
2339 pp. 319, AGU, Washington, D.C., doi: 10.1029/167GM24, 2006b.
- 2340 Kozyra, J.U., Manchester IV, W.B., Escoubet, C.P. et al.: Earth's collision with a solar filament  
2341 on 21 January 2005: Overview, *J. Geophys. Res. Spa. Phys.*, 118, doi:10.1002/jgra.50567, 2013.
- 2342 Krieger, A.S., Timothy, A.F., and Roelof, E.C.: A coronal hole and its identification as the source  
2343 of a high velocity solar wind stream, *Sol. Phys.* 23, 123, 1973.
- 2344 Lakhina, G.S.: Magnetic reconnection, *Bull. Astr. Soc. India*, 28, 593-646, 2000.
- 2345 Lakhina, G.S., Alex, S., Tsurutani, B.T., and Gonzalez, W.D.: Supermagnetic storms: Hazards to  
2346 society, in *Extreme Events and Natural Hazards: The Complexity Perspective*, Geophys. Mon.,  
2347 196, 267-278, 2012.

- 2348 Lakhina, G.S., and Tsurutani, B.T.: Satellite drag effects due to uplifted Oxygen neutrals during  
2349 super magnetic storms, *Nonl. Proc. Geophys.* 24, 745-750. [https://doi.org/10.5194/npg-24-745-](https://doi.org/10.5194/npg-24-745-2017)  
2350 [2017](https://doi.org/10.5194/npg-24-745-2017), 2017.
- 2351 Lakhina, G.S., and Tsurutani, B.T.: Supergeomagnetic storms: Past, present and future, Chapter 7  
2352 in *Extreme Events in Geospace*, 157, edited by N. Buzulukova, Elsevier, 2018.
- 2353 Lam, M.M., Chisham, G., and Freeman, M.P.: The interplanetary magnetic field influences mid-  
2354 latitude surface atmospheric pressure, *Env. Res. Lett.*, 8, doi:10.1088/1748-9326/8/4/045001,  
2355 2013.
- 2356 Lario, D.: Estimation of the solar flare neutron worst-case fluxes and fluences for missions  
2357 traveling close to the Sun, *Space Weather*, 10, S03002, doi: 10.1029/2011SW000732, 2012.
- 2358 Leamon, R.J., Canfield, R.C., Jones, S.L., Lambkin, K., Lundberg, B.J., and Pevtsov, A.A.:  
2359 Helicity of magnetic clouds and their associated active regions, *J. Geophys. Res.* 109, A05106.  
2360 <https://doi.org/10.1029/2003JA010324>, 2004.
- 2361 Lee, K. H.: Generation of parallel and quasi-perpendicular EMIC waves and mirror waves by fast  
2362 magnetosonic shocks in the solar wind, *J. Geophys. Res.*, 122, 7307-7322, 2017.
- 2363 Lepri, S.T., and Zurbuchen, T.H.: Direct observational evidence of filament material within  
2364 interplanetary coronal mass ejections, *Astrophys. J. Lett.*, 723, L22-L27.  
2365 <https://doi.org/10.1088/2041-8205/723/1/L22>, 2010.
- 2366 Li, X., Roth, I., Temerin, M., Wygant, J.R., Hudson, M.K., and Blake, J.B.: Simulation of the  
2367 prompt energization and transport of radiation belt particles during the March 24, 1991 SSC,  
2368 *Geophys. Res. Lett.*, 20, 22, 2423-2426, 1993.
- 2369 Li, X.-L., Temerin, M., Baker, D.N., Reeves, G.D., and Larson, D.: Quantitative prediction of  
2370 radiation belt electrons at geostationary orbit based on solar wind measurements, *Geophys. Res.*  
2371 *Lett.*, 28, 1887, 2001.
- 2372 Li, X., Baker, D.N., Temerin, M., Reeves, G., Friedel, R., and Shen, C.: Energetic electrons, 50  
2373 keV to 6 MeV, at geosynchronous orbit: their responses to solar wind variations, *Space Weather*,  
2374 3. S04001. <https://doi.org/10.1029/2004SW000105>, 2005.
- 2375 Li, X., Temerin, M., Tsurutani, B.T., and Alex, S.: Modeling of 1-2 September 1859 super  
2376 magnetic storm, *Adv. Spa. Res.*, 38(2), 273-279, <https://doi.org/10.1016/j.asr.2005.06.070>, 2006.
- 2377 Lui, A.T.Y, Chang, C.-L., Mankofsky, A., Wong, H.-K., and Winske, D.: A cross-field current  
2378 instability for substorm expansions, *J. Geophys. Res.*, 96, 11389, 1991.

- 2379 Lui, A.T.Y.: Current disruption in the Earth's magnetosphere: Observations and models, *J.*  
2380 *Geophys. Res.*, *101*, 13067-13088, doi:10.1029/96JA00079, 1996.
- 2381 Luhmann, J. G., Mays, M.L., Odstrcil, D., Li, Y., Bain, H., Lee, C.O., Galvin, A.B., Mewaldt,  
2382 R.A., Cohen, C.M.S., Leske, R.A., Larson, D., and Futaana, Y.: Modeling solar energetic particle  
2383 events using ENLIL heliosphere simulations, *Space Weather* *15*, 934-954, 2017.
- 2384 Manchester, W.B. IV, Ridley, A.J., Gombosi, T.I., and Dezeew, D.L.: Modeling the Sun-to-Earth  
2385 propagation of a very fast CME, *Adv. Space Res.*, *38*, 253-262, 2006.
- 2386 Mann, I.R., O'Brien, T.P., and Milling, D.K.: Correlations between ULF wave power, solar wind  
2387 speed, and relativistic electron flux in the magnetosphere: solar cycle dependence, *J. Atmosph.*  
2388 *Solar-Terr. Phys.*, *66*, 187, 2004.
- 2389 Mannucci, A.J., Tsurutani, B.T., Iijima, B.A., Konjathy, A., Saito, A., Gonzalez, W.D., Guarnieri,  
2390 F.L., Kozyra, J.U., and Skoug, R.: Dayside global ionospheric response to the major interplanetary  
2391 events of October 29-30, 2003 "Halloween storms", *Geophys. Res. Lett.*, *32*, L12S02,  
2392 doi:10.1029/2004GL021467, 2005.
- 2393 Mannucci, A.J., Tsurutani, B.T., Abdu, M.A., Gonzalez, W.D., Komjathy, A., Echer, E., Iijima,  
2394 B.A., Crowley, G., and Anderson, D.: Superposed epoch analysis of the dayside ionospheric  
2395 response to four intense geomagnetic storms, *J. Geophys. Res.*, *113*, A00A02,  
2396 doi:10.1029/2007JA012732, 2008.
- 2397 Matteini, L., Landi, S., Hellinger, P., and Velli, M.: Parallel proton fire hose instability in the  
2398 expanding solar wind: Hybrid simulations, *J. Geophys. Res.*, *111*, A10101,  
2399 <https://doi.org/10.1029/2006JA011667>, 2006.
- 2400 Matteini, L., Landi, S., Hellinger, P., Pantellini, F.G., Maksimovic, M., Velli, M., et al.: The  
2401 evolution of the solar wind proton temperature anisotropy from 0.3 to 2.5 AU, *Geophys. Res. Lett.*,  
2402 *34*, L20105, <https://doi.org/10.1029/2007GL030920>, 2007.
- 2403 Maunder, E. W.: Magnetic Disturbances, 1882 to 1903, as recorded at the Royal Observatory,  
2404 Greenwich, and their Association with Sun-spots, *Monthly Notices of the Royal Astronomical*  
2405 *Society*, *65*, 2-18, <https://doi-org.insu.bib.cnrs.fr/10.1093/mnras/65.1.2>, 1904.
- 2406 Mays, M. L., Thompson, B.J., Jian, L.K., Colaninno, R.C., Odstrcil, D., Mostl, C., Temmer, M.,  
2407 Savani, N.P., Collinson, G., Taktakishvili, A., MacNeice, P.J., and Zheng, Y.: *Astrophys J.*,  
2408 *812:145*, doi:10.1088/004-637X/812/2/145, 2015.



- 2409 McComas, D.J. et al.: Ulysses second fast latitude scan; complexity near solar maximum and the  
2410 reformation of polar coronal holes, *Geophys. Res. Lett.*, *29*(9), 1290, doi:10.1029/2001GL014164,  
2411 2002.
- 2412 McDonald, F.B., Teegarden, B.J., Trainor, J.H., Von Rosenvinge, T.T., and Webber, W.R.: The  
2413 interplanetary acceleration of energetic nucleons, *Astrophys. J. Lett.*, *203*, L149, 1976.
- 2414 Mendes, O., Domingues, M. O., Echer, E., Hajra, R., and Menconi, V. E.: Characterization of  
2415 high-intensity, long-duration continuous auroral activity (HILDCAA) events using recurrence  
2416 quantification analysis, *Nonlin. Processes Geophys.*, *24*, 407-417, 2017.
- 2417 Meng, X., Tsurutani, B.T., and Mannucci, A.J.: The solar and interplanetary causes of superstorms  
2418 (minimum  $Dst \leq -250$  nT) during the space age, *J. Geophys. Res.*, *124*. [https://](https://doi.org/10.1029/2018JA026425)  
2419 [doi.org/10.1029/2018JA026425](https://doi.org/10.1029/2018JA026425), 2019a.
- 2420 [Meng, X., Mannucci, A.J., Verkhoglyadova, O.P., Tsurutani, B.T., Ridley, A.J., and Shim, J.S.:](#)  
2421 [Thermosphere-ionosphere modeling with forecastable inputs: Case study of the June 2012 high](#)  
2422 [speed stream geomagnetic storm, submitted to \*J. Geophys. Res., Spa. Phys.\*, 2019b.](#)
- 2423 Meredith, N. P., Horne, R.B., Iles, R.H.A., Thorne, R.M., Heynderickx, D., and Anderson, R. R:  
2424 Outer zone relativistic electron acceleration associated with substorm-enhanced whistler mode  
2425 chorus, *J. Geophys. Res.*, *107*, A7, 1144, doi:10.1029/2001JA900146, 2002.
- 2426 Miyake, F., Nagaya, K., Masuda, K., and Nakamura, T.: A signature of cosmic-ray increase in AD  
2427 774-775 from tree rings in Japan, *Nature Lett.*, doi:10.1038/nature11123, 2012.
- 2428 Miyoshi, Y., Jordanova, V.K., Morioka, A., and Evans, D.S.: Solar cycle variations of the electron  
2429 radiation belts: Observations and radial diffusion simulation, *Space Weather*, *2*, S10S02,  
2430 doi:10.1029/2004SW000070, 2004.
- 2431 Monreal MacMahon, R., and Llop, C.: Ring current decay time model during geomagnetic storms:  
2432 A simple analytical approach, *Ann. Geophys.*, *26*, 2543-2550, 2008.
- 2433 Mostl, C., Rollett, T., Frahm, R.A., Liu, Y.D., Long, D.M., Colaninno, R.C., Reiss, M.A., Temmer,  
2434 M., Farrugia, C.J., Posner, A., Dumbovic, M., Janvier, M., Demoulin, P., Boakes, P., Devos, A.,  
2435 Kraaikamp, E., Mays, M.L., and Vrsnak, B.: Strong coronal channeling and interplanetary  
2436 evolution of a solar storm up to Earth and Mars, *Nat. Comm.*, *6*:7135, doi:10.1038/ncomms8135,  
2437 2015.
- 2438 Newton, H.W.: Solar flares and magnetic storms, *Mon. Not. R. Astron. Soc.*, *103*, 244, 1943.

- 2439 Ngwira, C.M., Pulkkinen, A., Kuznetsova, M.M., and Glocer, A.: Modeling extreme “Carrington-  
2440 type” space weather events using three dimensional global MHD simulations, *J. Geophys. Res.*  
2441 *Spa. Phys.* 119, 4456-4474, <https://doi.org/10.1002/2013JA019661>, 2014.
- 2442 Ngwira, C.M., Pulkkinen, A., Kuznetsova, M.M., and Glocer, A.: Reply to comments by Tsurutani  
2443 et al. on “Modeling extreme ‘Carrington-type’ space weather events using three-dimensional  
2444 global MHD simulations”, *J. Geophys. Res.* 123, 1393-1395.  
2445 <https://doi.org/10.1002/2017ja024928>, 2018.
- 2446 Nishida, A., and Jacobs, J.A.: Equatorial enhancement of world-wide changes, *J. Geophys. Res.*,  
2447 67, 12, 4937-4940, 1962.
- 2448 Nishida, A.: Coherence of geomagnetic DP2 fluctuations with interplanetary magnetic variations,  
2449 *J. Geophys. Res.*, 73, 5549, 1968.
- 2450 Nishida, A.: *Geomagnetic Diagnosis of the Magnetosphere*, Springer-Verlag, New York, 1978.
- 2451 Nishiura, M., Yoshida, Z., Saitoh, H., Yano, Y., Kawazura, Y., Nogami, T., Yamasaki, M.,  
2452 Mushiake, T., and Kashyap, A.: Improved beta (local beta > 1) and density in electron cyclotron  
2453 resonance heating on the RT-1 magnetosphere plasma, *Nuc. Fus.*, 55, 053019, doi:10.1088/0029-  
2454 5515/5/053019, 2015.
- 2455 Obayashi, T.: The interaction of solar plasma with geomagnetic field, disturbed conditions, in *Sol.*  
2456 *Terr. Phys.*, edited by J.W. King and W.S. Newman, 107 pp., Academic Press, London, 1967.
- 2457 O’Brien, T. P., and McPherron, R. L.: An empirical phase space analysis of ring current dynamics:  
2458 Solar wind control of injection and decay, *J. Geophys. Res.*, 105(A4), 7707–7719,  
2459 doi:10.1029/1998JA000437, 2000.
- 2460 O’Brien, T.P., McPherron, R.L., Sornette, D., Reeves, G.D., Friedel, R., and Singer, H.J.: Which  
2461 magnetic storms produce relativistic electrons at geosynchronous orbit?, *J. Geophys. Res.*, 106,  
2462 15533, 2001.
- 2463 Odstrcil, D., and Pizzo, V.J.: Three-dimensional propagation of coronal mass ejections (CMEs) in  
2464 a structured solar wind flow 1. CME launched within the streamer belt, *J. Geophys. Res.*, 104, A1,  
2465 483-492, 1999a.
- 2466 Odstrcil, D., and Pizzo, V.J.: Three-dimensional propagation of coronal mass ejections (CMEs) in  
2467 a structured solar wind flow 2. CME launched adjacent to the streamer belt, *J. Geophys. Res.*, 104,  
2468 493-503, 1999b.

- 2469 Olsen, J.V., and Lee, L.C.: PC1 wave generation by sudden impulses, *Plan. Spa. Sci.*, *31*, 295,  
2470 1983.
- 2471 Palmerio, E., Kilpua, E.K.J., Mostl, C., Bothmer, V., James, A.W., Green, L.M., Isavnin, A.,  
2472 Davies, J.A., and Harrison, R.A.: Coronal magnetic structure of earthbound CMEs and in situ  
2473 comparison, *Space Weather* *16*, 442-460, 2018.
- 2474 Pérez-Peraza, J., Vashenyuk, E. V., Miroshnichenko, L. I., Balabin, Yu. V., and Gallegos-Cruz,  
2475 A.: Impulsive, stochastic, and shock wave acceleration of relativistic protons in large solar events  
2476 of 1989 September 29, 2000 July 14, 2003 October 28, and 2005 January 20, *Astrophys. J.*, *695*,  
2477 865-873, 2009.
- 2478 Perreault, P., and Akasofu, S. I.: A study of geomagnetic storms, *Geophysical Journal*  
2479 *International*, *54*, 547-573, <https://doi.org/10.1111/j.1365-246X.1978.tb05494.x>, 1978.
- 2480 Pesses, M.E., Van Allen, J.A., and Goertz, C.K.: Energetic protons associated with interplanetary  
2481 active regions 1-5 AU from the sun, *J. Geophys. Res.*, *83*, 553, 1978.
- 2482 Pesses, M.E, Tsurutani, B.T., Van Allen, J.A., and Smith, E.J.: Acceleration of energetic protons  
2483 by interplanetary shocks, *J. Geophys. Res.*, *84*, 7297, 1979.
- 2484 Phillips, J.L., Bame, S.J., Feldman, W.C., Goldstein, B.E., Gosling, J.T., Hammond, C.M.,  
2485 McComas, D.J., Neugebauer, M., Scime, E.E., and Suess, S.T.: Ulysses solar wind plasma  
2486 observations at high southerly latitudes, *Science*, *268*, 1030, 1995.
- 2487 Pizzo, V.J., Koning, C., Cash, M., Millward, G., Biesecker, D.A., Puga, L., Codrescu, M., and  
2488 Odstrcil, D.: Theoretical basis for operational ensemble forecasting of coronal mass ejections,  
2489 *Space Weather* *13*, 676-697. <https://doi.org/10.1002/2015SW001221>, 2015.
- 2490 Rae, I.J., Murphy, K.R., Watt, C.E.J., Halford, A.J., Mann, I.R., Ozeke, L.G., Sibeck, D.G.,  
2491 Clilverd, M.A., Rodger, C.J., Degeling, A.W., Forsyth, C., Singer, H.J.: The role of localized  
2492 compressional ultra-low frequency waves in energetic electron precipitation, *J. Geophys. Res.* *123*,  
2493 1900-1914. <https://doi.org/10.1002/2017JA024674>, 2018.
- 2494 Randall, C.E., Harvey, V.L., Singleton, C.S., Bailey, S.M., Bernath, P.F., Codrescu, M., Nakajima,  
2495 H., and Russell, J.M.: Energetic particle precipitation effects on the Southern Hemisphere  
2496 stratosphere in 1992-2005, *J. Geophys. Res.* *112*, D08308. <https://doi.org/10.1029/2006JD007696>,  
2497 2007.

- 2498 Randall, C.E., Harvey, V.L., Siskind, D.E., France, J., Bernath, P.F., Boone, C.D., and Walker,  
2499 K.A.: NO<sub>x</sub> descent in the Arctic middle atmosphere in early 2009, *Geophys. Res. Lett.* *36*, L18811,  
2500 <https://doi.org/10.1029/2009GL039706>, 2009.
- 2501 Reames, D.V.: Particle acceleration at the Sun and in the heliosphere, *Spa. Sci. Rev.*, *90*, 413-491,  
2502 1999.
- 2503 Reeves, G.D., Spence, H.E., Henderson, M.G., Morley, S.K., Friedel, R.H.W., Funsten, H.O.,  
2504 Baker, D.N., Kanekal, S.G., Blake, J.B., Fennell, J.F., Claudepierre, S.G., Thorne, R.M., Turner,  
2505 D.L., Kletzing, C.A., Kurth, W.S., Larsen, B.A., and Niehof, J.T.: Electron acceleration in the  
2506 heart of the Van Allen radiation belts, *Science*, *341*, 991-994,  
2507 <https://doi.org/10.1126/science.1237743>, 2013.
- 2508 Reeves, G.D., Friedel, R.H.W., Larsen, B.A., Skoug, R.M., Funsten, H.O., Claudepierre, S.G.,  
2509 Fennell, J.F., Turner, D.L., Denton, M.H., Spence, H.E., Blake, J.B., and Baker, D.N.: Energy  
2510 dependent dynamics of keV to MeV electrons in the inner zone, outer zone, and slot regions, *J.*  
2511 *Geophys. Res.* *121*, 397-412, <https://doi.org/10.1002/2015JA021569>, 2016.
- 2512 Reikard, G.: Forecasting geomagnetic activity at monthly and annual horizons: Time series  
2513 models, *J. Atmos. Sol.-Terr. Phys.*, *133*, 111-120, 2015.
- 2514 Reikard, G.: Forecasting space weather over short horizons: Revised and updated estimates, *New*  
2515 *Astron.*, *62*, 62-69, 2018.
- 2516 Remya, B., Tsurutani, B.T., Reddy, R.V., Lakhina, G.S., and Hajra, R.: Electromagnetic cyclotron  
2517 waves in the dayside subsolar outer magnetosphere generated by enhanced solar wind pressure:  
2518 EMIC wave coherency, *J. Geophys. Res. Spa. Phys.*, *120*, 7536-7551, doi:10.1002/2015JA021327,  
2519 2015.
- 2520 Riley, P., Caplan, R.M., Giacalone, J., Lario, D., and Liu, Y.: Properties of the fast forward shock  
2521 driven by the 2012 July 23 extreme coronal mass ejection, *Astrophys. J.*, *819*:57,  
2522 doi:10.3847/0004-637X/819/1/57, 2016.
- 2523 Saikin, A.A., Zhang, J.-C., Smith, C., Spence, H.E., Torbert, R.B., and Kletzing, C.A.: The  
2524 dependence on geomagnetic conditions and solar wind dynamic pressure of the spatial  
2525 distributions of EMIC waves observed by the Van Allen Probes, *J. Geophys. Res. Spa. Phys.*, *121*,  
2526 4362-4377, doi:10.1002/2016JA022523, 2016.

- 2527 Saitoh, H., Yano, Y., Yoshida, Z., Nishiura, M., Morikawa, J., Kawazura, Y., Nogami, T., and  
2528 Yamasaki, M.: Observation of a new high- $\beta$  and high-density state of a magnetospheric plasma in  
2529 RT-1, *Phys. Plas.* *21*, 082511, 2014.
- 2530 Saldanha, R., S. Krucker, and R.P. Lin, Hard x-ray spectral evolution and production of solar  
2531 energetic particle events during the January 2005 x-class flares, *Astrophys. J.*, *673*, 1169-1173,  
2532 2008.
- 2533 Savani, N.P., Vourlidas, A., Szabo, A., Mays, M.L., Richardson, I.G., Thompson, B.J., Pulkkinen,  
2534 A., Evans, R., Nieves-Chinchilla, T.: Predicting the magnetic vectors within coronal mass ejections  
2535 arriving at Earth: 1. Initial architecture, *Space Weather* *13*, 374-385, doi:10.1002/2015SW001171,  
2536 2015.
- 2537 Savani, N. P., Vourlidas, A., Richardson, I. G., Szabo, A., Thompson, B. J., Pulkkinen, A., et al.:  
2538 Predicting the magnetic vectors within coronal mass ejections arriving at Earth: 2. Geomagnetic  
2539 response, *Space Weather* *15*, 441-461. <https://doi.org/10.1002/2016SW001458>, 2017.
- 2540 Scherhag, R.: Stratospheric temperature changes and the associated changes in pressure  
2541 distribution, *J. Meteor.*, *17*, 575, doi:10.1175/1520-0469(1960)017<0575:STCATA>2.0.CO;2,  
2542 1960.
- 2543 Schrijver, C.J., Kauristie, K., Aylward, A.D., Denardini, C.M., Gibson, S.E., Glover, A.,  
2544 Gopalswamy, N., Grande, M., Hapgood, M., Heynderickx, D., Jakowski, N., Kalegaev, V.V.,  
2545 Lapenta, G., Linker, J.A., Liu, S., Mandrini, C.H., Mann, I.R., Nagatsuma, T., Nandy, D., Obara,  
2546 T., O'Brien, T.P., Onsager, T., Opgenoorth, H.J., Terkildsen, M., Valladares, C.E., Vilmer, N.:  
2547 Understanding space weather to shield society: A global road map for 2015-2025 commissioned  
2548 by COSPAR and ILWS, *Adv. Spa. Res.* *55*, 2745-2807, 2015.
- 2549 Sckopke, N.: A general relation between the energy of trapped particles and the disturbance field  
2550 near the Earth, *J. Geophys. Res.*, *71*, 3125, 1966.
- 2551 Schrijver, C. J., Beer, J., Baltensperger, U., Cliver, E. W., Güdel, M., Hudson, H. S., McCracken,  
2552 K. G., Osten, R. A., Peter, T., Soderblom, D. R., Usoskin, I. G., and Wolff, E. W.: Estimating the  
2553 frequency of extremely energetic solar events, based on solar, stellar, lunar, and terrestrial records,  
2554 *J. Geophys. Res.*, *117*, A08103, doi: 10.1029/2012JA017706, 2012.
- 2555 Sharma, S., Kamide, Y., and Lakhina, G.S. (editors): *Storm-Substorm Relationship*, Amer.  
2556 Geophys. Un. Press, Wash. D.C.,142, 2004.

- 2557 Sheeley, N.R. Jr., Harvey, J.W., and Feldman, W.C.: Coronal holes, solar wind streams and  
2558 recurrent geomagnetic disturbances: 1973-1976, *Sol. Phys.*, *49*, 271, 1976.
- 2559 Sheeley, N.R. Jr., Asbridge, J.R., Bame, S.J., and Harvey, J.W.: A pictorial comparison of  
2560 interplanetary magnetic field polarity, solar wind speed and geomagnetic disturbance index during  
2561 the sunspot cycle, *Sol. Phys.*, *52*, 485, 1977.
- 2562 Simpson, J.A., Lentz, G.A., McKibben, R.B., O’Gallagher, J.J., Schroeder, W., and Tuzzolino,  
2563 A.J.: Preliminary documentation for the University of Chicago charged particle instrument data  
2564 from the Pioneer 10.11 spacecraft as submitted to NASA NSSDG, *NSSDC Doc. B.*, GSFC,  
2565 Greenbelt, Md, 1974.
- 2566 Siscoe, G. L.: A quasi-self-consistent axially symmetric model for the growth of a ring current  
2567 through earthward motion from a pre-storm configuration, *Planet. Spa. Sci.*, *27*, 285-295, 1979.
- 2568 Smith, E.J., Connor, B.V., and Foster Jr., G.T.: Measuring the magnetic fields of Jupiter and the  
2569 outer solar system, *IEE Trans. Magn.*, *MAG-11*, 962, 1975.
- 2570 Smith, E.J., and Wolfe, J.H.: Observations of interaction regions and corotating shocks between  
2571 one and five AU: Pioneers 10 and 11, *Geophys. Res. Lett.*, *3*, 137-140, 1976.
- 2572 Smith, E.J., Tsurutani, B.T., and Rosenberg, R.L.: Observations of the interplanetary sector  
2573 structure up to heliographic latitudes of 16°: Pioneer 11, *J. Geophys. Res.*, *83*, 717-723, 1978.
- 2574 Soraas, F., Aarsnes, K., Oksavik, K., Sandanger, M.I., Evans, D.S., and Greer, M.S.: Evidence for  
2575 particle injection as the case of Dst reduction during HILDCAA events, *J. Atmos. Sol.-Terr. Phys.*,  
2576 *66*, 177-187, 2004.
- 2577 Souza, A. M., Echer, E., Bolzan, M. J. A., and Hajra, R.: A study on the main periodicities in  
2578 interplanetary magnetic field Bz component and geomagnetic AE index during HILDCAA events  
2579 using wavelet analysis, *J. Atmos. Sol. Terr. Phys.*, *149*, 81-86, 2016.
- 2580 Souza, A. M., Echer, E., Bolzan, M. J. A., and Hajra, R.: Cross-correlation and cross-wavelet  
2581 analyses of the solar wind IMF Bz and auroral electrojet index AE coupling during HILDCAAs,  
2582 *Ann. Geophys.*, *36*, 205-211, 2018.
- 2583 [Srivastava, N.: A logistic regression model for predicting the occurrence of intense geomagnetic](#)  
2584 [storms, \*Ann. Geophys\* \*23\*, 2969-2974, 2005.](#)
- 2585 Stern, D.P.: The motion of a proton in the equatorial magnetosphere, *J. Geophys. Res.*, *80*, 595,  
2586 1975.

- 2587 Suess, S., and Tsurutani, B.T. (editors): *From the Sun: Auroras, Magnetic Storms, Solar Flares,*  
2588 *Cosmic Rays*, AGU monograph, Wash. D. C. 1998.
- 2589 Sugiura, M.: Hourly values of equatorial Dst for the IGY, *Annual International Geophysical Year,*  
2590 *vol. 35*, Pergamon, New York, p. 9, 1964.
- 2591 Summers, D., Ni, B., and Meredith, N.P.: Timescale for radiation belt electron acceleration and  
2592 loss due to resonant wave-particle interactions: 2. Evaluation for VLF chorus, ELF hiss, and  
2593 electromagnetic ion cyclotron waves, *J. Geophys. Res.*, *112*. A04207,  
2594 <https://doi.org/10.1029/2006JA011993>, 2007.
- 2595 Tan, B.: Small-scale microwave bursts in long-duration solar flares, *Astrophys. J.*, *773*, 165, 2013.
- 2596 Thomson, N. R., Rodger, C. J., and Clilverd, M. A.: Large solar flares and their ionospheric D  
2597 region enhancements, *J. Geophys. Res.*, *110*, A06306, doi: 10.1029/2005JA011008, 2005.
- 2598 Tang, F., Tsurutani, B.T., Gonzalez, W.D., Akasofu, S.I., and Smith, E.J.: Solar sources of  
2599 interplanetary southward Bz events responsible for major magnetic storms (1978-9), *J. Geophys.*  
2600 *Res.* *94*, A4, 3535-3541, 1989.
- 2601 Thorne, R.M., Smith, E.J., Fiske, K.J., and Church, S.R.: Intense variation of ELF hiss and chorus  
2602 during isolated substorms, *Geophys. Res. Lett.*, *1*, 193-196, doi:10.1029/GL001i005p00193, 1974.
- 2603 Thorne, R.M., O'Brien, T.P., Shprits, Y.Y., Summers, D., and Horne, R.B.: Timescale for MeV  
2604 electron microburst loss during geomagnetic storms, *J. Geophys. Res.*, *110*. A09202,  
2605 <https://doi.org/10.1029/2004JA010882>, 2005.
- 2606 Thorne, R.M., Li, W., Ni, B., Ma, Q., Bortnik, J., Chen, L., Baker, D.N., Spence, H.E., Reeves,  
2607 G.D., Henderson, M.G., Kletzing, C.A., Kurth, W.S., Hospodarsky, G.B., Blake, J.B., Fennell,  
2608 J.F., Claudepierre, S.G., and Kanekal, S.G.: Rapid local acceleration of relativistic radiation-belt  
2609 electrons by magnetospheric chorus, *Nature* *504*, 411-414, 2013.
- 2610 Thomson, N.R., Rodger, C.J., and Dowden, R.L.: Ionosphere gives the size of the greatest solar  
2611 flare, *Geophys. Res. Lett.*, *31*, L06803, doi:10.1029/2003GL019345, 2004.
- 2612 Tinsley, B.A., and Deen, G.W.: Apparent tropospheric response to MeV-GeV particle flux  
2613 variations: A connection via electrofreezing of supercooled water in high-level clouds?, *J.*  
2614 *Geophys. Res.*, *96*, 22,283, doi:10.1029/91JD02473, 1991.
- 2615 Tsurutani, B.T., and Smith, E.J.: Postmidnight chorus: A substorm phenomenon, *J. Geophys. Res.*,  
2616 *79*, 1, 118-127, 1974.

- 2617 Tsurutani, B.T., Smith, E.J., West Jr., H.I., and Buck, R.M.: Chorus, energetic electrons and  
2618 magnetospheric substorms, in *Wave Instabilities in Space Plasmas*, edited by P.J. Palmadesso and  
2619 K. Papadopoulos, 55, 1979.
- 2620 Tsurutani, B.T., Smith, E.J., Pyle, K.R., and Simpson, J.A.: Energetic protons accelerated at  
2621 corotating shocks: Pioneer 10 and 11 observations from 1 to 6 AU, *J. Geophys. Res.*, 87, A9, 7389-  
2622 7404, 1982.
- 2623 Tsurutani, B.T., and Lin, R.P.: Acceleration of  $>47$  keV ions and  $> 2$  keV electrons by  
2624 interplanetary shocks at 1 AU, *J. Geophys. Res.*, 90, A1, 1-11, 1985.
- 2625 Tsurutani, B.T., and Gonzalez, W.D.: The cause of high-intensity long-duration continuous AE  
2626 activity (HILDCAAs): Interplanetary Alfvén wave trains, *Plan. Spa. Sci.*, 35, 4, 405-412, 1987.
- 2627 Tsurutani, B.T., Gonzalez, W.D., Tang, F., Akasofu, S.-I., and Smith, E.J.: Origin of interplanetary  
2628 southward magnetic fields responsible for major magnetic storms near solar maximum (1978-  
2629 1979), *J. Geophys. Res.*, 93, A8, 8518-8531, 1988.
- 2630 [Tsurutani, B.T., Gould, T., Goldstein, B.E., and Gonzalez, W.D.: Interplanetary Alfvén waves and  
2631 auroral \(substorm\) activity: IMP 8, \*J. Geophys. Res.\*, 95, A3, 2241-2252, 1990.](#)
- 2632 Tsurutani, B.T., Gonzalez, W.D., Tang, F., and Lee, Y.T.: Great magnetic storms, *Geophys. Res.  
2633 Lett.*, 19, 73-76, 1992a.
- 2634 Tsurutani, B.T., Gonzalez, W.D., Tang, F., Lee, Y.T., Okada, M., and Park, D.: Reply to L.J.  
2635 Lanzerotti: Solar wind ram pressure corrections and an estimation of the efficiency of viscous  
2636 interaction, *Geophys. Res. Lett.*, 19, 19, 1993-1994, 1992b.
- 2637 Tsurutani, B.T., and Gonzalez, W.D.: The causes of geomagnetic storms during solar maximum,  
2638 *EOS*, 75, 5, 49-56, 1994.
- 2639 Tsurutani, B.T., Gonzalez, W.D., Zhou, X.-Y., Lepping, R.P., and Bothmer, V.: Properties of slow  
2640 magnetic clouds, *J. Atmos. Sol.-Terr. Phys.*, 66, 147-151, 1994.
- 2641 Tsurutani, B.T., Gonzalez, W.D., Gonzalez, A.L.C., Tang, F., Arballo, J.K., and Okada, M.:  
2642 Interplanetary origin of geomagnetic activity in the declining phase of the solar cycle, *J.  
2643 Geophys. Res.*, 100, 21,717, 1995.
- 2644 Tsurutani, B.T., and Lakhina, G.S.: Some basic concepts of wave-particle interactions in  
2645 collisionless plasmas, *Rev. Geophys.*, 35, 4, 491-502, 1997.
- 2646 [Tsurutani, B.T., Gonzalez, W.D., Kamide, Y., and Arballo, J.K. \(editors\): \*Magnetic Storms\*, Amer.  
2647 Geophys. Un. Press, Wash. D.C., 98, 1997a.](#)



- 2648 Tsurutani, B.T., and Gonzalez, W.D.: The interplanetary causes of magnetic storms: A review, in  
2649 *Magnetic Storms*, edited by Tsurutani, Gonzalez, Kamide and Arballo, AGU Press, Wash. D.C.,  
2650 98, 77-89, 1997b.
- 2651 Tsurutani, B.T., Arballo, J.K., Lakhina, G.S., Ho, C.M., Ajello, J., Pickett, J.S., Gurnett, D.A.,  
2652 Lepping, R.P., Peterson, W.K., Rostoker, G., Kamide, Y., and Kokubun, S.: The January 10, 1997  
2653 auroral hot spot, horseshoe aurora and first substorm: A CME loop?, *Geophys. Res. Lett.*, 25, 15,  
2654 3047-3050, 1998.
- 2655 Tsurutani, B. T., Arballo, J. K., Lakhina, G. S., Ho, C. M., Ajello, J., Pickett, J. S., Gurnett, D. A.,  
2656 Lepping, R. P., Peterson, W. K., Rostoker, G., Kamide, Y., and Kokubun, S.: The January 10,  
2657 1997 auroral hot spot, horseshoe aurora and first substorm: A CME loop?, *J. Geophys. Res.*, 25,  
2658 3047-3050, 1998.
- 2659 Tsurutani, B.T., Solar/interplanetary plasma phenomena causing geomagnetic activity at Earth, in  
2660 *Proc. Inter. Sch. Phys. "Enrico Fermi" Course CXLII*, edited by B. Coppi, A. Ferrari and E.  
2661 Sindoni, IOS Press, Amsterdam, 273, 2000.
- 2662 Tsurutani, B.T., Gonzalez, W.D., Lakhina, G.S., and Alex, S.: The extreme magnetic storm of 1-  
2663 2 September 1859, *J. Geophys. Res.* 108, A7, 1268, doi:10.1029/JA009504, 2003.
- 2664 Tsurutani, B.T., Gonzalez, W.D., Zhou, X.-Y., Lepping, R.P., and Bothmer, V.: Properties of slow  
2665 magnetic clouds, *J. Atmos. Sol.-Terr. Phys.*, 66, 147-151, 2004a.
- 2666 Tsurutani, B.T., Gonzalez, W.D., Guarnieri, F., Kamide, Y., Zhao, X., and Arballo, J.K.: Are high-  
2667 intensity long-duration continuous AE activity (HILDCAA) events substorm expansion events?,  
2668 *J. Atmos. Sol.-Terr. Phys.*, 66, 167-176, 2004b.
- 2669 Tsurutani, B.T., Mannucci, A., Iijima, B., Abdu, M.A., Sobral, J.H.A., Gonzalez, W., Guarnieri,  
2670 F., Tsuda, T., Saito, A., Yumoto, K., Fejer, B., Fuller-Rowell, T.J., Kozyra, J., Foster, J.C., Coster,  
2671 A., and Vasyliunas, V.M.: Global dayside ionospheric uplift and enhancement associated with  
2672 interplanetary electric fields, *J. Geophys. Res.* 109, A08302, doi:10.1029/2003JA010342, 2004c.
- 2673 Tsurutani, B.T., Gonzalez, W.D., Lakhina, G.S., and Alex, S.: Reply to comment by S.-I. Akasofu  
2674 and Y. Kamide on "The extreme magnetic storm of 1-2 September 1859", *J. Geophys. Res.*, 110,  
2675 A09227, doi:10.1029/2005JA011121, 2005a.
- 2676 Tsurutani, B.T., Judge, D.L., Guarnieri, F.L., Gangopadhyay, P., Jones, A.R., Nuttall, J., Zambon,  
2677 G.A., Didkovsky, L., Mannucci, A.J., Iijima, B., Meier, R.R., Immel, T.J., Woods, T.N., Prasad,  
2678 S., Floyd, L., Huba, J., Solomon, S.C., Straus, P., and Viereck, R.: The October 38, 2003 extreme

2679 EUV solar flare and resultant extreme ionospheric effects: Comparison to other Halloween events  
2680 and the Bastille day event, *Geophys. Res. Lett.*, *32*, L03S09, doi:10.1029/2004GL021475, 2005b.

2681 Tsurutani, B.T., McPherron, R.L., Gonzalez, W.D., Lu, G., Sobral, J.H.A., and Gopalswamy, N.  
2682 (editors): *Recurrent Magnetic Storms: Corotating Solar Wind Streams*, Amer. Geophys. Un. Press,  
2683 Wash. D.C., 167, 2006a.

2684 Tsurutani, B.T., Gonzalez, W.D., Gonzalez, A.L.C., Guarnieri, F.L., Gopalswamy, N., Grande,  
2685 M., Kamide, Y., Kasahara, Y., Lu, G., Mann, I., McPherron, R., Soraas, F., and Vasyliunas, V.:  
2686 Corotating solar wind streams and recurrent geomagnetic activity: A review, *J. Geophys. Res.*,  
2687 *111*, A07S01, doi:10.1029/2005JA011273, 2006b.

2688 Tsurutani, B.T., McPherron, R.L., Gonzalez, W.D., Lu, G., Gopalswamy, N., and Guarnieri, F.L.:  
2689 Magnetic storms caused by corotating solar wind streams, in *Recurrent Magnetic Storms*  
2690 *Corotating Solar Wind Streams*, edited by B.T. Tsurutani et al., AGU Press, Wash. DC, 167, 1-17,  
2691 2006c.

2692 Tsurutani, B.T., Echer, E., Guarnieri, F.L., and Kozyra, J.U.: CAWSES November 7-8, 2004  
2693 superstorm: Complex solar and interplanetary features in the post-solar maximum phase, *Geophys.*  
2694 *Res. Lett.*, *35*, L06S05, doi:10.1029/2007GL031473, 2008a.

2695 Tsurutani, B.T., Verkhoglyadova, O.P., Mannucci, A.J., Saito, A., Araki, T., Yumoto, K., Tsuda,  
2696 T., Abdu, M.A., Sobral, J.H.A., Gonzalez, W.D., McCreddie, H., Lakhina, G.S., and Vasyliunas,  
2697 V.M.: *J. Geophys. Res.*, *113*, A05311, doi:10.1029/2007HA012879, 2008b.

2698 Tsurutani, B.T., Horne, R.B., Pickett, J.S., Santolik, O., Schriver, D., and Verhoglyadova, O.P.: *J.*  
2699 *Geophys. Res.*, *115*, AF0010, doi:10.1029/2010JA015870, 2010.

2700 Tsurutani, B.T., Lakhina, G.S., Verkhoglyadova, O.P., Gonzalez, W.D., Echer, E., and Guarnieri,  
2701 F.L.: A review of interplanetary discontinuities and their geomagnetic effects, *J. Atmos. Sol.-Terr.*  
2702 *Phys.*, *73*, 5-19, 2011.

2703 Tsurutani, B.T., Verkhoglyadova, O.P., Mannucci, A.J., and Lakhina, G.S.: Extreme changes in  
2704 the dayside ionosphere during a Carrington-type magnetic storm, *J. Spa. Weath. Spa. Clim.*, *2*,  
2705 A05, doi:10.1051/swsc/2012004, 2012.

2706 Tsurutani, B.T., and Lakhina, G.S.: An extreme coronal mass ejection and consequences for the  
2707 magnetosphere and Earth, *Geophys. Res. Lett.*, *41*, doi:10.1002/203GL058825, 2014.

2708 Tsurutani, B.T., Echer, E., Shibata, K., Verkhoglyadova, O.P., Mannucci, A.J., Gonzalez, W.D.,  
2709 Kozyra, J.U., and Paetzold, M.: The interplanetary causes of geomagnetic activity during the 7-

- 2710 17 March 2012 interval: a CAUSES II overview, *J. Spa. Weath. Spa. Clim.*, 4, A02,  
2711 doi:10.1051/swsc/2013056, 2014.
- 2712 Tsurutani, B. T., Hajra, R., Echer, E., and Gjerloev, J. W.: Extremely intense ( $SML \leq -2500$  nT)  
2713 substorms: isolated events that are externally triggered?, *AnGeo Comm.*, 33, 519-524, 2015.
- 2714 Tsurutani, B. T., Hajra, R., Echer, E., Gonzalez, W. D., and Santolik, O.: Predicting  
2715 magnetospheric relativistic  $>1$  MeV electrons, *NASA Tech Briefs*, 40, 20, 2016a.
- 2716 Tsurutani, B.T., Hajra, R., Tanimori, T., Takada, A., Bhanu, R., Mannucci, A.J., Lakhina, G.S.,  
2717 Kozyra, J.U., Shiokawa, K., Lee, L.C., Echer, E., Reddy, R.V., and Gonzalez, W.D.: Heliospheric  
2718 plasma sheet (HPS) impingement onto the magnetosphere as a cause of relativistic electron  
2719 dropouts (REDs) via a coherent EMIC wave scattering with possible consequences for climate  
2720 change mechanisms, *J. Geophys. Res. Spa. Phys.*, 121, doi:10.1002/2016JA022499, 2016b.
- 2721 Tsurutani, B.T., Lakhina, G.S., Echer, E., Hajra, R., Nayak, C., Mannucci, A.J., and Meng, X.:  
2722 Comment on “Modeling extreme “Carrington-type” space weather events using three-dimensional  
2723 global MHD simulations” by C.M. Ngwira, A. Pulkkinen, M.M Kuznetsova and A. Glocer”, *J.*  
2724 *Geophys. Res. Spa. Phys.*, 123, 1388-1392, <https://doi.org/10.1002/2017JA024779>, 2018a.
- 2725 Tsurutani, B.T., Lakhina, G.S., Sen, A., Hellinger, P., Glassmeier, K.-H., and Mannucci, A.J.: A  
2726 review of Alfvénic turbulence in high-speed solar wind streams: Hints from cometary plasma  
2727 turbulence, *J. Geophys. Res. Spa. Phys.*, 123, <https://doi.org/10.1002/2017JA024203>, 2018b.
- 2728 Turner, N. E., Mitchell, E. J., Knipp, D. J., and Emery, B. A.: Energetics of magnetic storms driven  
2729 by corotating interaction regions: a study of geoeffectiveness, in *Recurrent Magnetic Storms:*  
2730 *Corotating Solar Wind Streams*, Geophys. Monogr. Ser., vol. 167, edited by B. T. Tsurutani et al.,  
2731 pp. 113, AGU, Washington, D.C., doi:10.1029/167GM11, 2006.
- 2732 Turner, D.L., and Li, X.: Quantitative forecast of relativistic electron flux at geosynchronous orbit  
2733 based on low energy electron flux, *Space Weather*, 6, S05005,  
2734 <https://doi.org/10.1029/2007SW000354>, 2008.
- 2735 Usanova, M.E., Mann, I.R., Bortnik, J., Shao, L., and Angelopoulos, V.: THEMIS observations of  
2736 electromagnetic ion cyclotron wave occurrence: Dependence on AE, SYMH and solar wind  
2737 dynamic pressure, *J. Geophys. Res.*, 117, A10218, doi:10.1029/2012JA018049, 2012.
- 2738 Usoskin, I.G., and Kovaltsov, G.A.: Occurrence of extreme solar particle events: Assessment from  
2739 historical proxy data, *Astrophys. J.*, 757:92, doi:10.1088/0004-637X/757/1/92, 2012.

- 2740 Usoskin, I.G., Kromer, B., Ludlow, F., Beer, J., Friedrich, M., Kovaltsov, G.A., Solanki, S.K., and  
2741 Wacker, L.: The AD775 cosmic event revisited: the Sun is to blame, *Astron. Astrophys.*, *L3*,  
2742 doi:10.1051/0004-6361/201321080, 2013.
- 2743 Vaisberg, O.L., and Zastenker, G.N.: Solar wind and magnetosheath observations at Earth during  
2744 August 1972, *Spa. Sci. Rev.*, *19*, 687, 1976.
- 2745 Volland, H.: A semi-empirical model of large-scale magnetospheric electric fields, *J. Geophys.*  
2746 *Res.*, *78*, 171, 1973.
- 2747 Wang, C. B., Chao, J. K., and Lin, C.-H.: Influence of the solar wind dynamic pressure on the  
2748 decay and injection of the ring current, *J. Geophys. Res.*, *108*(A9), 1341,  
2749 doi:10.1029/2003JA009851, 2003.
- 2750 Wang, J., Zhao, M., and Zhou, G.: Magnetic changes in the course of the X7.1 solar flare on 2005  
2751 January 20, *Astrophys. J.*, *690*, 862-874, 2009.
- 2752 Wanliss, J. A., and Showalter, K. M.: High-resolution global storm index: Dst versus SYM-H,  
2753 *Journal of Geophysical Research*, *111*, A02202. <https://doi.org/10.1029/2005JA011034>, 2006.
- 2754 West, H.I., Jr., Buck, R.M, and Walton, J.R.: Shadowing of electron azimuthal-drift motions near  
2755 the noon magnetopause, *Nature Phys. Sci.*, *240*, 6, doi:10.1038/physci240006a0, 1972.
- 2756 Weygand, J. M., and McPherron, R. L.: Dependence of ring current asymmetry on storm phase, *J.*  
2757 *Geophys. Res.*, *111*, A11221, doi:10.1029/2006JA011808, 2006.
- 2758 Wilcox, J.M., Scherrer, P.H., Svalgaard, L., Roberts, W.O., and Olson, R.H.: Solar magnetic sector  
2759 structure: Relation to circulation of the Earth's atmosphere, *Science*, *180*, 185,  
2760 doi:10.1126/science.180.4082.185, 1973.
- 2761 Williams, D. J., Mitchell, D. G., Huang, C. Y., Frank, L. A., and Russell, C. T.: Particle  
2762 acceleration during substorm growth and onset, *Geophys. Res. Lett.*, *17*, 587-590,  
2763 <https://doi.org/10.1029/GL017i005p00587>, 1990.
- 2764 Wing, S., Johnson, J.R., Jen, J., Meng, C.I., Sibeck, D.G., Bechtold, K., Freeman, J., Costello, K.,  
2765 Balikhin, M., and Takahashi, K.: Kp forecast models, *J. Geophys. Res.* *110*, A04203,  
2766 doi:10.1029/2004JA0105002005.
- 2767 Wing, S., Johnson, J.R., Camporeale, E., Reeves, G.D.: Information theoretical approach to  
2768 discovering solar wind drivers of the outer radiation belt, *J. Geophys. Res. Spa. Phys.*, *121*, 9378-  
2769 9399, 2016.

- 2770 Winterhalter, D.E., Smith, E.J., Burton, M.E., Murphy, N., and McComas, D.J.: The heliospheric  
2771 plasma sheet, *J. Geophys. Res.*, *99*, 6667, doi:10.1029/93JA03481, 1994.
- 2772 Wolff, E.W., Bigler, M., Curran, M.A.J., Dibb, J.E., Frey, M.M., Legrand, M., and McConnell,  
2773 J.R.: The Carrington event not observed in most ice core nitrate records, *Geophys. Res. Lett.*, *39*,  
2774 L08503, doi:10.1029/2012GL051603, 2012.
- 2775 Wygant, J., Mozer, F., Temerin, M., Blake, J., Maynard, N., Singer, H., and Smiddy, M.: Large  
2776 amplitude electric and magnetic field signatures in the inner magnetosphere during injection of 15  
2777 MeV electron drift echos, *Geophys. Res. Lett.*, *21*, 16, 1739-1742, 1994.
- 2778 Wygant, J., Rowland, D., Singer, H.J., Temerin, M., Mozer, F., and Hudson, M.K.: Experimental  
2779 evidence on the role of the large spatial scale electric field in creating the ring current, *J. Geophys.*  
2780 *Res.*, *103*, A12, 29527-29544, 1998.
- 2781 Yashiro, S., Gopalswamy, N., Michalek, G., St. Cyr, O. C., Plunkett, S. P., Rich, N. B., and  
2782 Howard, R. A.: A catalog of white light coronal mass ejections observed by the SOHO spacecraft,  
2783 *J. Geophys. Res.*, *109*, A07105, doi:10.1029/2003JA010282, 2004.
- 2784 [Yurchyshyn, V., Hu, Q., Lepping, R.P., Lynch, B.J., Krall, J.: Orientations of LASCO halo CMEs  
2785 and their connection to the flux rope structure of interplanetary CMEs, \*Adv. Spa. Res.\*, \*40\*, 1821-  
2786 1826, 2007.](#)
- 2787 Zastenker, G.N., Temny, V.V., d'Uston, C., and Bosqued, J.M.: The form and energy of the shock  
2788 waves from the solar flares of August 2, 4 and 7, 1972, *J. Geophys. Res.*, *83*, 1035, 1978.
- 2789 Zhao, X., and Dryer, M.: Current status of CME/shock arrival time prediction, *Spa. Weath.*, *12*,  
2790 448-469, doi:10.1002/2014SW001060, 2014.
- 2791 Zhang, J., Woch, J., and Solanki, S.: Polar coronal holes during solar cycles 22 and 23, *Chin. J.*  
2792 *Astron. Astrophys.*, *5*, 5, 531-538, 2005.
- 2793 Zhou, X., and Tsurutani, B. T.: Rapid intensification and propagation of the dayside aurora: Large  
2794 scale interplanetary pressure pulses (fast shocks), *Geophys. Res. Lett.*, *26*, 8, 1097-1100, 1999.
- 2795 Zhang, J., et al.: Solar and interplanetary sources of major geomagnetic storms ( $Dst \leq -100$  nT)  
2796 during 1996-2005, *J. Geophys. Res.*, *112*, A10102, doi:10.1029/2007JA012321, 2007.
- 2797 Zhou, X., and Tsurutani, B.T.: Interplanetary shock triggering of nightside geomagnetic activity:  
2798 Substorms, pseudobreakups, and quiescent events, *J. Geophys. Res.*, *106*, A9, 18,957-18,967,  
2799 2001.

2800 Zhou, X.-Y., Strangeway, R.J., Anderson, P.C., Sibeck, D.G., Tsurutani, B.T., Haerendel, G., Frey,  
2801 H.U., and Arballo, J.K.: Shock aurora: FAST and DMSP observations, *J. Geophys. Res.*, 108, A4,  
2802 doi:10.1029/2002JA009701, 2003.

2803  
2804 **Acknowledgements.** This paper was solicited by an Editor of Reviews of Geophysics to be the  
2805 main article for Space Weather for the AGU Centennial. The paper was written with that in mind  
2806 but was rejected by two referees. GSL thanks the National Academy of Sciences, India for support  
2807 under the NASI-Senior Scientist Platinum Jubilee Fellowship Scheme. The work of RH is funded by the  
2808 Science & Engineering Research Board (SERB), a statutory body of the Department of Science &  
2809 Technology (DST), Government of India through the Ramanujan Fellowship.